INTERNATIONAL ATOMIC ENERGY AGENCY

INDC(CCP)-435
Distr.: L0

I N D C INTERNATIONAL NUCLEAR DATA COMMITTEE

Articles Translated from Journal Yadernye Konstanty (Nuclear Constants)

(Series: Nuclear Constants, Issue No. 2, 2001)

Translated by the IAEA

December 2002

IAEA NUCLEAR DATA SECTION, WAGRAMER STRASSE 5, A-1400 VIENNA

Nuclear Data Section
International Atomic Energy Agency
P.O. Box 100
Wagramer Strasse 5
A-1400 Vienna
Austria

Produced by the IAEA in Austria
December 2002

INDC(CCP)-435
Distr.: L0

Articles Translated from Journal Yadernye Konstanty (Nuclear Constants)

(Series: Nuclear Constants, Issue No. 2, 2001)

Abstract

This report contains translations of three papers published in the Nuclear Constants journal (Voprosy Atomnoj Nauki I Teknniki, seriya: Yadernye Konstanty (YK), vypusk 2, 2001). They are marked as "Translated from Russian". Three original YK papers published in English and one sent by the author are included with corrections of misprints and small format changes. As a result the report contains seven of nine papers presented in YK, 2 (2001).

December 2002

Contents

02-11288 (150) [1]
Translated from Russian

UDC 539.17

EVALUATION OF THE ENERGY DEPENDENCE OF THE MEAN NUMBER OF PROMPT NEUTRONS $\bar{\nu}_p$ FOR NEPTUNIUM AND FOR AMERICIUM ISOTOPES

B.D. Kuz'minov, A.I. Sergachev, V.A. Khryachkov
National Research Centre - Institute for Physics and Power Engineering, Obninsk, Russia

EVALUATION OF THE $\bar{\nu}_p$ ENERGY DEPENDENCE FOR NEPTUNIUM AND AMERICIUM ISOTOPES. A new evaluation of the $\bar{\nu}_p$ energy dependence for neptunium and americium isotopes in the neutron energy range up to 20 MeV is described. Existing experimental data and some systematics are used. The adopted curves are approximated by linear functions.

Introduction

Recent years have seen increased research into such promising nuclear technologies as the closed fuel cycle, transmutation of minor actinides, and the use in reactors of plutonium from weapons and power applications. A characteristic of these areas is that the technological process involves comparatively large amounts of minor actinides.

As a result it has become desirable to update the nuclear data on the minor actinides and, in particular, the prompt fission neutron multiplicity as the main factor affecting the neutron multiplication coefficient in a medium.

The present paper gives a new evaluation of the energy dependence $\bar{\nu}_p(E_n)$ for ^{237}Np, ^{241}Am, ^{242m}Am and ^{243}Am in the reactor range of fission neutron energies.

1. Basic principles of the approach to evaluating $\bar{\nu}_p$

The energy balance in neutron-induced fission of nuclei is composed as follows:

$$\bar{E}_f + B_n + E_n = \bar{E}_k + \bar{E}_\gamma + \bar{\nu}_p\,(\bar{\varepsilon} + \bar{S}_n) \qquad (1)$$

Here $\bar{E}_f$ is the mean fission energy, equal to the mass difference between the fissioning nucleus and the fission fragments. B_n and E_n are the binding energy and kinetic energy of the neutron inducing the fission, $\bar{E}_k$ is the mean total kinetic energy of paired fission fragments, $\bar{E}_\gamma$ is the energy carried away by prompt gamma rays, $\bar{\nu}_p$ and $\bar{\varepsilon}$ are the mean number and

mean kinetic energy of prompt fission neutrons, and $\overline{S}_n$ is the mean binding energy of neutrons in the fission fragments. Let us take an average over all fission paths.

$$\overline{\nu}_p = \frac{\overline{E}_f - \overline{E}_k - \overline{E}_\gamma}{\overline{\varepsilon} + \overline{S}_n} + \frac{B_n + E_n}{\overline{\varepsilon} + \overline{S}_n} \qquad (2)$$

If we divide the energy scale for the fission-inducing neutrons into intervals within which all the averaged quantities in Eq. (2) remain practically unchanged, then the energy dependence of $\overline{\nu}_p$ can be written as a piecewise-linear function.

There are a few values of the neutron energy E_n^i which must be taken as the boundaries for this division into intervals.

Specifically, these include the thresholds for the (n,n′f) and (n,2n′f) reactions. In this case a contribution appears from several fissioning isotopes with different excitation energies, which accordingly leads to a change in all the terms of the fission energy balance.

Those cases where changes in the mean kinetic energy of the fragments or in their mass distributions are known must also be taken into account in dividing the energy scale into intervals.

Numerous examples can be given where such phenomena occur.

Figure 1 gives the energy dependence of $\overline{\nu}_p$ and $\overline{E}_k$ for fission of ^{232}Th by neutrons. Near and below the fission barrier the sign of the rate of growth of $\overline{\nu}_p$ is observed to change; qualitatively, this correlates with changes in $\overline{E}_k$.

Figure 2 gives results on the change in the distributions of fragments by mass and kinetic energy at the transition from spontaneous fission of ^{242}Pu to fission of ^{241}Pu induced by thermal and fast neutrons [1].

An analogous picture is observed for the fissioning nucleus ^{240}Pu [2].

Table 1 gives data characterizing the growth rate of $\overline{\nu}_p$ in the fission of nuclei below and above the fission barrier (the main figures are taken from Ref. [3]).

These data show that the growth rates of $\overline{\nu}_p$ are substantially different for below-barrier and above-barrier fission of one and the same nucleus: in below-barrier fission significantly more energy is expended on the emission of a single neutron. However, such a conclusion has no physical meaning, as the difference observed is due to the significant change in the fission fragment distributions by mass and kinetic energy at the transition from spontaneous to induced fission (see Fig. 2).

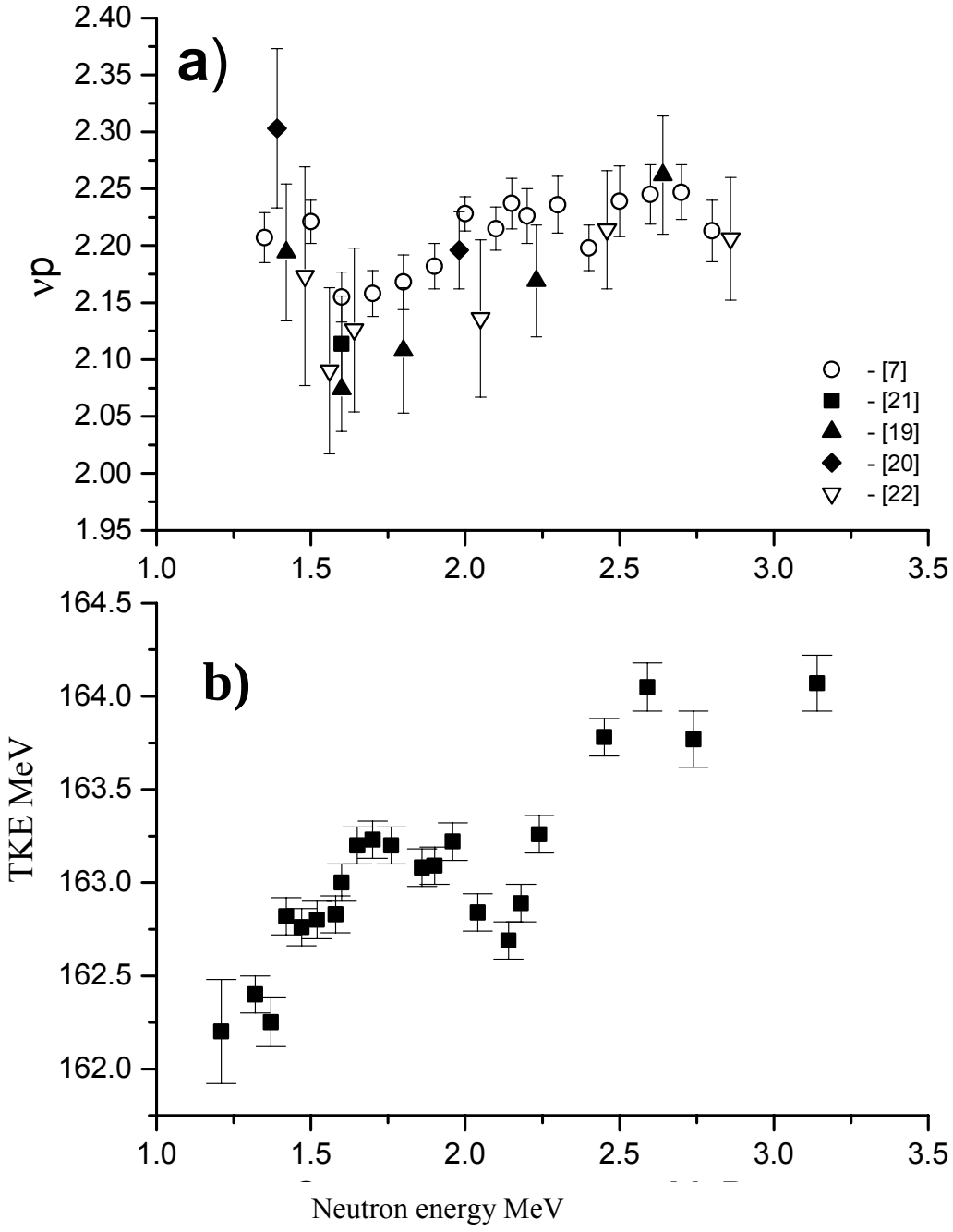

Fig. 1. Energy dependence of $\bar{\nu}_p$ (a) and total kinetic energy of fragments in fission of ^{232}Th by fast neutrons (b) - [18].

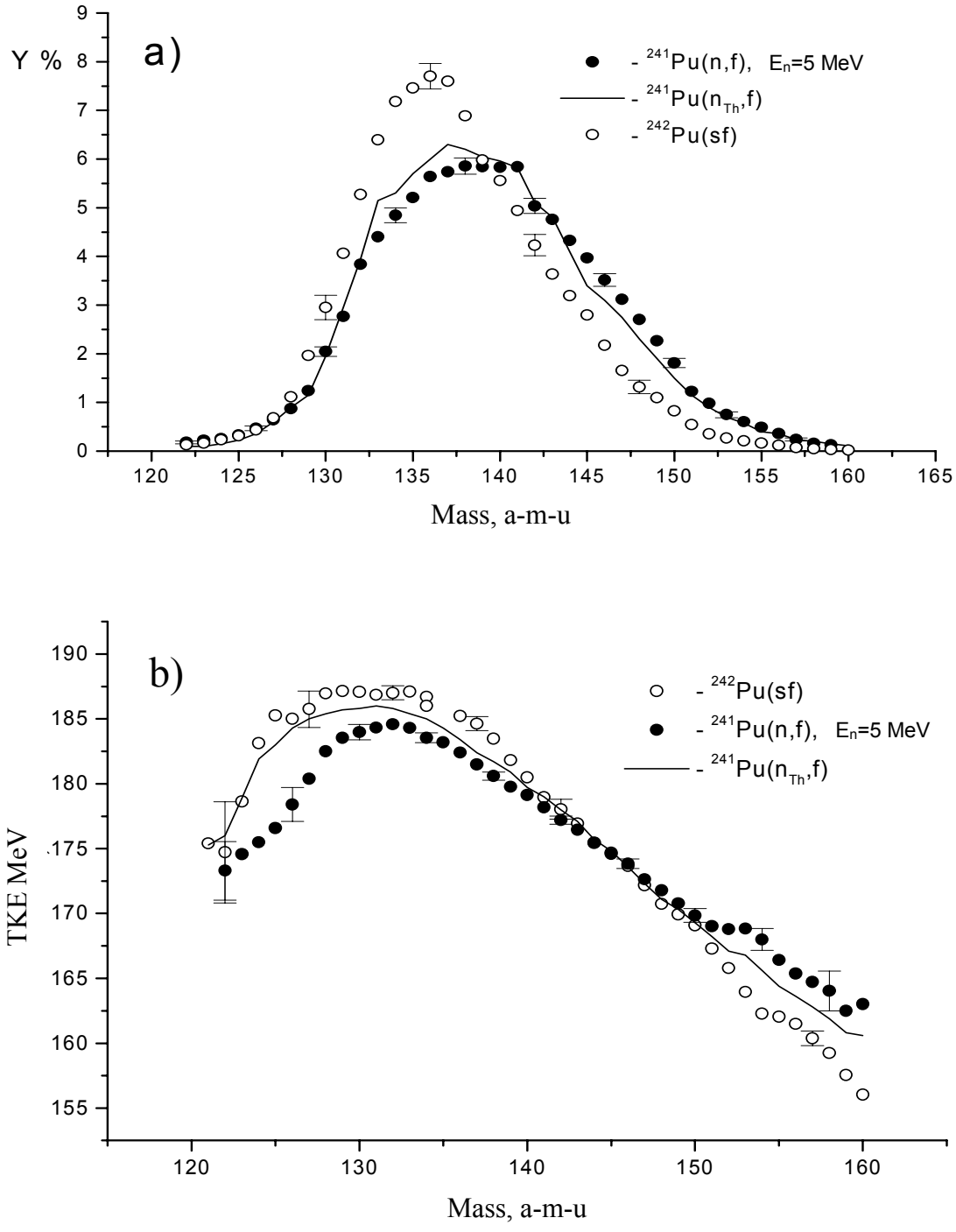

Fig. 2. Yields (a) and kinetic energy of fragment pairs (b) in spontaneous fission of ^{242}Pu and fission of ^{241}Pu by thermal neutrons and 5 MeV neutrons [1].

Table 1

Fissioning nuclei	$\bar{\nu}_p(spont.)$	$\bar{\nu}_p(therm.)$	$\frac{d\bar{\nu}_p}{dB_n}\frac{1}{MeV}$	Neutron energy range E_n MeV	$\frac{d\bar{\nu}_p}{dE_n}\frac{1}{MeV}$
^{236}U	1.89±0.05	2.415±0.004	0.080±0.008	0.44-6.4	0.143±0.012
^{240}Pu	2.16±0.01	2.875±0.013	0.109±0.02	2.0-7.0	0.158±0.010
^{242}Pu	2.15±0.02	2.929±0.009	0.125±0.004	0.0-5.9	0.143±0.017
^{246}Cm	2.95±0.02	3.82±0.03	0.135±0.007	0.5-9.0	0.146±0.009

Thus it must be concluded that linear extrapolation of the dependence of $\bar{\nu}_p$ from the below-barrier to the above-barrier region of nuclear fission is not legitimate.

Specifically, in the case of fissioning nuclei with a threshold shape of the fission cross-section, extrapolation of the linear dependence $\bar{\nu}_p(E_n)$ obtained in the fast neutron range to thermal neutrons is not appropriate. Near the fission barrier appreciable variations in $\bar{\nu}_p$ may be expected due to specific changes in the fragment distributions by mass and kinetic energy (see Fig. 1).

To evaluate the energy dependence $\bar{\nu}_p(E_n)$ we selected a piecewise-linear description of the experimental data using the least squares method.

All the experimental data used are reduced to a uniform standard - the mean number of prompt neutrons in spontaneous fission of ^{252}Cf: $\bar{\nu}_p$ = 3.757 [4].

2. Neptunium-237

There are four papers devoted to measurements of the energy dependence $\bar{\nu}_p$ (E_n) for ^{237}Np [5-8].

Reference [5] describes measurements involving monoenergetic neutrons. Fission neutrons were recorded using a large (240 L) liquid scintillator with an efficiency of about 70%. Fission events were recorded by means of a spiral fission chamber with a ^{237}Np layer thickness of 1 mg/cm^2. The monoenergetic neutrons were obtained from T(p,n), D(d,n) and T(d,n) reactions in an electrostatic accelerator. The measurement error is estimated at 2-2.5%.

In Ref. [6] the fission neutron detector was an array of 16 ^{3}He counters placed in a polyethylene moderator. Fission events were recorded by an ionization chamber. The measurements were carried out on an electrostatic accelerator operating in continuous mode. Monoenergetic neutrons in the energy range 1-6 MeV were used.

To take into account incomplete recording of fission events, the measurements of $\bar{\nu}_p$ were made with different fissionable layer thicknesses and different ionization chamber designs (flat single-layer and spiral multilayer). The error in the relative measurements was less than 1%.

In Ref. [7] the fission neutron detector was a large liquid scintillator with a volume of 240 L. Fission events were recorded by a multilayer fast ionization chamber containing a total quantity of 100 mg of ^{237}Np in a layer about 1 mg/cm^2 thick. Neutrons were obtained from the T(p,n) reaction on a tandem electrostatic accelerator operating in pulsed mode. Fission events caused by background neutrons were eliminated by the time-of-flight method. The measurement error given by the authors is less than 1%.

In Ref. [8] the neutron source was a uranium target bombarded by 50 MeV electrons. Fission neutrons were detected using a large liquid scintillator with a volume of 400 L containing gadolinium in the solution. The fission neutron recording efficiency was about 65%.

The fission fragments were recorded with a plane-parallel cascade detector. The ^{237}Np sample weighed 3.5 mg. The fission fragment recording efficiency was about 95%.

The energy of the neutrons produced by fission of ^{237}Np nuclei was determined by the time-of-flight method.

Measurements of $\bar{\nu}_p(E_n)$ were performed in the neutron energy range 0.5-12 MeV. The measurement error is estimated at 1-1.5%.

Comparison of the measurement results of Refs [5-8] shows that the results in Refs [5, 6, 8] agree to within the measurement error. The results in Ref. [7] are 2-3% lower than those in Refs [5, 6, 8] in the neutron energy range below 5 MeV.

In the evaluation the statistical weight of the measurement results was chosen according to the errors given by the respective authors.

Figure 3 shows the results from Refs [5-8] and the evaluated function of the energy dependence $\bar{\nu}_p(E_n)$.

Extrapolation to a neutron energy E_n=20 MeV was done by calculation based on averaging the growth rate of $\bar{\nu}_p$ for a wide range of nuclei from ^{232}Th to ^{242m}Am for which evaluated values of this quantity in the neutron energy range 15-20 MeV were available. The mean value of the growth rate of $\bar{\nu}_p$ in this energy range was obtained as 0.11±0.005 MeV^{-1}, where the error was determined as the mean variation of the values of $\frac{d\nu_p}{dE_n}$ for the various nuclei in the energy range mentioned.

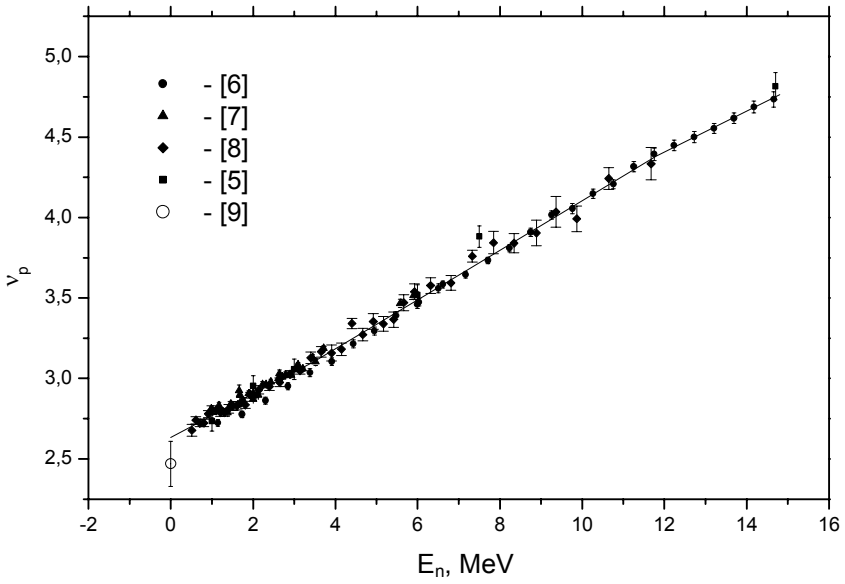

Fig. 3. Energy dependence $\overline{\nu}_p(E_n)$ for ^{237}Np. Solid line - evaluation.

Table 2

Neutron energy, MeV	$\overline{\nu}_p^i$	$\Delta\overline{\nu}_p^i$
0.0	2.633	0.02
3.45	3.100	0.015
6.20	3.519	0.028
11.80	4.382	0.056
14.80	4.763	0.12
20.00	5.335	0.14

Table 2 gives the boundaries selected for the intervals within which the linear description of $\overline{\nu}_p(E_n)$ was used and the corresponding evaluated values of $\overline{\nu}_p^i$.

In Ref. [9] the mean number of prompt neutrons from fission of ^{237}Np by thermal neutrons was measured: $\overline{\nu}_p \approx 2.47\pm0.14$. This value is lower than the evaluated value extrapolated to zero neutron energy. As noted in Section 2, extrapolation of $\overline{\nu}_p(E_n)$ to zero neutron energy for nuclei with a threshold shape of the fission cross-section has no physical meaning, but is only a formal step taken for convenience in calculating the evaluated values of $\overline{\nu}_p(E_n)$.

The low value of $\bar{\nu}_p$=2.47±0.14 agrees qualitatively with the high value of the mean kinetic energy for fission of ^{237}Np by thermal neutrons, E_k=174.7±0.6 MeV, obtained in Ref. [10].

3. Americium-241

Only one paper [8] has been published giving measurement results for the energy dependence $\bar{\nu}_p(E_n)$ in fission of ^{241}Am by fast neutrons. The research was carried out in the neutron energy range 1-11 MeV. The measurement method is described in Section 3. In addition, the value of $\bar{\nu}_p$ in the fission of ^{241}Am by thermal neutrons was measured in Refs [11, 12]. The difference between the results obtained, 3.08±0.025 [11] and 3.216±0.038 [12], exceeds the measurement errors indicated. Reference [12] gives a thorough analysis of the possible errors. Several standards were used for the relative measurements. The problem of superposition of pulses from α-particles and the difference between the fission neutron spectra for ^{241}Am and the standards used were taken into consideration. The authors of this paper also measured $\bar{\nu}_p$ for a number of other isotopes and their results agree with those of other authors to within the measurement errors.

In Ref. [11] the difference between the prompt fission neutron spectra for ^{241}Am and ^{235}U was not considered. The amount of ^{241}Am loaded into the ionization chamber was about 250 μg, which apparently made it necessary to introduce a high level of discrimination owing to superposition of pulses from α-particles and thus led to low fission event recording efficiency.

The paper does not mention the introduction of corrections for this low recording efficiency. Moreover, when the neutron beam is switched on, the recording of false pulses in the fission fragment detector due to superposition of extraneous noise pulses is not ruled out. These problems are not discussed in Ref. [11].

The neglect of all these effects may lead to a reduced measured value of $\bar{\nu}_p$.

Thus we can give preference to the value of $\bar{\nu}_p$ obtained in Ref. [12] for fission of ^{241}Am by thermal neutrons.

In the evaluation of the energy dependence $\bar{\nu}_p(E_n)$ the values of $\bar{\nu}_p$ at thermal neutron energy from Refs [11, 12] were not considered (see Section 2).

Two evaluations of $\bar{\nu}_p(E_n)$ were performed with the boundary points of the intervals set at 0, 6 and 11 MeV and with E_n=0 and 11 MeV. For both cases identical results were obtained. For this reason the second option was selected to simplify the description of the energy dependence $\bar{\nu}_p(E_n)$.

Figure 4 shows the results from Ref. [8] and the evaluated dependence $\bar{\nu}_p(E_n)$ obtained for fission of ^{241}Am by neutrons.

Table 3 gives the boundaries E^i of the intervals of the linear description of $\bar{\nu}_p$ (E_n) and the corresponding values of $\bar{\nu}_p^i$.

The values of $\bar{\nu}_p^i$ at E_n=15 MeV and 20 MeV are calculated as for ^{237}Np.

As in the case of ^{237}Np, extrapolation to zero neutron energy has no physical meaning, and the agreement of the extrapolated values of $\bar{\nu}_p$ with those measured in Ref. [11] must apparently be considered coincidental.

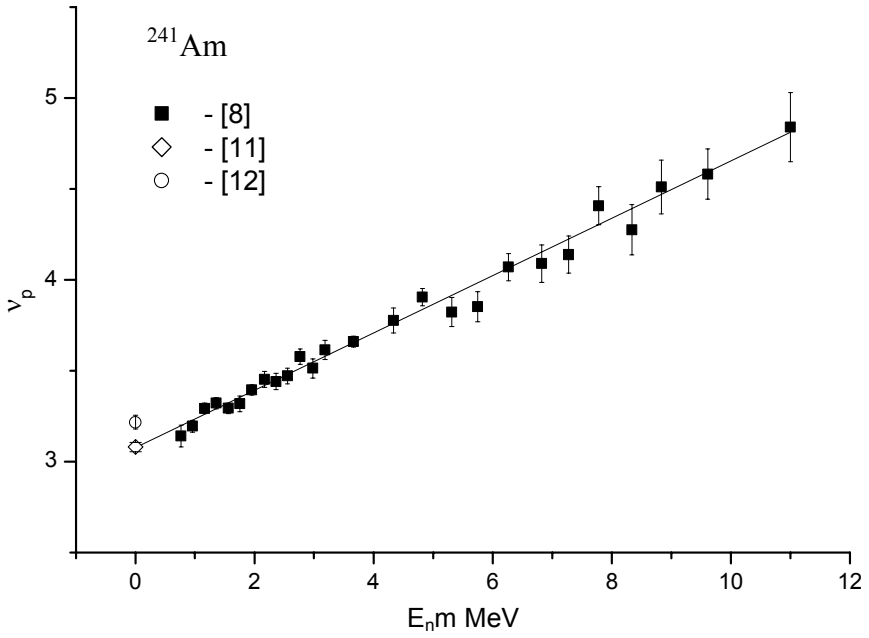

Fig. 4. Energy dependence $\bar{\nu}_p$ (E_n) for ^{241}Am. Solid line - evaluation.

Table 3

E_i, MeV	$\bar{\nu}_p^i$	$\Delta\bar{\nu}_p^i$
0	3.08	0.06
11	4.81	0.19
15	5.34	0.21
20	5.92	0.25

4. Americium-242m

Measurement results on the energy dependence $\bar{\nu}_p(E_n)$ for ^{242m}Am are given in Ref. [13]. Fission fragments were recorded using an ionization chamber with polyspheric electrodes. The amount of fissionable material loaded was about 200 μg. The fission event recording efficiency was about 95%.

The liquid scintillator NE213 was used as a neutron detector.

The neutron source was a 100 MeV linear electron accelerator. The energy of the neutrons produced by fission of nuclei was determined by the time-of-flight method.

The measurements of $\bar{\nu}_p$ for ^{242m}Am were performed relative to $\bar{\nu}_p$ for ^{235}U.

As a result of the measurements, corrections were introduced to account for the experimental geometry, the difference in the fission neutron spectra, etc.

The statistical measurement error was large, increasing from 3% at neutron energies around 0.5-1 MeV to 14% at $E_n \approx 20$ MeV.

In Refs [12, 14, 15] the mean number of prompt neutrons from fission of ^{242m}Am by thermal neutrons was measured. The results in the three papers agree to within the indicated measurement errors: 3.262±0.024 [12], 3.27±0.010 [14] and 3.20±0.12 [15].

The present paper's evaluation of the energy dependence $\bar{\nu}_p(E_n)$ for ^{242m}Am is based on the experimental results in Ref. [13] as well as the values of $\bar{\nu}_p$ for thermal neutrons from Refs [12, 14, 15].

Owing to the large statistical error in the results of Ref. [13], a detailed rendering of $\bar{\nu}_p(E_n)$ did not appear justified, so the energy dependence $\bar{\nu}_p(E_n)$ for the entire reactor neutron energy range from 0 to 20 MeV has been described by a single line.

Figure 5 shows results from Refs [12, 13, 14, 15] and also the evaluated dependence $\bar{\nu}_p(E_n)$.

Table 4 gives evaluated values of $\bar{\nu}_p^i$ at the energy interval boundaries.

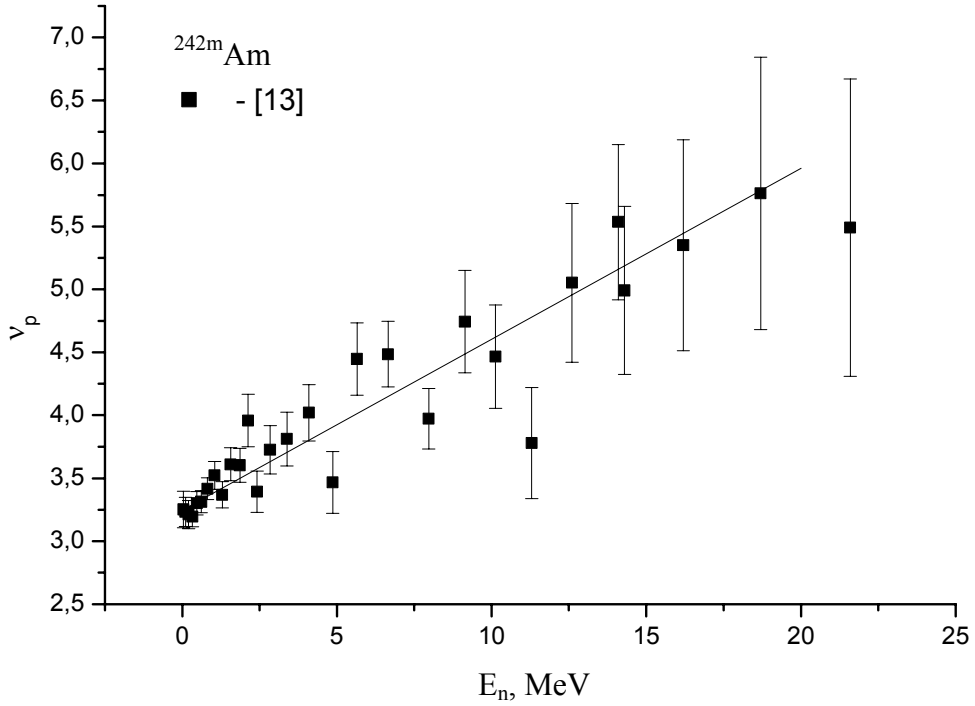

Fig. 5. Energy dependence $\overline{\nu}_p(E_n)$ for ^{242m}Am. Solid line - evaluation.

Table 4

E_n^i, MeV	$\overline{\nu}_p^i$	$\Delta\overline{\nu}_p^i$
0	3.24	0.1
20	5.96	1.1

5. Americium-243

The energy dependence of $\overline{\nu}_p$ in fission of ^{243}Am by neutrons was experimentally studied in Refs [8, 16].

The measurement method used in Ref. [8] is briefly described in Section 3.

The neutron energy range studied was 0.8-11 MeV.

In Ref. [16] measurements were made by the same method as in Ref. [6] (see Section 3) in the energy range 6-12 MeV. In Ref. [17] the mean number of prompt neutrons from fission of ^{243}Am by thermal neutrons was measured.

In evaluating the energy dependence of $\overline{\nu}_p$ for ^{243}Am the neutron energy scale was divided into 4 intervals: 0-6; 6-11; 11-15; 15-20.

In the first two intervals the evaluation was based on the experimental results of Refs [8, 16]. In the third and fourth intervals the evaluated data were calculated as described in Section 3.

The value of $\bar{\nu}_p$ for thermal neutrons was not considered in the evaluation.

Figure 6 shows results from Refs [11, 17] and the evaluated dependence of $\bar{\nu}_p$ on E_n. The agreement of the evaluated value of $\bar{\nu}_p$ for E_n=0 and the measured value of $\bar{\nu}_p$ for ^{243}Am fission by thermal neutrons appears to be coincidental (see Section 2).

Table 5 gives evaluated values of $\bar{\nu}_p^i$ at the boundaries of the corresponding energy intervals.

Conclusion

For the present paper, evaluated data were obtained on the energy dependence of $\bar{\nu}_p$ for ^{237}Np, ^{241}Am, ^{242m}Am and ^{243}Am. In the most important neutron energy range (0-10 MeV) the evaluated values of $\bar{\nu}_p$ are based on available experimental data.

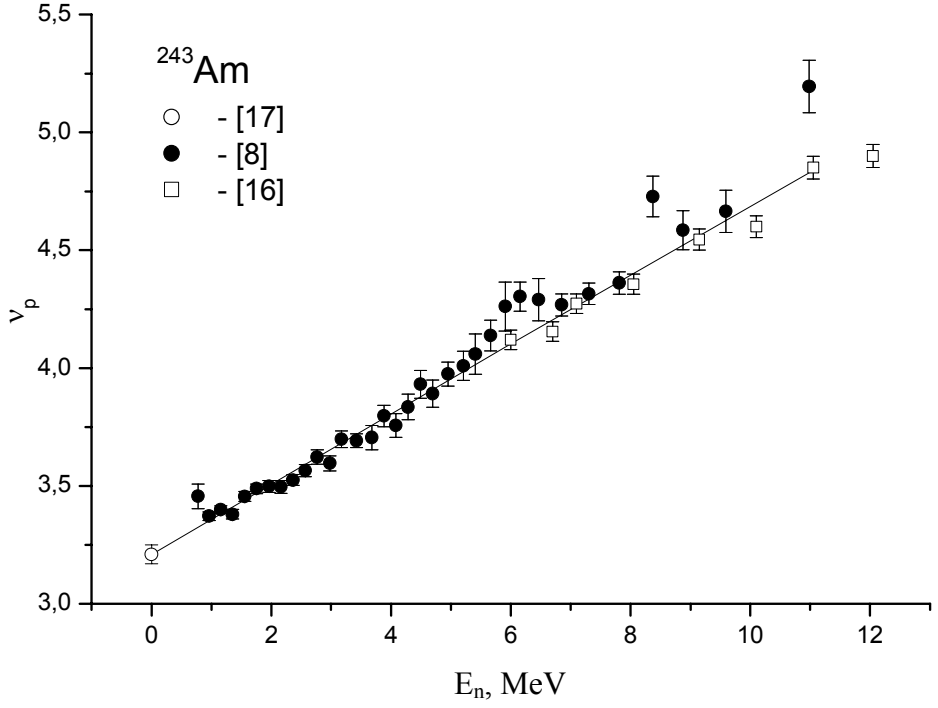

Fig. 6. Energy dependence $\bar{\nu}_p(E_n)$ for ^{243}Am. Solid line - evaluation.

Table 5

E_n^i, MeV	$\bar{\nu}_p^i$	$\Delta\bar{\nu}_p^i$
0	3.21	0.04
6	4.10	0.06
11	4.83	0.12
15	5.36	0.14
20	5.94	0.25

Unfortunately, the results for each of the americium isotopes were obtained, as a rule, by a single method and a single group of researchers. However, analysis of the experimental work done by these groups on other fissionable nuclei shows that the methods used are well designed, and the measurement results agree with data sets obtained by other methods and research groups. Hence there is no reason to expect large hidden methodical errors in the measurements of $\bar{\nu}_p$ for the minor actinides reviewed. In the energy range 15-20 MeV the evaluated data were obtained by calculation from systematics which take into account the growth rate of $\bar{\nu}_p$ for a set of nuclei for which evaluated values of $\bar{\nu}_p$ are known in this energy range.

The errors in the evaluated data on $\bar{\nu}_p(E_n)$ for the minor actinides studied are greater than the corresponding errors for the main fissionable materials, but in view of the role played by the minor actinides in nuclear technology these errors can for the present be considered satisfactory.

The evaluated values of $\bar{\nu}_p$ for ^{237}Np, ^{241}Am, ^{242m}Am and ^{243}Am obtained in this work have been included in the files of evaluated neutron data on these isotopes produced for the updated national library BROND-3.

The work was carried out with the support of the Department of Nuclear Science and Technology of the Russian Federation Ministry of Atomic Energy under contract 6.27.19.19.02/882.

REFERENCES

1. D'yachenko N.P., Kabenin V.N., Kolosov N.P., Kuz'minov B.D., Sergachev A.I., Yadernaya Fizika 17(1973)696.
2. Wagemans C., Schillebeeckx P., Nucl. Phys. A502(1989)287.
3. Handbook "Low Energy Neutron Physics", edited by H. Schopper, publisher Springer. Subvolume A Part I, p.9-145.
4. Nuclear Data Standards for Nuclear Measurements. 1991 NEANDC/INDC Nuclear Standards File. NEANDC-311 «U» INDC(SEC)-101, p.110.
5. Veeser L.R., Phys. Rev. C17(1978)385.
6. Frehaut J., Bois R., Bertin A., Proc. Intern. Conf. on Nuclear Data for Science and Technology, Antwerp, 1982, p.78.
7. Malinovskij V.V., Vorob'eva V.G., Kuz'minov B.D., Piksajkin V.M., Semenova N.N., Solov'ev S.M., Soloshenkov P.S., Atomnaya Ehnergiya 54(1983)208.
8. Khokhlov Yu.A., Ivanin I.A., In'kov V.I., Vinogradov Yu.I., Danilin L.D., Polynov V.N., Proc. Int. Conf. on Nuclear Data for Science and Technology, Gatlinburg, 1994, Vol.1, p.272.
9. Thierens H., Jacobs E., D′Hondt, De Frenne D., De Clercq P., Deruytter A.J., Blachot J., Perrin P., Nucl. Phys. A342(1980)229.
10. Wagenmans C., Allaert E., Caitucoli F., D′Hondt, P., Barreau G., Perrin P., Nucl. Phys. A369(1981)1.
11. Lebedev V.I., Kalashnikov V.I., Atomnaya Ehnergiya 5 (1958)176.
12. Jaffey A.H., Lerner J.L., Nucl. Phys. A145 (1970)1.
13. Howe R.E., Browne J.C., Dougan R.J., Dupzyk R.J., Landrum J.H., Nucl. Sci. Eng. 77 (1981)454.
14. Kroshkin N.I., Zamyatnin Yu.S., Atomnaya Ehnergiya 29 (1970)95.
15. Fultz S.C., Caldwell J.T., Berman B.L., Bramblett R.L., Kelly M.A., Wilson H.D., Coops M.S., Lougheed R.W., Evans J.E., Hoff R.W., Phys. Rev. 152 (1966)1046.
16. Frehaut J., Bertin A., Bois R., in Comptes rendus d′activité du Service de Physique Nucléaire pour l′année 1983. CEA-N-2396, Centre d′Etudes de Bruyeres-le-Chatel, 92-Montroge (France) p.69(1984).
17. Mughabgahab S.F., Neutron Cross Section. Vol.1, Part B, BNL, Academ. Press Inc. (1984). New York, USA.
18. D'yachenko N.P., Kuz'minov B.D., Sergachev A.I., Proc. IX Intern. Symposium on the Interactions of Fast Neutrons with Nuclei, Dresden, 1980, p.97.
19. Conde H., Halmberg M., Arkiv foer Fysik 29 (1965)33.
20. Mather D.S., Fieldhouse P., Moot A., Nucl. Phys. 66 (1965)149.
21. Meadows J.W., Whalen J.F., Rep. WASH-1033(1961)2.
22. Prokhorova L.I., Smirenkin G.N., Yadernaya Fizika 7 (1968)961.

UDC 539.172

NEW TECHNIQUE FOR A SIMULTANEOUS ESTIMATION OF THE LEVEL DENSITY AND RADIATIVE STRENGTH FUNCTIONS OF DIPOLE TRANSITIONS AT $E_{ex} \leq B_n$ -0.5 MeV

V.A. Khitrov, A.M. Sukhovoj
Frank Laboratory of Neutron Physics, Joint Institute for Nuclear Research, 141980 Dubna, Russia

The new, model-independent method to estimate simultaneously the level densities excited in the (n,γ) reaction and the radiative strength functions of dipole transitions is developed. The method can be applied for any nucleus and reaction followed by cascade γ-emission. It is just necessary to measure the intensities of two-step γ-cascades depopulating one or several high-excited states and determine the quanta ordering in the main portion of the observed cascades. The method provides a sufficiently narrow interval of most probable densities of levels with given J^{π} and radiative strength functions of dipole transitions populating them.

1 Introduction

The observed parameters of the cascade γ-decay of the compound nucleus can be reproduced in the calculation if one determines (in the frameworks of some model) at least

(a) the mean density ρ of the excited states with given spin and parity J^{π}, and

(b) the mean width $\Gamma_{\lambda i}$ of γ-transitions between the arbitrary states λ and i.

The objects of primary interest are the total radiative width Γ_{γ} of the compound nucleus (neutron resonance) and the spectrum of γ-emission. It may be, for example, the intensity $I_{\gamma\gamma}$ of the cascades of two successive γ-transitions between the compound state and given low-lying level via a great number of intermediate levels. The experimental data on $I_{\gamma\gamma}$ (as a function of the energy of their intermediate level) are obtained for over 30 nuclei from the mass region $114 \leq A \leq 200$ (see, e.g., [1] with a precision of approximately 10\%. The experimental values of Γ_{γ} are known within the same accuracy. Unfortunately, such accuracy cannot be achieved in the calculation of these parameters for an arbitrary nucleus because there are no models that would predict ρ and $\Gamma_{\lambda i}$ with the mentioned above precision.

This is seen from the data of Table 1 which represent the mean ratio between the experimental cascade intensities $I_{\gamma\gamma}^{exp}$ and those calculated $I_{\gamma\gamma}^{cal}$ using the known enough models of level density [2,3] and radiative strength functions [4,5].

Table1.

The ratio $R = I_{\gamma\gamma}^{exp} / I_{\gamma\gamma}^{cal}$ averaged over 30 nuclei

Models:	[2,4]	[2,5]	[3,4]	[3,5]
R	2.2(2)	2.7(2)	1.5(1)	1.7(1)

Precise γ-decay parameters are, however, necessary for the calculation of the interaction cross-sections of neutrons with unstudied target nuclei and the understanding of the behavior of nuclear matter with increasing excitation energy. An analysis of the existing methods for the determination of the level density [6,7] and radiative strength functions (k) [8]

$$k = \Gamma_{\lambda i}/(E_{\gamma}^{3} \times A^{2/3} \times D_{\lambda}) \quad (1)$$

in deformed nuclei, for example, shows that it is not possible to obtain sufficiently precise experimental level densities for certain intervals of their energies and quantum numbers as well as the widths of the corresponding transitions. Analysis of contributions of different sources of systematical errors in determination of the level density from the evaporation spectra was performed by H.Vonach [9] mainly for light spherical nuclei. The total uncertainty evaluated by him amounts to about 20-30%. It should be noted, however, that an accuracy in calculation of cascade intensities within the models [2-5] in the lightest nuclei (from the range of the minimum of the neutron strength function) studied by us is also considerably better than that for deformed nuclei: the ratio R for ^{114}Cd and ^{124,125}Te varies in limits from 0.7 (^{124}Te) up to 1.4 (^{114}Cd).

Therefore, without developing new methods for the determination of nuclear parameters under discussion one cannot expect any progress in the modification of the existing theoretical models, first of all, for deformed nuclei. (In eq. (1) $\Gamma_{\lambda i}$ is the partial radiative width of γ-transition with the energy E_{γ}, D_{λ} is the average level spacing of the decaying state and quantity A is the nucleon number).

A new and sufficiently perspective way to obtain such information for the entire energy interval below B_n seems to be the investigation [10,11] of the two-step γ-cascades between the compound state λ and the given low-lying level f through all possible intermediate states i. The algorithms [10,11] developed for the analysis of γ-γ coincidences registered by ordinary Ge detectors allow one to determine the intensity distribution of the cascades as a function of the

energy of the cascade intermediate levels over the whole energy region up to $E_{ex} \approx B_n$ with an acceptable systematic error (which decreases as the efficiency of the γ-spectrometer increases).

The intensity $i_{\gamma\gamma}$ of an individual cascade is

$$i_{\gamma\gamma} = \Gamma_{\lambda i}/\Gamma_\lambda \times \Gamma_{if}/\Gamma_i \qquad (2)$$

where $\Gamma_{\lambda i}$ and Γ_{if} are the partial widths of the transitions connecting the levels $\lambda \to i \to f$; Γ_λ and Γ_i are the total widths of the decaying states λ and i, respectively. The sum intensity $I_{\gamma\gamma}$ of the cascades is related to an unknown number of intermediate levels $n_{\lambda i} = \rho \times \Delta E$ and unknown widths of primary and secondary transitions via the equation

$$I_{\gamma\gamma} = \sum_{j,\pi} (\Gamma_{\lambda i}/\langle\Gamma_{\lambda i}\rangle \times m_{\lambda i}) \times n_{\lambda i} \times (\Gamma_{if}/\langle\Gamma_{if}\rangle \times m_{if}). \qquad (3)$$

The summation is over a certain set of quantum numbers of intermediate, initial, and final states for the purpose of comparison with the experimental data. The thermal neutron capture cross-section for two possible spins of compound states are listed in [15], for example. The J^π values for the initial and final cascade levels are also known. The latter, however, is true if the energy E_f of the final state does not exceed ≈1 MeV. The optimal width of the interval ΔE and the number N of such intervals in eq. (3) are determined by the statistics of γ-γ coincidences (as a square detector efficiency) and the necessity to obtain detailed energy dependence for $I_{\gamma\gamma}$. The width of ΔE does not exceed 0.5 MeV even in the case of a 10% efficiency detector, however. The total radiative widths Γ_λ of the capturing states are also known from the corresponding experiments for all stable nuclei [15]. The mean partial widths $\langle\Gamma_{\lambda i}\rangle$, $\langle\Gamma_{if}\rangle$ and the total numbers $m_{\lambda i}$, m_{if} of levels excited by E1 and M1 transitions after the decay of the states λ and i, respectively, to be found in the analysis are related to the total radiative widths as

$$\Gamma_\lambda = \langle\Gamma_{\lambda i}\rangle \times m_{\lambda i}$$
$$\Gamma_i = \langle\Gamma_{if}\rangle \times m_{if} \qquad (4)$$

The contribution of higher multipolarities to eqs. (3) and (4}) is smaller than the error of the determination of $I_{\gamma\gamma}$. Equations (3) and (4) and their obvious combination

$$\Gamma_\lambda \times I_{\gamma\gamma} = \Sigma\, \Gamma_{\lambda i} \times n_i \times (\Gamma_{if}/\langle\Gamma_{if}\rangle m_{if}) \qquad (5)$$

allow three ways of the estimation of the parameters of the cascade γ-decay using the experimental data on $I_{\gamma\gamma}$ and Γ_λ:

(a) the level density can be estimated from eq. (3) using model calculated partial radiative widths;

(b) the partial widths of cascade transitions can be estimated from eq. (5) using model calculated level densities with certain J^π;

(c) simultaneous estimation of the intervals of probable level densities and radiative strength functions which satisfy eqs. (3) and (4) in general.

It is clear that the level density and strength functions found according to variants (a) and (b) inevitably contain errors caused by the uncertainties of experimental and model values used as parameters of the analysis. However, the influence of these uncertainties on the final result is suppressed because of the correlation (determinated by the used type of the functional relations (3) and (5)) between the experimental Γ_λ^{exp}, $I_{\gamma\gamma}^{exp}$ and the parameters under study ρ, Γ .

In accordance with the variant (a) the sufficiently narrow interval of probable ρ was determined for almost 30 nuclei from the mass region 114≤A≤200 for some set of possible models of γ-transition strength functions. An important conclusion made in [16] is that the best description of the level density in the interval from ≈0.5B_n to B_n was achieved in the framework of the generalized model of the superfluid nucleus [3]. Besides, simple enough models [4,5] of radiative strength functions cannot provide a correct description of the experiment and also need modification. An analysis by variant (b) was performed by us, as well. The main result is that there are no strength function models for E1 and M1 transitions in deformed nuclei which could reproduce the dependence $\Gamma_\lambda \times I_{\gamma\gamma}$ at primary transition energies E_1≤2-3 MeV if the level density is set by the model of a non-interacting Fermi-gas. Wherefore, the understanding and correct description of the γ-decay of the compound nucleus with a high level density require experimental determination of the level density and radiative strength functions over the entire excitation energy region.

Further investigations [17] have shown that the level density at excitations from 1-2 to 3-4 MeV in, first of all, deformed nuclei deviates strongly from the exponential energy dependence derived on the basis of the idea that the nucleus is a non-interacting Fermi-gas [2]. Moreover, it is not excluded that the level density in this energy interval can be almost constant or even decrease with increasing excitation energy. These confirm and complement the results obtained in [16].

2 Analysis

The variant (c) of analysis of the experimental intensities of two-step γ-cascades between the capturing state and several low-lying levels allowed us to suggest an original method for the solution (although partial) of this problem. It is based on an obvious circumstance that N+1 equations (3) and (4) together with 6N conditions

$$\rho(\pi = +) > 0; \quad \rho(\pi = -) > 0$$
$$\Gamma(E1) > 0; \Gamma(M1) > 0 \qquad (6)$$

(separately for primary and secondary transitions in the case of radiative widths) restrict some interval of possible level densities and partial radiative widths which provide a simultaneous reproduction of Γ_λ^{exp} and $I_{\gamma\gamma}^{exp}$. This interval can be estimated using modern computers and the existing computational algorithms. Its width, however, cannot equal zero even at zero uncertainty of the experiment. It should be added that $I_{\gamma\gamma}$ in the form of eq. (3) is inversely proportional (qualitatively) to the total number of states excited in the process under study and is proportional to the ratio of cascade transition widths to their mean values. Therefore, the method of analysis described below has a maximum sensitivity at minimum density of the excited states (unlike the methods [6,7].

As in the case of other reactions (followed by γ-emission) used for the determination of ρ, all values obtained experimentally in the (n_{th},γ) measurements are determined by the product $\Gamma_{\lambda i} \times \rho$. Hence, in the calculation deviation of one of the two parameters from its mean value is compensated by deviation of the other one with the corresponding magnitude and sign. This circumstance should be taken into account in data processing --- a minimum or maximum value of the level density derived from the experimental data results, e.g., in a maximum or minimum value of the corresponding strength functions.

It should be noted that deviation of the calculated level density from the true value is completely compensated by deviation of strength functions when Γ_λ is only calculated. In the case of the calculation of $I_{\gamma\gamma}$ the compensation is incomplete. This very circumstance allows one to select the intervals of ρ and $\Gamma_{\lambda i}$ which provide the description of the $I_{\gamma\gamma}$ and Γ_λ parameters with an acceptable uncertainty. This analysis can be performed by means of finding large enough sets of random values of ρ and $\Gamma_{\lambda i}$ which reproduce completely the parameters Γ_λ^{exp} and $I_{\gamma\gamma}^{exp}$ and belong to the intervals that contain true values. This means that most probable values of the level density and radiative strength functions of dipole γ-transitions and intervals of their uncertainties can be found by selection of pairs of random ρ and k which obey, in general, eqs. (3) and (4) or (3) and (5). This requires numerous repetitions of the procedure and statistical methods of analysis.

It is clear that the widths of the intervals of probable ρ and k satisfying eqs. (3) and (4) increase with increasing number of unknown parameters in the equations. According to experimental conditions, the summation in eqs. (3) and (5) as over all intermediate states of the cascades. Since the summed data included cascade transitions of different multipolarities, we could not obtain the strength functions of E1 and M1 transitions and the level density for different parities separately with a good precision. In practice, from a combination of eqs. (3) and (5) the sum of strength functions and the sum of level densities of both parities should be only derived and compared with model predictions. The corresponding summation reduces considerably the uncertainty of the observed result due to anti-correlation of elements.

Indeed, an analysis of the available data confirms that the dispersion of each set of ρ(π=+), ρ(π=-), k(E1) and k(M1) random values is too large to make any conclusions about independent correspondence of individual values to the model.

A sufficiently large N and the nonlinearity of eqs. (3) and (4) stipulate the choice of the way to solve the system of equations and inequalities - the Monte Carlo method. The simplest iterative algorithm [16] was used for this aim: we set some initial values for Γ(E1), Γ(M1), ρ(π=-), and ρ(π=+) and then distort them by means of random functions. If these distortions decrease the parameters $\Delta=(I_{\gamma\gamma}^{exp} - I_{\gamma\gamma}^{cal})^2$ at this step of the iteration procedure, then the distorted values are used as initial parameters for the next iteration. Agreement between the experimental and calculated cascade intensities and the total radiative widths, respectively, is usually achieved after several thousand iterations. As a result we get two random ensembles of level densities and partial widths for every N energy intervals. Examples of intermediate and final results of one of many variants of the calculation for two nuclei are shown in Figs. 1 and 2. It is obvious that such iterative process can be realized in an unlimited number of ways. We chose a sufficiently simple and effective way: the Gaussian curve is used as a distorting function for logarithms of ρ and f

$$f(E)=A \times \exp(-(E - E_0)^2/\sigma^2) \qquad (7)$$

Its parameters are independently chosen for the level density and strength functions from the intervals [-0.2;0.2], $[E_d;B_n]$ and [0.3 MeV;B_n] for A, E_0, and σ, respectively using a standardized random value distributed uniformly in [0;1]. Here E_d is the maximum excitation energy of the known discrete level involved in the calculation. Numerous repetitions of the iterative calculation with different initial parameters (including obviously unreal values of Γ and ρ for ≈30 nuclei from the mass region $114 \le A \le 200$ show that this algorithm yields rather narrow intervals of the sum level density of both parities and of the sum partial widths of E1 and M1 transitions. The use of eq. (7) with mentioned parameters allows one to get a set of different, smooth enough functional dependence for both ρ and k. In this case for the majority of the studied nuclei the values of level density are in good agreement with the number of the observed intermediate levels of the cascades resolved as the pairs of peaks. In some nuclei, however, the mean level density (which together with the mean strength functions provides reproduction of cascade intensities) is less than the number of intermediate levels

observed below ≈ 2 MeV. The main portion of this discrepancy is removed in all cases if one foresees a possibility of additional local variation of k for high-energy transitions in the energy interval which, as a rule, does not exceed 0.1-0.2 MeV. One of the examples of this kind is shown in Fig. 1. The necessity to account this effect can be due to both insufficient averaging of the random partial widths of primary transitions and their possible dependence on the structure of the excited low-lying level. This can result, for instance, from concentration of the strength of the fragmented single-particle or phonon states.

3 Asymptotical uncertainty of the obtained parameters

The method suggested by us for estimation of ρ and k cannot give unique value of these parameters at a given energy of the excitation or quantum energy. Therefore the question arises about the value of their uncertainty at different energies and degree of possible systematical deviations of the observed parameters from the modal values. The results of modelling for ^{156}Gd and ^{198}Au shown in Fig. 3 answer these questions. Intensity of cascades for these nuclei were calculated under assumption that the strength function k(E1) is described by model [4] and value of k(M1)=const; level density exponentially increases with the energy or have some step-like structure. Below the excitation energy ≈ 1-2 MeV the calculation used experimental decay scheme. Consequently, the calculated intensity distribution of cascades in function of the primary transition energy has one or two maxima. (Other conditions of the calculation completely corresponded to the experiment).

Figure 3(b) shows that the model level density is reproduced practically without systematical error and the width of the interval of its probable values does not exceed 20-30%.

Discrepancy between the experimental and model sum k(E1)+k(M1) results from that the total radiative width calculated according model [4] does not correspond to the experimental value. Energy dependence of k(E1)+k(M1) is reproduce rather well – sharp changes in the first derivative with respect to the quantum energy is not observed (unlike some other nuclei studied by us). So, one can summarize that the suggested method provides reliable enough estimation of the level density and radiative strength functions of dipole transitions.

4 Approach used in calculation

The insufficient experimental data on cascade γ-transitions (only cascades terminating at low-lying levels (E_f<1 MeV) of nuclei were studied [1] does not allow us to determine the level densities and gamma-widths without the following important assumption: the strength functions of transitions of a given multipolarity only depend on the transition energy and do not depend on the structure and energy of the corresponding excited states. Their nonequal values for γ-transitions of equal energies but populating different levels is, in part, compensated by the circumstance that the left part of eq. (5) depends on absolute radiative strength function values of primary transitions and depend only on the ratio of strength functions in the case of secondary transitions. These decrease the effect of the discussed assumption on the k(E1)+k(M1) values but do not remove it completely. There is no necessity in introduction of any hypotheses of spin dependence of level density differing from that predicted in models [2,3].

5 Sources of errors in the determination of strength functions and level densities

The presence of the statistic and systematic errors in determination of $I_{\gamma\gamma}$, Γ_λ and specific problems of extraction of level density and radiative strength functions cause noticeable uncertainties of the determined parameters. The influence of the different sources of errors on the obtained results manifest itself in a different degree.

1. Uncertainties of the measuring of terms in eqs. (3) and (5 result in errors of strength functions and level density. Owing to a linear relation between Γ_λ, $I_{\gamma\gamma}$ and $\Gamma_{\lambda i}$ in eq. (5), ≈10% errors of Γ_λ and $I_{\gamma\gamma}$ achieved in the experiment cause rather a small error in the determination of $\Gamma_{\lambda i}$ and ρ as compared to dispersion of the obtained data.

2. The more considerable source of uncertainty in the determination of the strength functions and ρ is a systematic error of decomposition [13,14] of the experimental spectra into two components corresponding to solely primary and solely secondary transitions. The analysis [17] showed that the error in $\Delta I_{\gamma\gamma}$ caused by this procedure does not usually exceed ≈ 20% for primary transition energy E_1<3-4 MeV. Intensities of cascades (histograms in Figs. 1, 2, 4-13) at these primary transition energies can be overestimated, as a maximum, by the above value. At the higher energies they can be decreased by the same value (the total intensity is preserved). In order to estimate the influence of $\Delta I_{\gamma\gamma}$ on the final results, the $I_{\gamma\gamma}$ values were varied within a level of 25%. These variations caused changes in k(E1)+k(M1) and ρ which did not exceed the dispersion of the data plotted in Figs. 4-13.

3. The maximum uncertainty of level density and radiative strength functions results from the use of condition (6). It dominates at any possible precision in determination of $I_{\gamma\gamma}$ and Γ_λ. The simplest way to estimate these errors at any E_1 and E_{ex} is the following:

(a) taking into account that the probabilities of deviations with opposite sign of the random ρ_i and k_i values with respect to their mean values are equal and decrease as the absolute values of deviations increase; and

(b) assuming that mathematical expectations of the random ensembles of the ρ_i and k_i values satisfying eqs. (3)-(5) correspond to their real values one can consider the mean-square deviations of the random values relative to their arithmetical means as the estimations of the errors. These errors can be attributed to level density and strength functions separately in spite of their strong anti-correlation. Just these uncertainties are shown for the radiative strength functions and level density plotted in Figs.4-13.

On the whole we can summarize the situation as the following. At the presently achieved accuracy for experimental determination of $I_{\gamma\gamma}$ and Γ_λ, level densities and strength functions are derived from eqs. (3)-(5) with the mean total uncertainties of about 40-50% in the worst case. Asymptotic value of this uncertainty at zero statistic and systematic errors of the experiment is equal, in the average, for both ρ and k and cannot be less than $\approx 20\%$.

4. There are two ways to decrease the errors of the level density and strength functions determined from eqs. (3)-(5):

(a) the increase of the volume of the experimental data on the cascade intensities;

(b) the reduction of the number of parameters in eqs. (3)-(5) owing to the use of additional information or introduction of some new assumptions.

In the first case the problem can be easily solved experimentally: the use of a Compton-suppressing spectrometer consisting of HPGe detectors with an efficiency of not less than 30-40% allows the selection from a mass of γ-γ coincidences of two-step cascades for a considerably larger number of their final levels than at present. From a combination of eq. (3) for the sum over all final levels of cascades and an individual final level k one can determine the ratio $\Gamma_{if}/\langle\Gamma_{if}\rangle \times m_{if}$ for all possible values of i and f, i. e., determine energy dependence of the experimental sum k(E1)+k(M1) for any possible secondary transitions, get rid of the only approach used in the analysis, and reduce the number of parameters in the analysis.

The data shown in Figs. 4-13 were obtained under assumption about a constancy of the ratio

$$\Gamma_{\lambda i}/\Gamma_{if} = \text{const} \qquad (8)$$

for the transitions with equal multipolarity and energy E_1 in all interval of the neutron binding energy.

The comparison of the total γ-spectra and population of low-lying levels calculated in this way with the available experimental data including spectroscopic information [1] shows that even such assumption provides better accuracy in calculating the parameters of cascade γ-decay than the approach using the models [2-5]. Unfortunately, we could not achieve complete correspondence between the estimated level density and available spectroscopic information. Nevertheless, the obtained values demonstrate certain correspondence of our level density with the numbers of the excited levels observed in the experiment [1]. Some nuclei, however, demonstrate residual discrepancy (for example, ^{170}Tm, Fig. 1). This discrepancy can be attributed, partially, to both insufficient precision of assumption (8) and inexactitude of the spectroscopic data. Their errors can be also considerably decreased using more efficient spectrometer of γ-γ coincidences than that used by authors [1].

On the whole, in spite of the uncertainties mentioned above one can conclude that at a given stage of the experimental investigation of the cascade γ-decay of compound states our method provides more reliable results than methods [6-8].

6 Main results of analysis

The type of relation between k and ρ on the one hand and between Γ_λ and $I_{\gamma\gamma}$ on the other hand does not allow one to determine k and ρ unambiguously and independently. Some deviation of, for example, ρ from a real value is inevitably compensated by deviation of strength functions of the corresponding magnitude and sign. Nevertheless, the results obtained in the present analysis can be used for the verification of nuclear models and, if necessary, for the determination of the direction of the further development of these models. The main argument in favour of this statement is relatively week dependence of the final results on the initial values of strength functions and ρ in the iterative process. As an example, Figs. 1 and 2 show the strength function and ρ values obtained for their unreal initial values: $\rho(E_{ex})=\rho(B_n)$, the strength functions decrease linearly as the transition energy increases. Nevertheless, the final results of the iterative process quite agree with a general picture obtained for a large enough set of different real and unreal initial values of k and ρ. This confirms the conclusion that the strength functions and level density obtained from the analysis can be considered as most probable.

The strength functions k(E1)+k(M1) and level densities ρ obtained in the present analysis are plotted in Figs. 4-13. For every set of random ρ at a given excitation energy E_{ex} and k(E1)+k(M1) at a given primary transition energy $E_1=B_n-E_{ex}$ there were determined both their mean values and probable dispersion using usual relationships of statistical mathematics. The results of the analysis are compared with predictions of the level density models [2,3] and models of radiative widths [4,5]. In the case of radiative strength functions a comparison is performed in the following manner: the k(E1) values calculated according to the models [4] and [5] (upper and lower curves, respectively) are summed with

k(M1)=const which is normalized so that the ratio $\Gamma(M1)/\Gamma(E1)$ would be approximately equal to the experimental data at $E_\gamma \approx B_n$.

A comparison of the results of the analysis with predictions of the models [2-5] (often used by experimentalists) shows that:

(a) k(E1)+k(M1) and ρ are not monotonic functions of the energy and, probably, reflect the most common peculiarities of the structures of the states connected by the corresponding γ-transitions;

(b) the energy dependence of k(E1)+k(M1) differs strongly from predictions of the models [4,5] in the case of even-even compound nuclei from the region of the 4s-resonance of the neutron strength function, at least;

(c) the k(E1)+k(M1) functions increase from near-magic to deformed nuclei and from complicated highly-excited states to simpler low-lying levels which are populated by γ-transitions under consideration;

(d) relative deviations of the obtained strength functions and level densities from the mean values are characterized by strong negative correlation. In the majority of nuclei the correlation coefficient changes from -0.6 to -1.0. This means that the strength functions and level densities are not independent variables in eqs. (3) and (5), which provides the possibility of their simultaneous determination;

(e) the probable level density determined in the present analysis conforms to the picture obtained in previous experiments [16,17]: up to the excitation energy 1-2 MeV, our data are not in contradiction with the exponential extrapolation of $\rho(E_{ex})$ predicted by the Fermi-gas back-shift model [2]. The energy dependence of the level density in the interval from 1-2 to some threshold value E_b is considerably weaker than it follows from any existing level density model. Above $E_b \approx 3$ MeV for N-odd and ≈ 4 MeV for N-even nuclei, the level density, most probably, corresponds better to the predictions of the generalized model of the superfluid nucleus in its simplest form [3].

This change in the behavior of the level density in the vicinity of the excitation energy E_b may signify a qualitative change in the nuclear properties. The observation [18] of the probable harmonicity of the excitation spectra of the intermediate levels of the most intense cascades in a large group of nuclei from the mass region $114 \le A \le 200$ allows an assumption that the nuclear properties at low energy are mainly determined by vibrational excitations (probably, a few phonons of rather high energy). A very quick exponential increase in the level density above E_b says about the probable dominant influence of the inner, many-quasiparticle type of excitations of these states.

7 Discussion

The method suggested in present work allows model independent, simultaneous estimation of intervals of probable values of the level densities with given spins and summed strength functions of primary dipole transitions populating them. The method is effective in investigations of any stable nucleus. The main differences of this algorithm from the known methods of determination of level densities [6,7,9] and radiative strength functions [8] are the following:

1. Our method does not permit one to get the sole values of ρ and k for a given energy. But the width of the intervals of their probable magnitudes depends very weakly on the uncertainty in determination of Γ_λ and $I_{\gamma\gamma}$ at the achieved precision of the experiment, at the one hand, and is narrow enough in order to get new information on nuclear matter, from the other hand.

2. The most correct and reliable data on the level density is derived from the evaporation spectra at the highest excitation energies; analysis of the cascade intensities provides similar data for the lowest energies. So, both methods mutually add each other.

3. Analysis of cascade intensities allows direct determination of the absolute level densities, evaporation spectra usually provide [6,7] information on nuclear temperature.

4. Systematical uncertainties of both methods do not relate. Discrepancies in the independently determined level densities at some energies indicate to necessity, for example, to determine more precisely the barrier transmission factor for the evaporated particle or to take into account different energy dependence of k of the primary and secondary transitions of the γ-cascades. Besides, they can testify to necessity to describe more correctly direct and pre-equilibrium processes in nuclear reactions for deformed nuclei or to define more precisely the nuclear excitation energy above which thermodynamical parameters of a nucleus are determined mainly by quasiparticle excitations.

5. Energy dependence of the data in Figs. 4-13 can be reproduced well enough in the framework of modern version of the generalized model of the superfluid nucleus [19] if the temperature of the phase transition is diminished up to the value $T'_{cr} \approx 0.7 T_{cr}$, where

$$T_{cr} = \delta/1.76 \qquad (9)$$

is the temperature of the transition from the superfluid to normal phase of homogeneous Fermi-system [20]. But re-determination of the entropy and temperature predicted by model [19] should be done so that nuclear temperature below T'_{cr} will not increase with decreasing excitation energy.

6. Additional and independent arguments in favor of reliability of step-like structure in level density are:

(a) combinatorical calculation [21] of density of the states with $K^\pi = 1/2+$ in ^{165}Dy below B_n, providing similar to Figs. 4-13 picture;

(b) analysis [22] of the experimental data from the reaction ^{165}Ho(p,n)^{165}Er. This also demonstrates some step-like structure in the total level density at low excitations;

(c) precise analysis [23] of the neutron cross sections for actinides testify to necessity to take into account the influence of the pairing interaction on the level density for the wide interval of the neutron energies manifesting itself, in particular, as irregularities in the energy dependence of the level density.

7. It is obvious that the structures shown in Figs.4-13 can be inherent not to the total level density with given J^{π}, but only to that part of them which are really excited in (n,γ) reaction.

Then, unlike the existing notions, this reaction is selective and structures of the excited states must be taken into account in any calculations of parameters of this reaction in the entire excitation energy region below B_n.

8 Conclusions

A new method is suggested for a simultaneous estimation of the probable level density populated by dipole primary transitions in the (n_{th},γ) reaction and the sum strength functions k(E1)+k(M1) of these transitions. Unlike other methods used for the investigations of nuclear properties below the excitation energy 6-9 MeV, this method allows the estimation of ρ, radiative strength functions, and intervals of their probable variations without any model notions of the nucleus.

The method is universal - it can be used for any nucleus and reaction with γ-emission. The latter is possible if the excitation energy interval of high-lying states is narrow enough in order to use the sum coincidence technique. Besides, the most probable quanta ordering in the cascades must be determined for the main part of the observed cascade intensity. It should be noted, that in the case of a lack of the experimental values of the total radiative widths of decaying high-lying states the absolute radiative strength functions cannot be determined. In this case only relative energy dependence of the radiative strength functions can be obtained.

The most important (although preliminary and qualitative) physical result is that the level density below the neutron binding energy (first of all in deformed nuclei) cannot be reproduced to a precision achieved in the experiment without more precise than in [19] accounting for the co-existence and interaction of superfluid and usual phases of nuclear matter in this whole excitation energy interval.

The obtained results demonstrate very serious and obvious discrepancies with the existing ideas of the structure of the deformed nuclei. These data agree completely with an earlier obtained qualitative picture [18] of the studied process: considerable influence of vibrational excitations on the nuclear properties below the excitation energy E_b and a transition to dominant influence of quasiparticle excitations above this energy.

This work was supported by RFBR Grant No. 99-02-17863

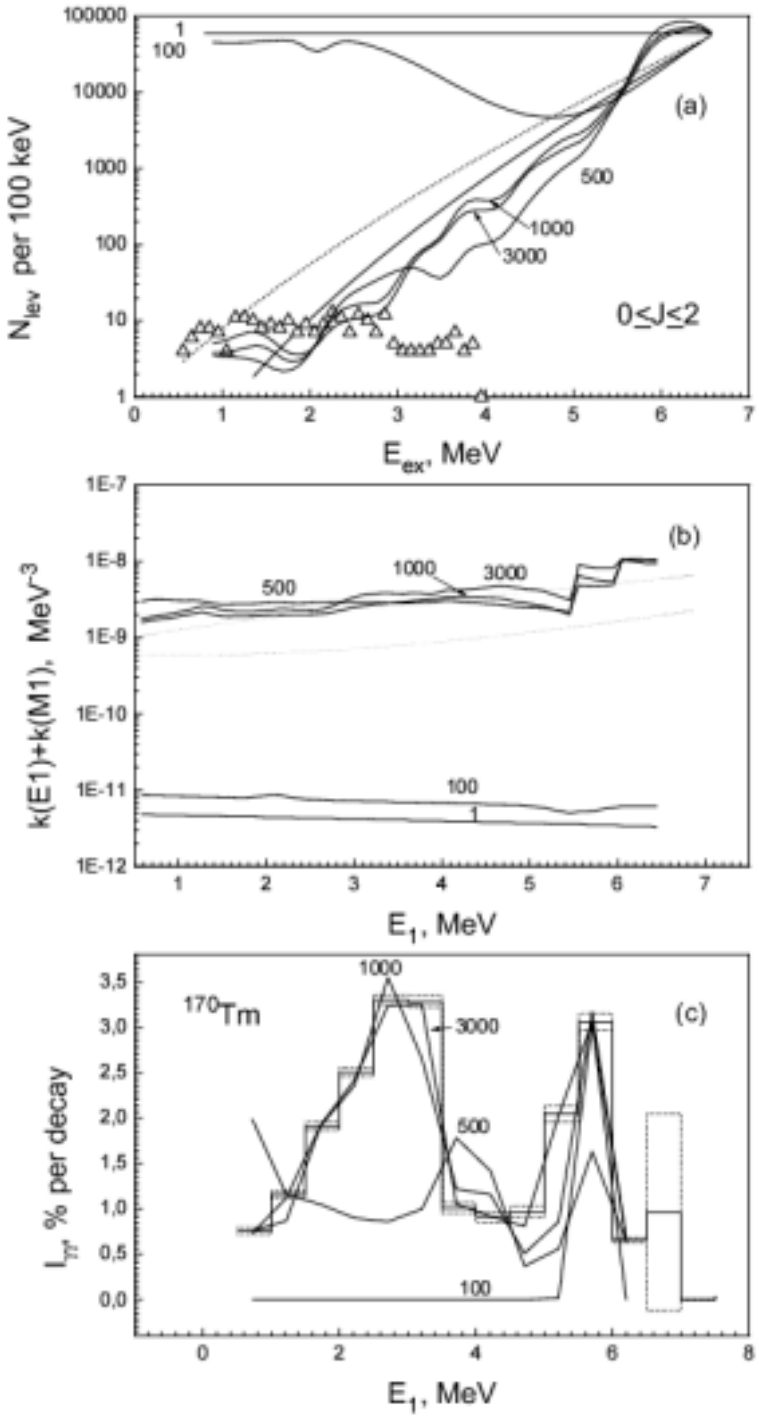

Fig. 1. The examples of ρ (a) and k (b) intermediate values and the corresponding distributions of cascade intensities (c) for the ^{170}Tm odd-odd nucleus in function of the primary transition energy E_1 or excitation energy E_{ex}. Letters next to the lines mean the number of iterations. Triangles show number of levels excited by the primary dipole transitions with the energy E_1 in the energy interval of 100 keV. The dashed curve (a), (b) represents model predictions, the histograms (c) represent the experimental cascade intensities with statistical errors.

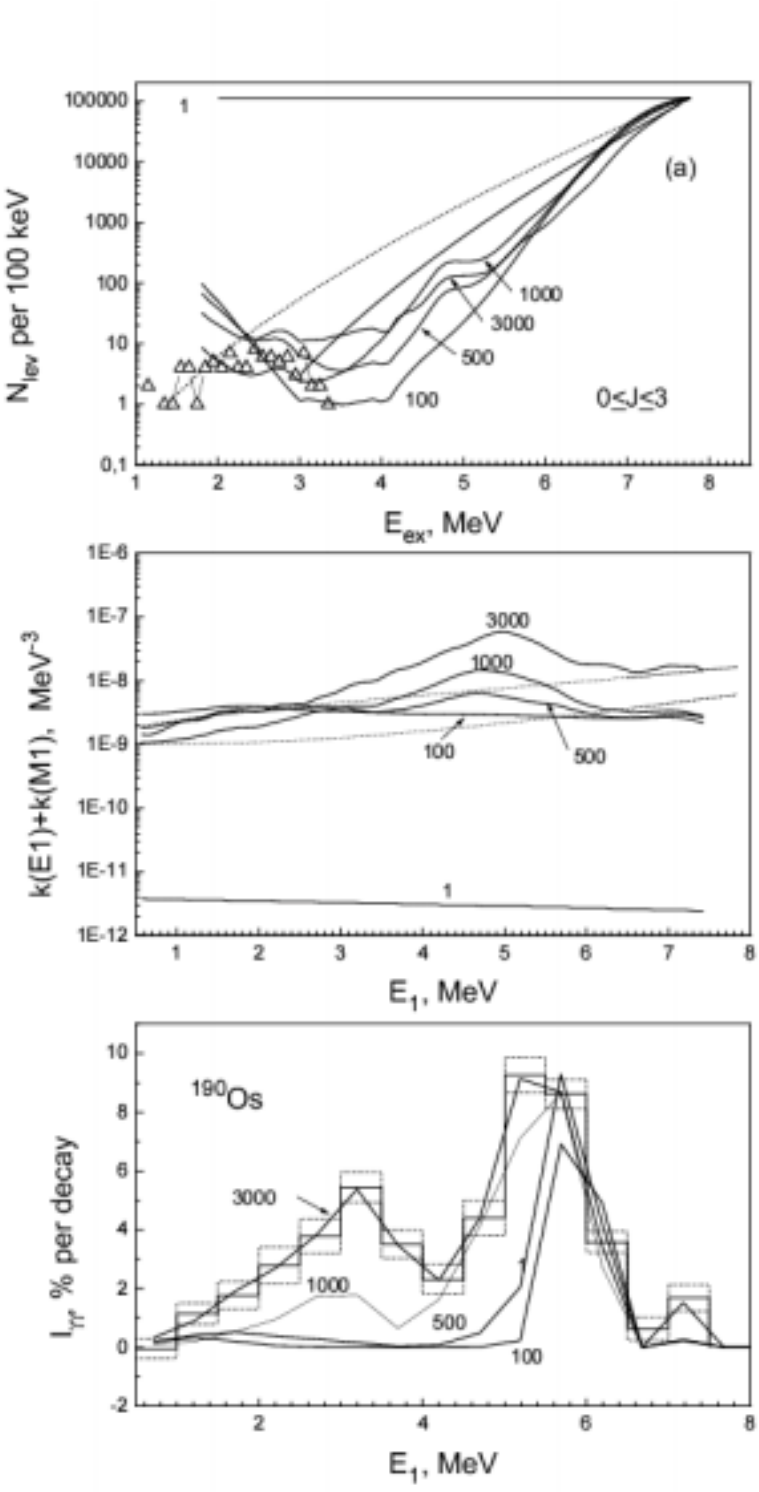

Fig.2. The same as in Fig. 1, for the ^{190}Os even-even nucleus.

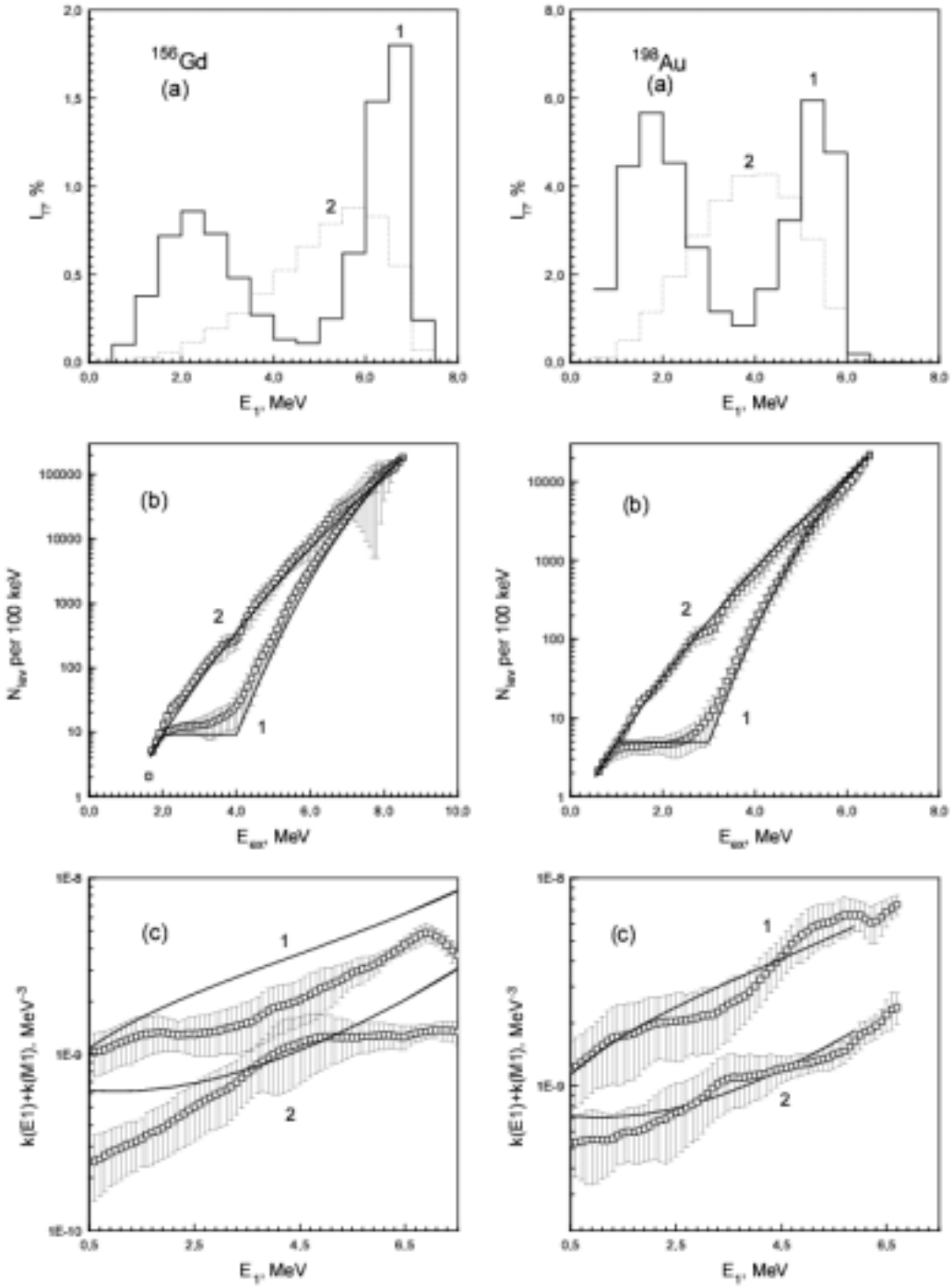

Fig. 3 The intensity of two-step cascades (a) calculated with level density [2,3] shown by solid lines in (b) and radiative strength [4,5] functions - line 1 in (c) (line 2 in (c) represents predictions of model [5]). Points with error bars represent the interval of possible values of ρ (b) and k (c) providing acceptable precision in reproduction of cascade intensities shown in (a).

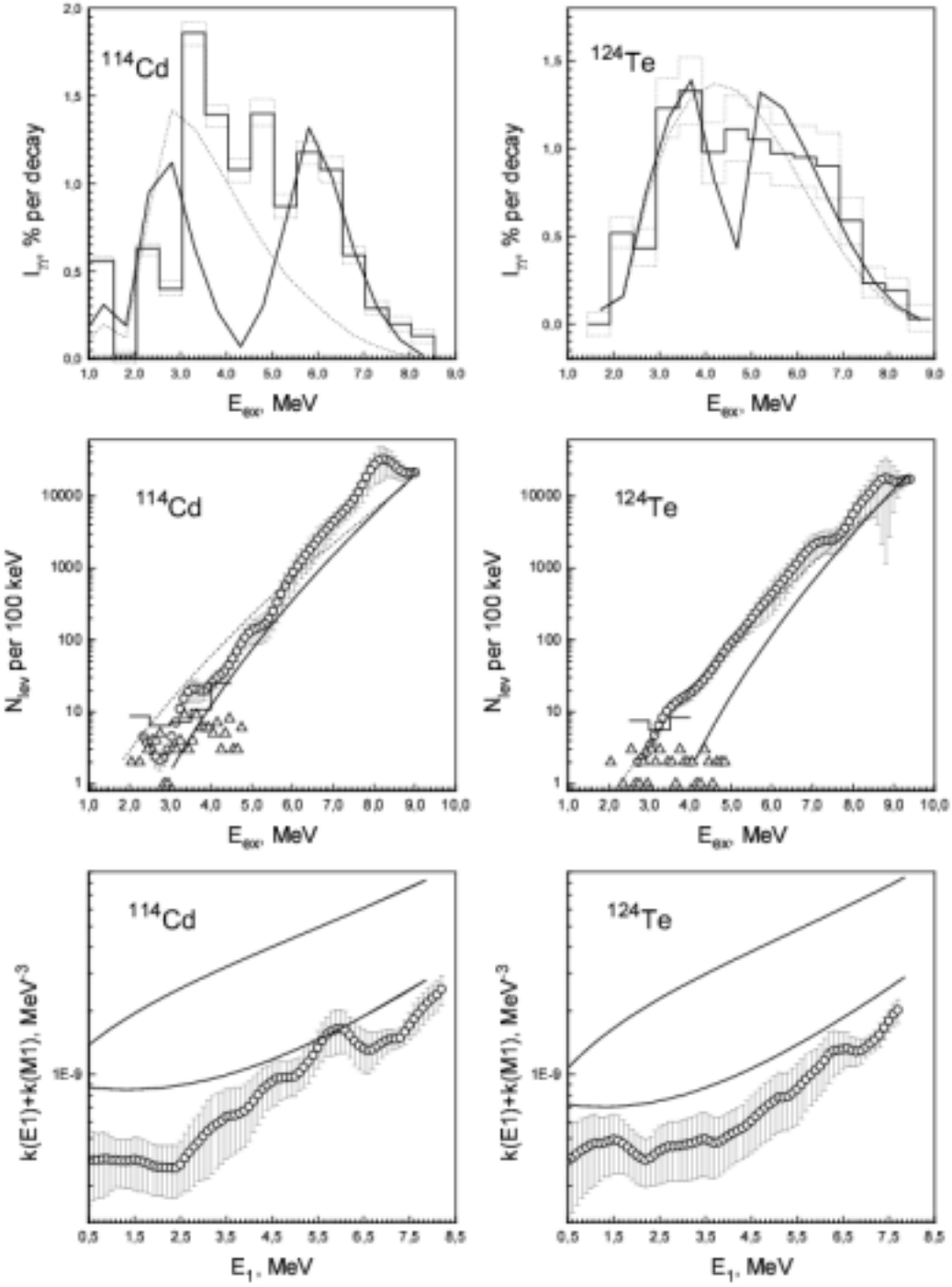

Fig. 4. Experimental cascade intensities $I_{\gamma\gamma}$ in 0.5 MeV energy bins with ordinary statistical errors for ^{114}Cd and ^{124}Te (histograms). Curves represent calculation performed like that shown in Fig. 3. Points with errors represent number of levels per 100 keV energy interval and sums k(E1)+k(M1), respectively.

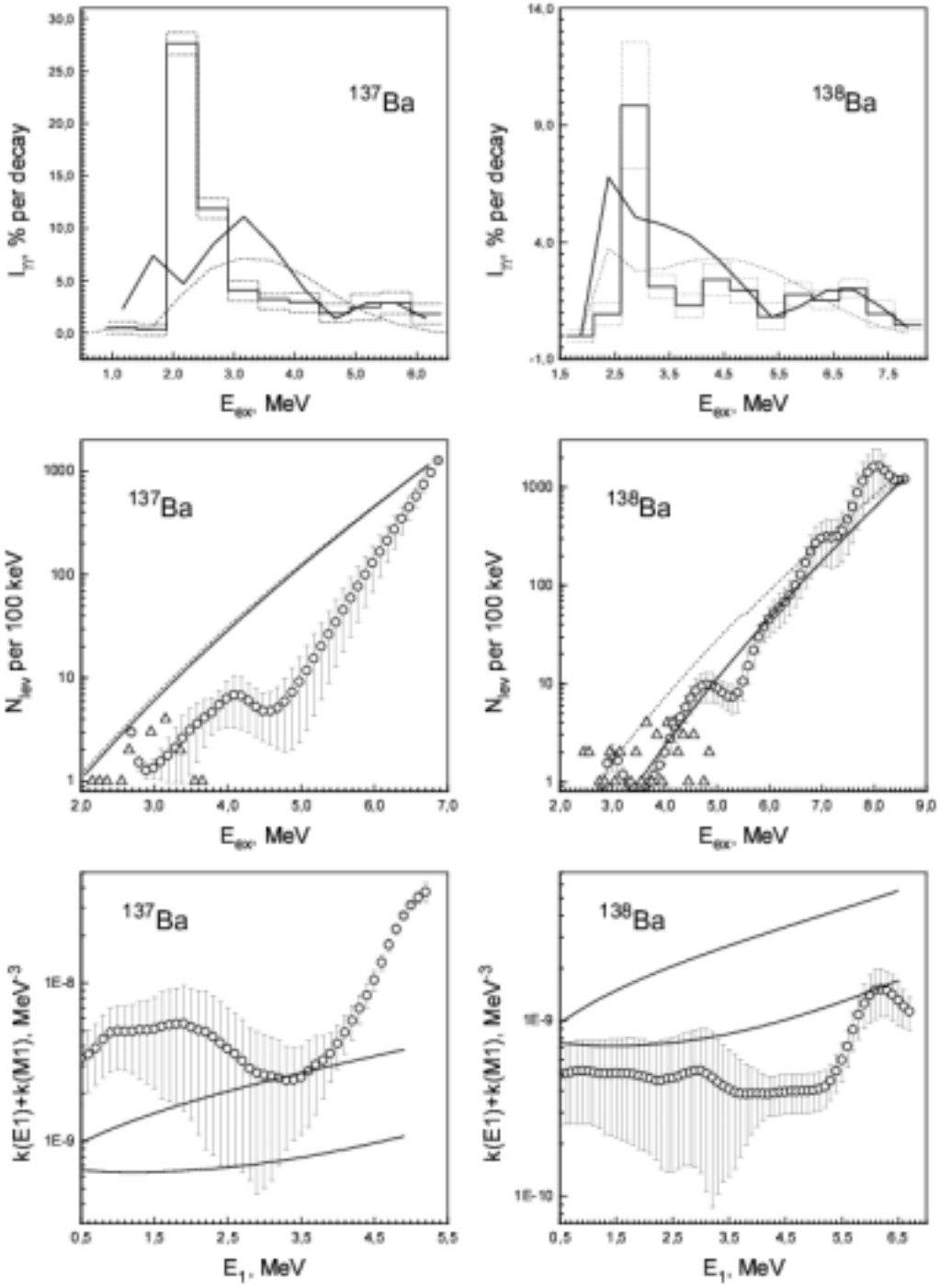

Fig. 5. The same as in Fig. 4 ^{137}Ba and ^{138}Ba.

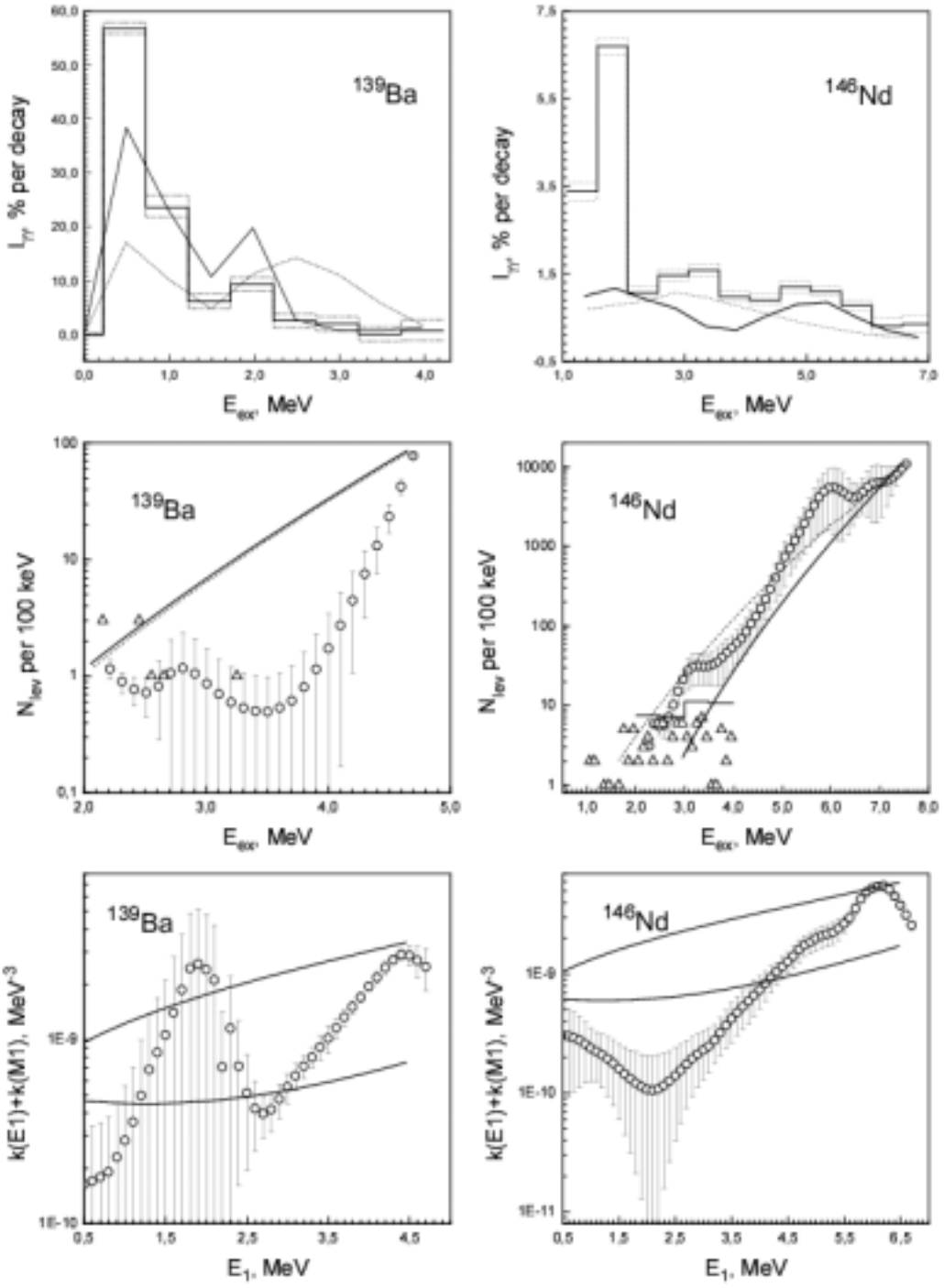

Fig. 6. The same as in Fig. 4 for ^{139}Ba and ^{146}Nd.

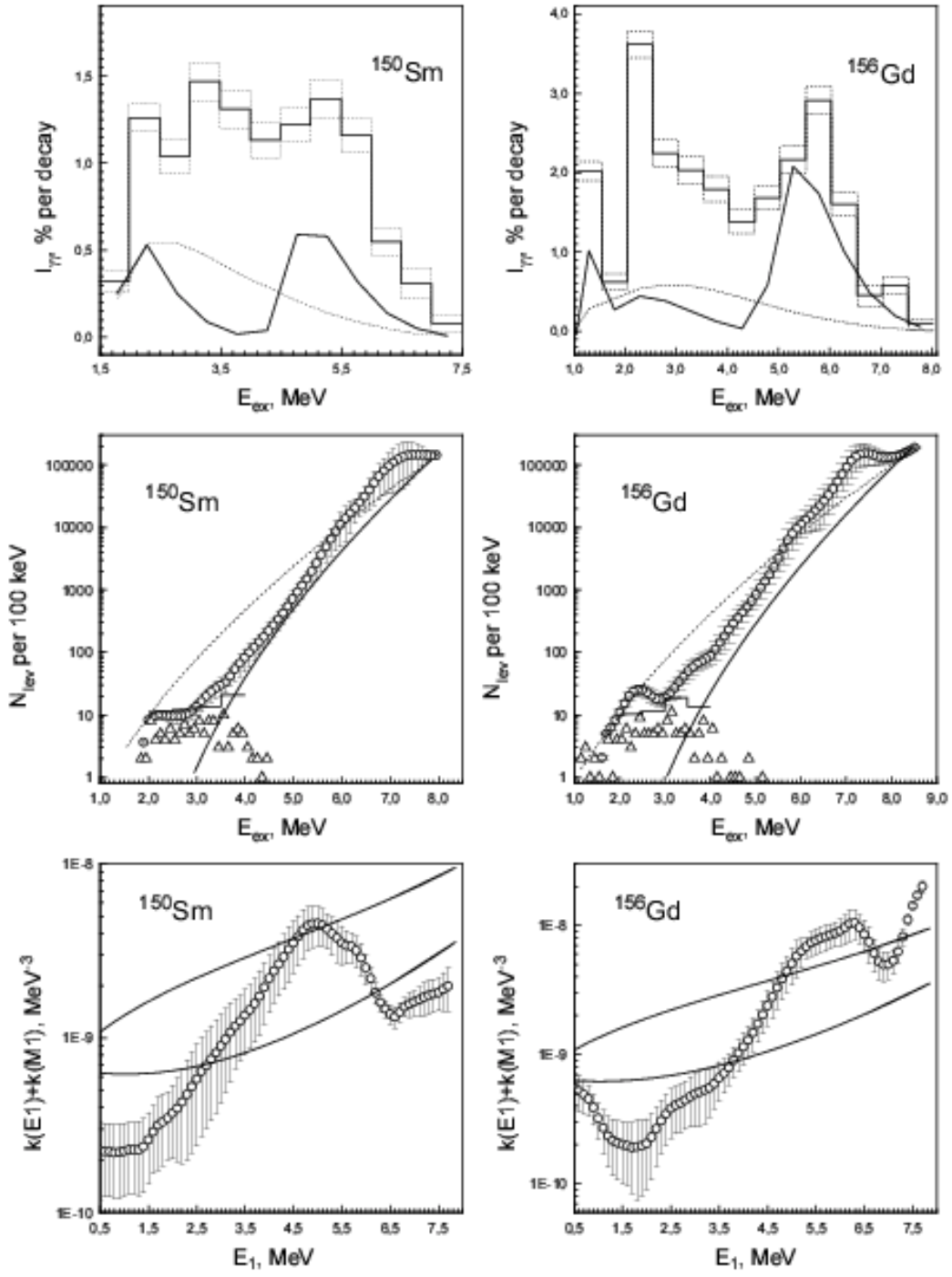

Fig. 7. The same as in Fig. 4 for ^{150}Sm and ^{156}Gd.

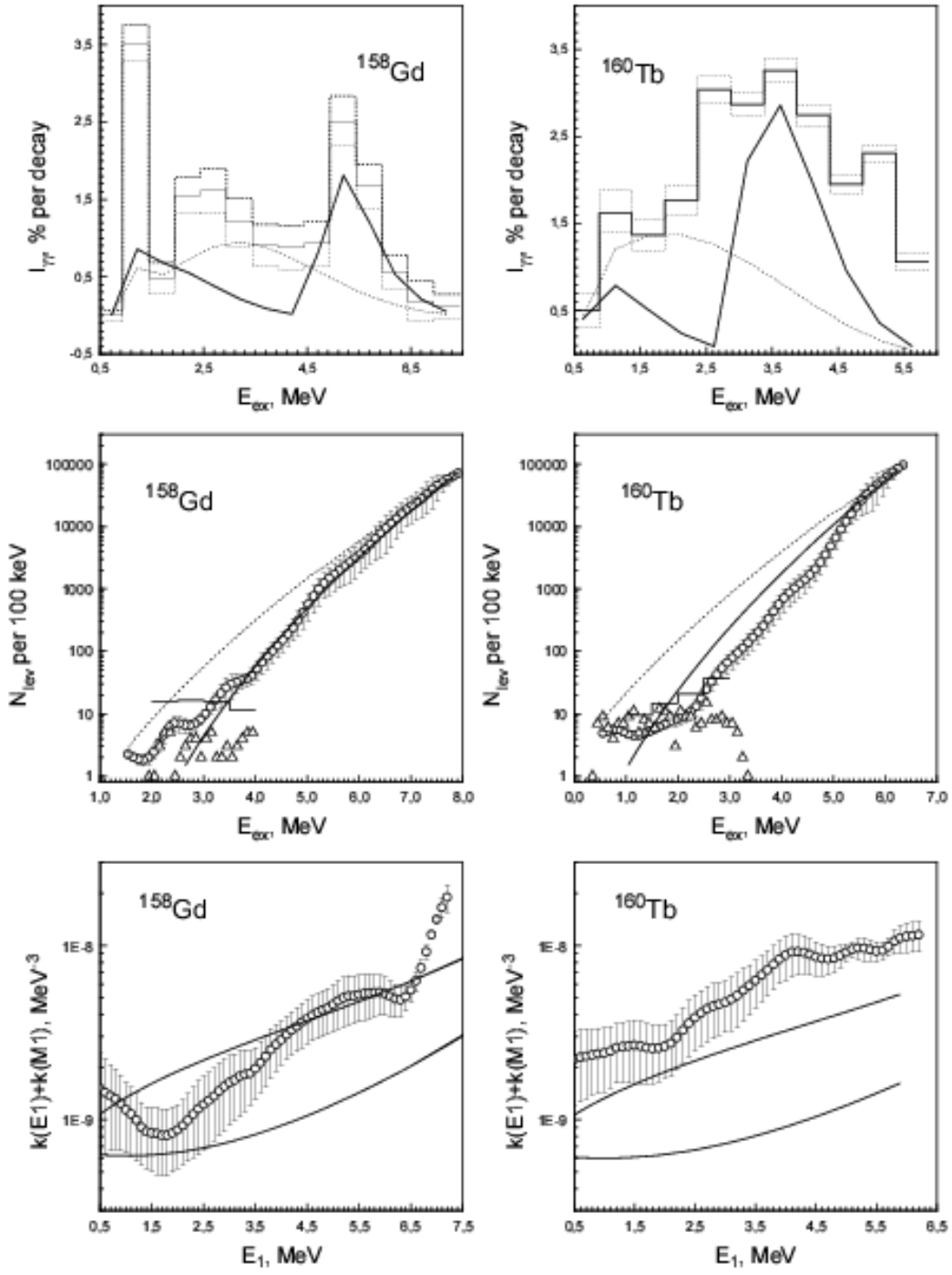

Fig. 8. The same as in Fig. 4 for ^{158}Gd and ^{160}Tb.

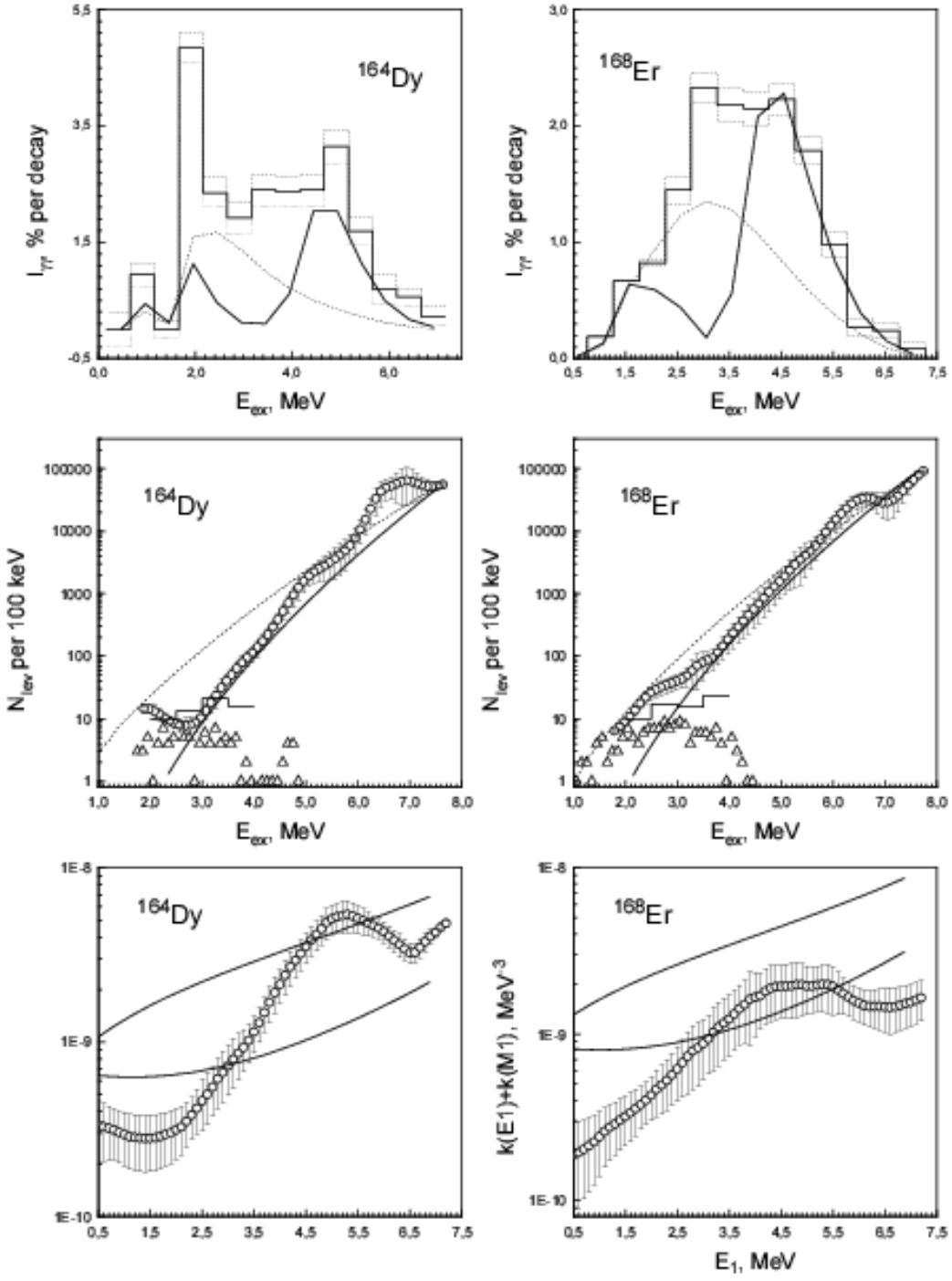

Fig. 9. The same as in Fig. 4 for ^{164}Dy and ^{168}Er.

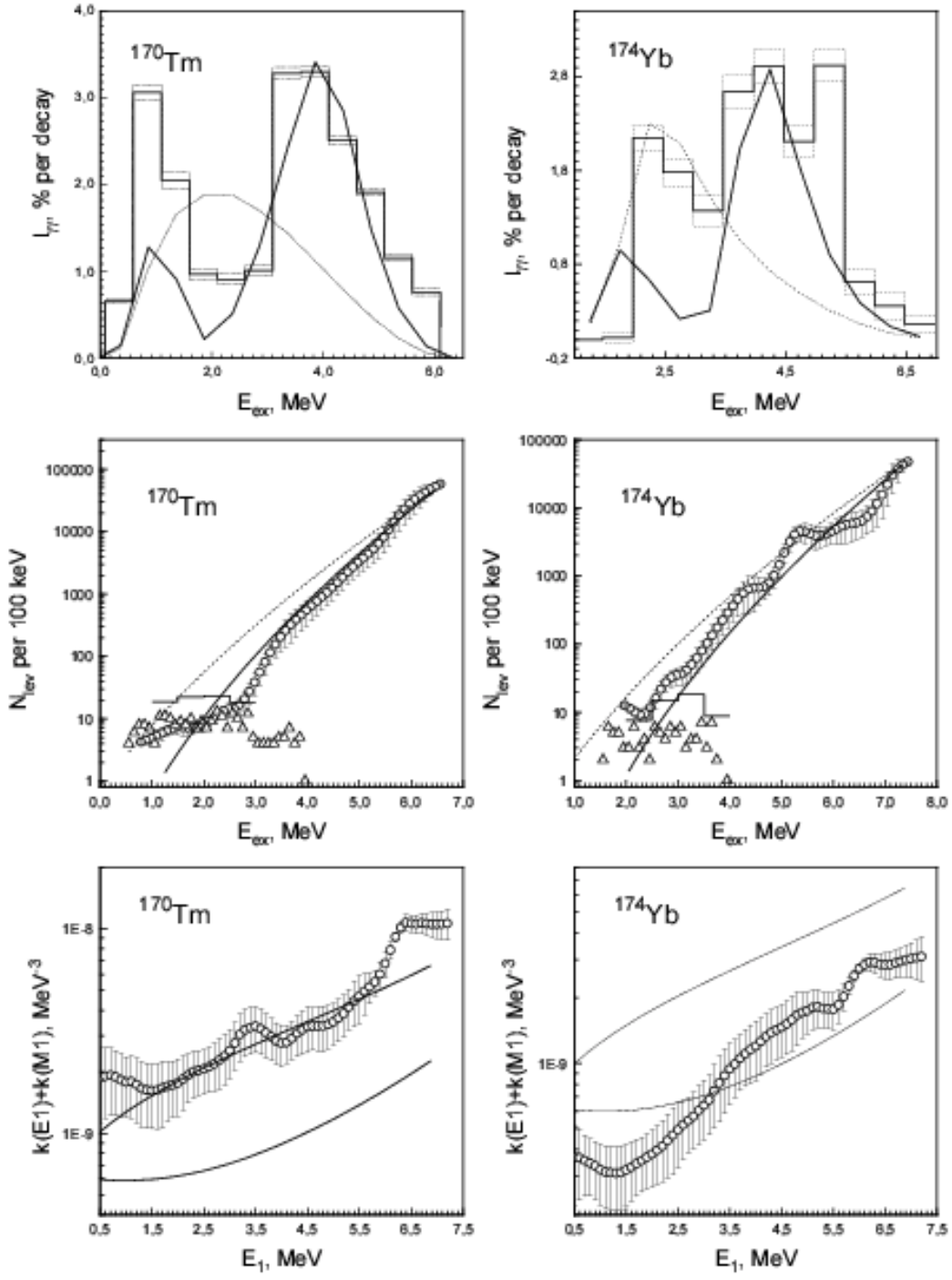

Fig. 10. The same as in Fig. 4 for ^{170}Tm and ^{174}Yb.

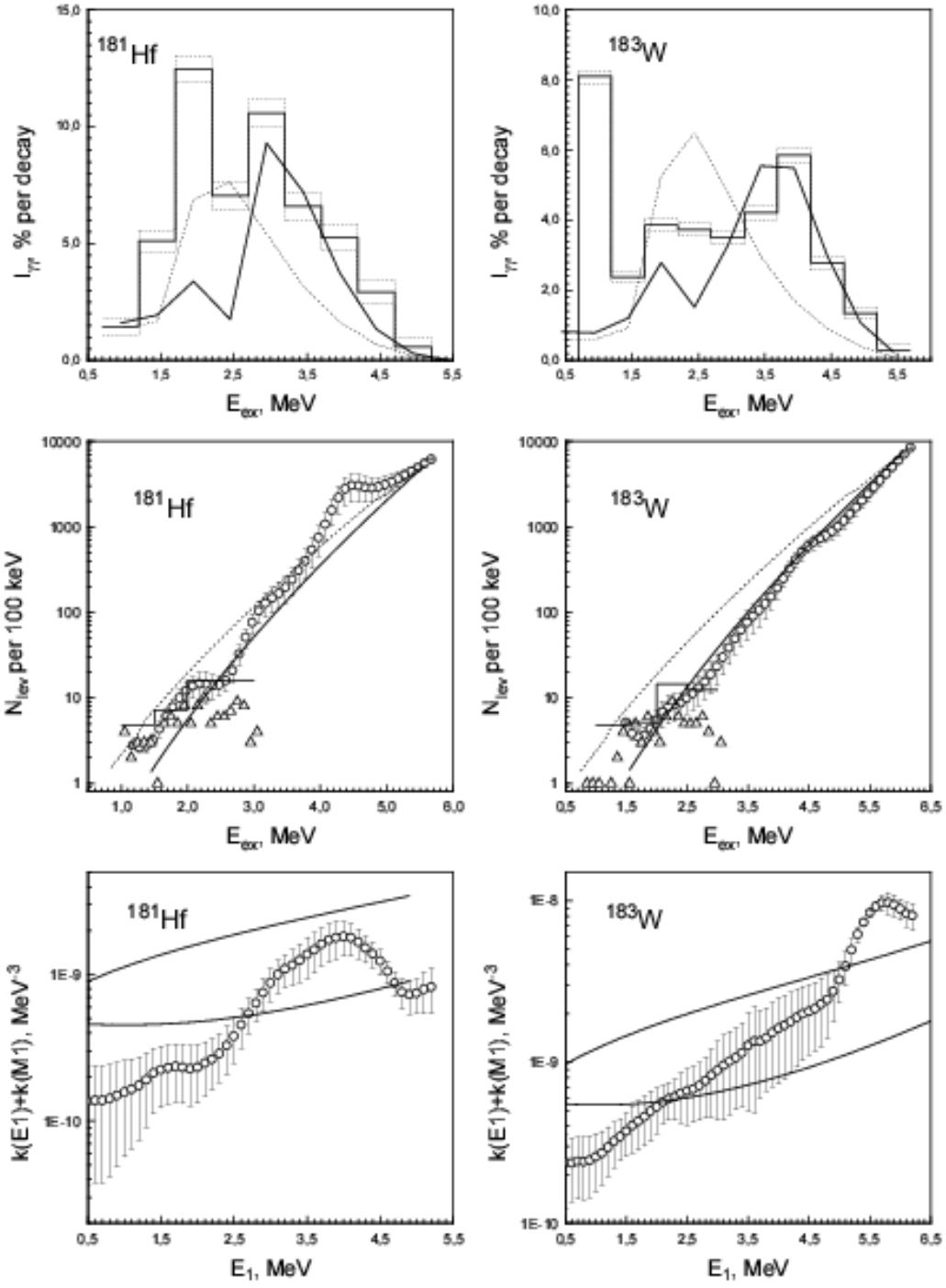

Fig. 11. The same as in Fig. 4 for ^{181}Hf and ^{183}W.

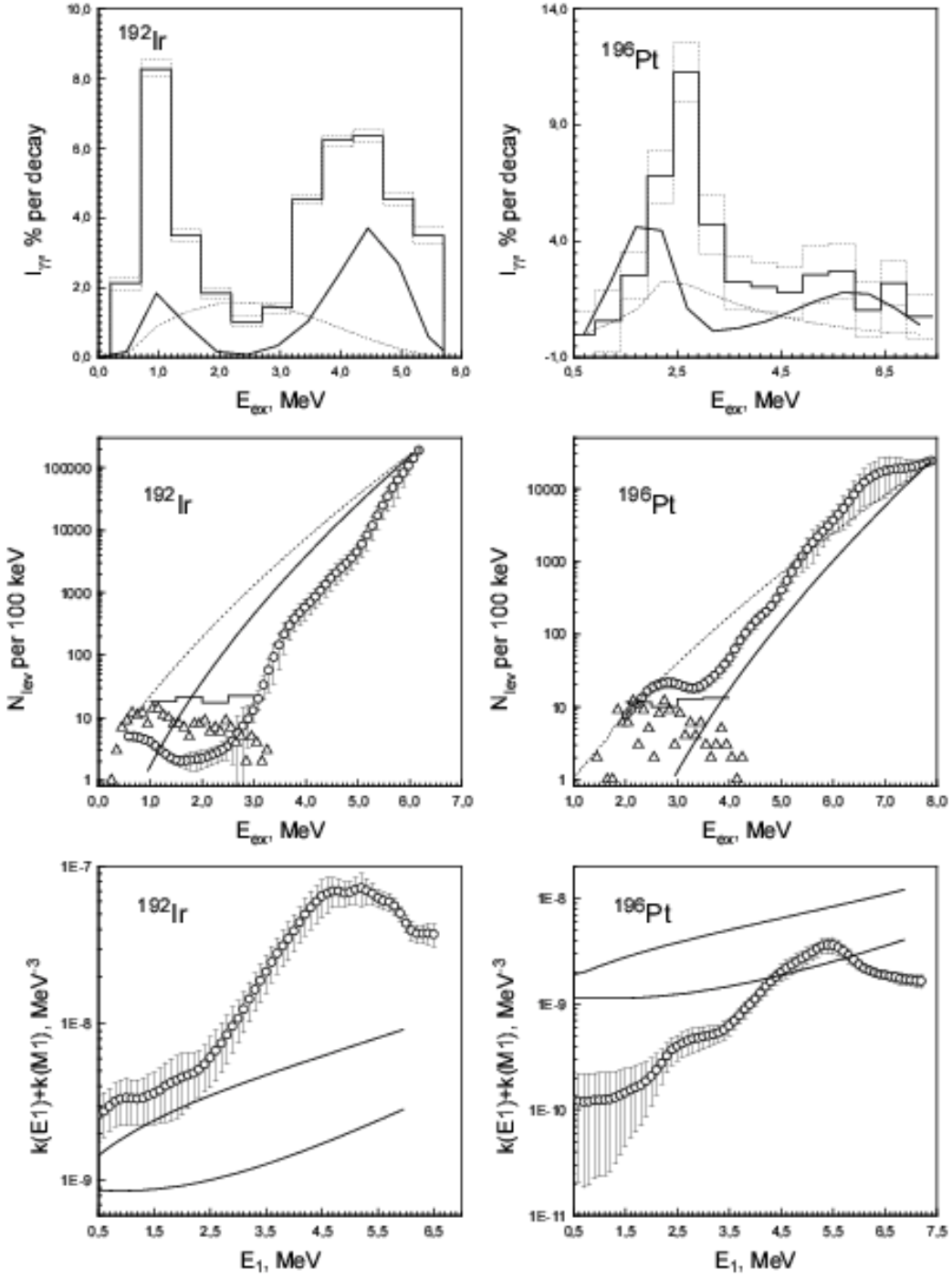

Fig. 12. The same as in Fig. 4 for ^{192}Ir and ^{196}Pt.

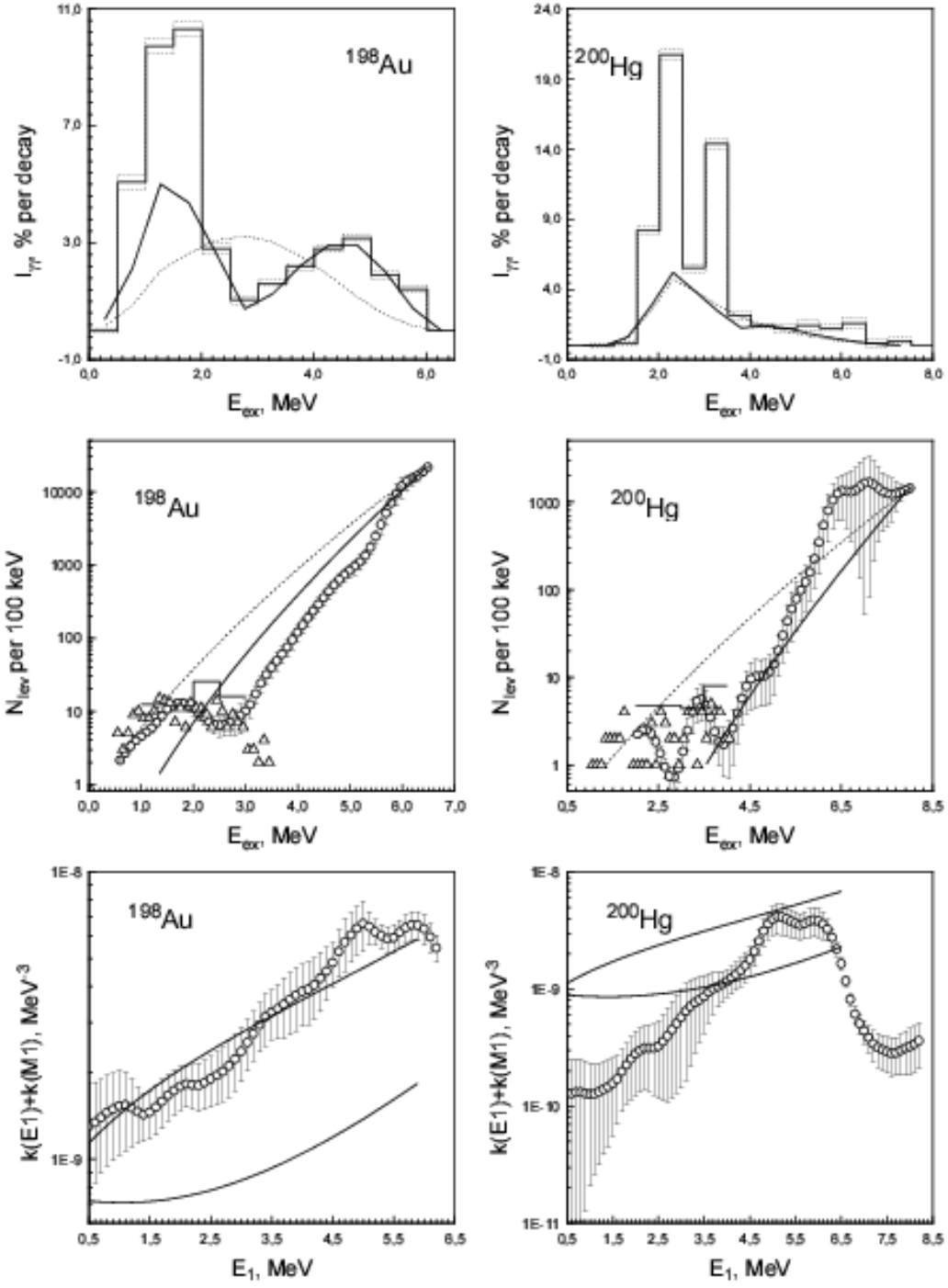

Fig. 13. The same as in Fig. 4 for ^{198}Au and ^{200}Hg.

References

1. S.T. Boneva et al., Phys. of Atomic Nuclei, **62(5)** (1999) 832
2. W. Dilg, W. Schantl, H. Vonach, M. Uhl, Nucl. Phys., **A217** (1973) 269
3. A.V. Ignatyuk, Proc. of IAEA Consultants Meeting on the Use of Nuclear Theory and Neutron Nuclear Data Evaluation (Trieste, 1975) IAEA-190, Vol.1 (1976), P.211
4. P.Axel, Phys. Rev. **126(2)** (1962) 671

M. Blatt and V. F. Weisskopf, Theoretical Nuclear Physics, New York (1952)

5. S.G. Kadmenskij, V.P. Markushev, W.I. Furman, Sov. J. Nucl. Phys. 37 (1983), p.165
6. M.I. Svirin, G.N. Smirenkin, Yad. Fiz. 47 (1988) 84
7. A.V. Ignatyuk et al., Sov. J. Nucl. Phys. 29 (1978) 875
8. G.A. Bartholomew et al., Advances in nuclear physics, 7 (1973) 229
9. H. Vonach, Proc. IAEA Advisory Group Meeting on Basic and Applied Problems Nuclear Level Densities (New York, 1983), INDC(USA)-092/L, (1983) P.247
10. S.T. Boneva et al., Sov. J. Part. Nucl. 22(2) (1991) 232
11. S.T. Boneva et al., Sov. J. Part. Nucl. 22(6) (1991) 698
12. Yu.P. Popov, A.M. Sukhovoj, V.A. Khitrov, Yu.S. Yazvitsky, Izv. AN SSSR, Ser. Fiz., 48 (1984) 1830
13. S.T. Boneva, V.A. Khitrov, A.M. Sukhovoj, A.V. Vojnov, Z. Phys. A338 (1991) 319
14. S.T. Boneva, V.A. Khitrov, A.M. Sukhovoj, A.V. Vojnov, Nucl. Phys. A589 (1995) 293
15. S.F. Mughabghab, Neutron Cross Sections V.1, part B, NY.: Academic Press (1984) 406
16. V.A. Khitrov, A.M. Sukhovoj, Proc. of VI International Seminar on Interaction of Neutrons with Nuclei, (Dubna, 1998) E3-98-202, Dubna, 1988, P.172
17. A.M. Sukhovoj, V.A. Khitrov, Physics of Atomic Nuclei 62(1) (1999) 19
18. A.M. Sukhovoj, V.A. Khitrov, Bulletin of the Russian Academy of Sciences, Physics 61(11) (1997) 1611
19. A.V. Ignatyuk, Report IAEA INDC-233(L) IAEA, Vienna 1985

E.M. Rastopchin, M. I. Svirin and G. N. Smirenkin, Yad. Fiz. **52** (1990) 1258

20. J. Bardin, L. Cooper, J. Schriffer, Phys.Rev. 108 (1957) 1175
21. A.I. Vdovin et al., Sov. J. Part. Nucl. 7(4) (1976) 380
22. B.V. Zhuravlev, Izv. RAN, Ser. Fiz. 63(1) (1999) 148
23. V.M. Maslov, Phys. of Atomic Nuclei 63(2) (2000) 161

UDC 539.17

NEUTRON CROSS SECTION EVALUATIONS FOR ACTINIDES AT INTERMEDIATE ENERGIES: ^{239}PU.

A.V. Ignatyuk, V.P. Lunev, Yu.N. Shubin[*]*,*
E.V. Gai, N.N. Titarenko
Institute of Physics and Power Engineering, 249020 Obninsk, Russia

W.Gudowski
Royal Institute of Technology, 100-44 Stockholm, Sweden

Investigations aimed at the development of neutron cross section evaluations for actinides performed at IPPE in collaboration with Royal Institute of Technology, Stockholm at intermediate energies in the range of 0 – 200 MeV are briefly described on the example of ^{239}Pu. The coupled-channels optical model is used to calculate the neutron total, elastic and reaction cross sections and the elastic scattering angular distributions. Evaluations of the neutron and charged particle emission cross sections and of the fission cross sections are obtained on the basis of the statistical description that includes direct, preequilibrium and equilibrium mechanisms of nuclear reactions. The Kalbach parametrization of angular distributions is used to describe the double-differential cross sections of emitted neutrons and charged particles in ENDF/B-VI format. These investigations resulted in creation of complete neutron and proton data files for ^{238}U and ^{232}Th and neutron data file for^{239}Pu up to 150 MeV. These files were processed with NJOY.

INTRODUCTION

In order to develop main concepts of the accelerator-driven power systems and the corresponding nuclear waste management it is necessary to know nuclear data on spectra and reaction cross sections for structural materials, fissile actinides and most important fission products in a very broad energy range. In practice, the energy interval from thermal energies to a few thousand MeV should be covered [1]. The status of available nuclear data differs strongly for the energy regions below and above of 20 MeV. Huge efforts have been made to create libraries of evaluated neutron data (ENDF/B, JENDL, BROND etc.), for the low energy region. In spite of some differences between the evaluations the most data are reasonable enough and their accuracy satisfy requests of major current applications. For energies higher than 20 MeV data are rather scarce and are not systematised yet.

A lack of experimental data has to be compensated by the development of reliable calculation methods. The codes based on the intranuclear cascade model combined with the evaporation model have been successfully applied for the energies above a few hundred MeV [2-5]. At lower energies, however, nuclear structure effects are so prominent that their description requires more detailed consideration of competitive reaction mechanisms. Therefore, it was decided that the energy region from 20 to 150 MeV requires special consideration and the evaluated data files for this region should be prepared for most important structural and fissile materials in the same manner as for the energy region below 20 MeV [1]. In accordance with that, the evaluated data files for about 30 of most important structural and shielding materials were extended in the ENDF/B-VI library up to 150 MeV by the Los Alamos group [6].

Plutonium isotopes are in the priority list of the most important nuclei to be evaluated. The main results of experimental data analysis and calculations recommended for the intermediate energy neutron data file of ^{239}Pu are briefly discussed below.

INCIDENT NEUTRON ENERGIES BELOW 20 MeV

Below 20 MeV the evaluation is based on the evaluations of ENDF/B-VI. As the recent analysis shows the difference between various evaluations is essential for many data, but at this moment we have not enough experimental data to improve considerably the existent evaluations. However some corrections of the fission cross section was made above 14 MeV in accordance with the experimental data by Lisowski [23] and Staples [21].

To provide the uniformity of the representation of the evaluation results on the angular distributions in a whole energy range 0.03<E<150 MeV, the ENDF/B-VI data on the angular distributions of neutrons in elastic (MF=4, MT=2) and inelastic scattering (MF=4, MT=51-54) in the region below E<20 MeV were transformed from the Legendre polynomial expansion coefficients to the normalised probability distribution representation.

[*] Corresponding author. E-mail address: shubin@ippe.rssi.ru

INCIDENT NEUTRON ENERGIES ABOVE 20 MeV

Evaluations above 20 MeV are based on nuclear model calculations, whose parameters are to be adjusted on the available experimental data. A coupled-channels optical model is used to calculate the transmission coefficients for neutrons and protons particles, and to evaluate the angular distributions for neutron scattering as well.

The GNASH code [7] was used to calculate the integral and double differential cross sections and to prepare data in ENDF/B-VI format.

The level density description for all channels was obtained on the basis of the Gilbert-Cameron approach fitted to experimental data on the density of low-lying levels and neutron resonances.

TOTAL AND SCATTERING CROSS SECTIONS

Evaluations of neutron total cross sections are based on the coupled-channels optical model calculations with potential parameters fitted to experimental data. The analysis of such data was performed in many laboratories, and the deformed optical model parameters obtained were used for the neutron cross section evaluations of actinides [9-11]. These sets of parameters give approximately the same total cross sections. However, the calculated neutron absorption cross sections differ essentially for various sets. Discrepancies of the absorption cross section evaluations are essential at neutron energies above 10 MeV, and their effects appear in the evaluated cross sections of (n,xn), fission and other reactions.

The optimal set of optical model parameters has been estimated from the analysis of experimental data of neutron total cross sections, angular distributions for proton elastic and inelastic scattering and proton absorption cross sections.

Table 1.

Optical potential parameters for neutrons and protons*

Well depth (MeV);	Energy Range (MeV):
V_r = 51.50 +/- 16h + 0.2420*E + D_c	0 < E < 40
V_r = 50.58 +/- 16h - 0.2190*E + D_c	40 < E < 100
V_r = 49.34 +/- 16h - 0.2066*E + D_c	100 < E < 150
r_r = 1.21	0 < E < 150
a_r = 0.7	
r_{Coul} = 1.26	
W_d = 3.36 +/- 5h + 0.4681*E - 0.02381*E**2	0 < E < 5.24
W_d = 2.079 +/- 5h + 0.686*E - 0.0212*E**2	5.24 < E < 22.
W_d = 9.053 + 5h - 0.0867*E	22. < E < 35.
W_d = 9.053 +/- 5h - 0.0867*E	35. < E < 100.
W_d = 1.523 +/- 5h - 0.0114*E	100. < E < 150.
r_d= 1.32 - 0.0055*E	0 < E < 22.
a_d = 0.63	
r_d= 1.2	22. < E < 35.
a_d = 0.47 +0.008*E	
r_d= 1.2	35. < E < 150.
a_d = 0.75	
W_v = -1.708 + 0.122*E - 0.000022*E**2	0 < E < 100
W_v = -0.408 + 0.107*E - 0.0002*E**2	100 < E < 150
r_v = 1.26	0 < E < 150
a_v = 0.35 + 0.0018*E	
V_{so} = 6.18	0 < E < 150
r_{so} = 1.16	
a_{so} = 0.667	

Here Lane isospin correction term h = (A-2Z)/A; A and Z are the atomic mass and proton number of the target nucleus; Coulomb correction term (for protons only) Dc = 0.4Z/A**1/3 , (the plus sign refers to protons) deformation parameters: beta2 = 0.205, beta4 = 0.075, and the scheme of 1/2+ - 3/2+ - 5/2+ - 7/2+ -9/2+ coupled levels is accepted. These parameters are close to those used for the intermediate energy neutron cross section evaluations of lead isotopes [13].

The total cross section calculated with the parameters given above is compared with available experimental data and other calculations in Fig. 1. A reasonable agreement of our calculations with the Barashenkov's systematics [14] and experimental data [15-19] is obtained for all energies above 20 MeV.

The corresponding calculations of neutron elastic scattering and absorption cross sections are shown in Figs. 2 and 3, respectively. There are no direct measurements of the elastic and inelastic cross sections at high energies. However, a reasonable estimation of them is given by Barashenkov's systematics, based mainly on proton reaction data [14]. The optical model calculations reproduce well the proton absorption cross section in the whole energy region from the Coulomb barrier to 200 MeV, and at high energies they are in reasonable agreement with the Barashenkov evaluations for both protons and neutrons.

The coupled-channels model makes it possible to calculate also the cross sections and angular distributions for elastic and inelastic scattering of neutrons with excitation of low-lying collective levels in the whole energy range. Evaluated neutron inelastic scattering cross sections to low-lying collective levels of ^{239}Pu are shown in Fig. 4.
Experimental data of elastic scattering angular distributions are available only at incident neutron energy up to 14.1 MeV [15]. Our calculations are compared with these data in Fig. 5. The contributions of the first collective levels 3/2+, 5/2+, 7/2+, 9/2+ to the scattering cross sections should be taken into account in such a comparison with experiments, because a resolution is not high enough to separate the elastic and inelastic scattering cross sections. The reasonable agreement of calculations with experimental data allow us to apply the optical model to the evaluation of the elastic and inelastic scattering angular distributions for all higher energies. The results of such calculations are shown in Figs. 6, 7 and 8 for the energies of 50, 100 and 150 MeV, respectively. Unfortunately, there are no measurements of the neutron elastic scattering angular distributions for high energies.

FISSION CROSS SECTIONS AND FISSION PROMPT NEUTRONS

The fission cross section above 20 MeV was measured by several groups [20-25]. Data [25] have a preliminary status and they should be taken in careful consideration only after the complete processing of measurement results.
The calculated fission cross section was fitted to the ENDF/B-VI evaluation, considered as the neutron standard at energies below 14 MeV, in order to obtain the fission barrier parameters. For higher energies, the effects of nuclear viscosity were included in the calculations of the fission widths of highly excited compound nuclei [26]. An accurate description of the fission cross sections is very important for consistent evaluation of multiple emission of neutron and charged particles. The evaluated fission cross section is compared with experimental data in Fig. 9.

The evaluation of the average number of prompt neutrons per fission is based on the Cascade Evaporation Fission Model calculations fitted to the experimental data [27] below 50 MeV. The results of our evaluation for $<\nu>$, the average number of prompt neutrons per fission, are shown in Fig. 10 in the energy region up to 150 MeV. The evaluation is based on the Cascade Evaporation Fission Model calculations fitted to the experimental data below 50 MeV. In the upper part of Fig. 10 the corresponding temperature of the Maxwellian fission neutron spectra is shown as a function of the incident neutron energy.

NEUTRON PRODUCTION CROSS SECTIONS AND SPECTRA

Evaluations of particle emission spectra and corresponding production cross sections are performed in accordance with the rules of the ENDF/B-VI format for the double-differential cross sections, by using the Kalbach-Mann representation of such data [28]. Differential cross sections are described in this approach by the integral production cross section for the corresponding emitted particle multiplied by a normalised angular distribution function of the following form

$$f(\mu_b, E_a, E_b) = f_0(E_a, E_b)\left\{\frac{a(E_a, E_b)}{\sinh a(E_a, E_b)}\left[\cosh\left(a(E_a, E_b)\mu_b\right) + r(E_a, E_b)\sinh\left(a(E_a, E_b)\mu_b\right)\right]\right\},$$

where E_a is the incident particle energy in the laboratory system, μ_b is the scattering angle cosine of the emitted particle b and E_b is its energy in the center-of-mass system, $f_0(E_a,E_b)$ is the normalized spectrum of the emitted particle, $r(E_a,E_b)$ is the pre-compound fraction of this spectrum, and $a(E_a,E_b)$ is the simple function proposed in Ref. [34], which depends mainly on the center-of-mass emission energy E_b and, to a lesser extent, on particle type and incident energy at higher values of E_a. In accordance with such a description, the two energy-dependent functions $f_0(E_a,E_b)$ and $r(E_a,E_b)$ determine completely the shape of emitted particle spectra and the anisotropy of the corresponding angular distributions, respectively.
E_a is the incident particle energy in the laboratory system, E_b is the emitted particle energy in the center-of-mass system. The preequilibrium components of spectra become larger with increasing incident neutron energy while, the soft equilibrium components change only a little.

The neutron emission is a dominant reaction that competes with nuclear fission. The evaluated neutron production cross section is shown in Fig. 11. Below 20 MeV these calculations agree well enough with the evaluations of the (n,2n) and (n,3n) reactions based on experimental data and included in the files of BROND-2 or ENDF/B-VI. Above 20 MeV, there are no direct experimental data on neutron emission cross sections or on the multiplicity of secondary neutrons, which can be evaluated as the ratio of the calculated neutron production cross section to the reaction cross section considered above.

The evaluated normalized spectra of emitted neutrons are shown in Fig. 12 for incident neutron energies from 20 to 150 MeV. The preequilibrium components of spectra become larger with increasing incident neutron energy while, the soft equilibrium components change only a little. The calculated r-factors that define the anisotropy of secondary neutron angular distributions are given in Fig. 15 for several incident neutron energies.

CHARGED PARTICLE EMISSION CROSS SECTIONS AND SPECTRA

In order to calculate the transmission coefficients for protons, we used the same potential as for neutrons, with the corresponding Lane components. The calculated absorption cross section for such a potential agrees rather well with Barashenkov's systematics of the proton induced reaction cross sections at high energies [14], but, at the present time, the experimental data are not accurate enough to test such calculations for energies close to the Coulomb barrier.

The proton production cross section calculated with such transmission coefficients is shown in Fig. 13. The corresponding normalized proton spectra and r-factors are presented in Figs. 14 and 15, respectively.

For similar calculations of deuteron, triton and α-particle yields, which should be lower than the proton yields, we used the spherical optical model with the parameters given in Tables 2, 3 and 4, respectively.
The corresponding potential parameters for deuterons were taken from [29]:

Table 2.

Optical potential parameters for deuterons

V_r= 81.32-0.24E+ D_{Coul}
r_v=1.18
a_v=0.636+0.035A**1/3
D_{Coul}= 1.43Z/A**1/3 r_{Coul}=1.30

W_v= 0.0 E< 45 MeV
W_v= 0.132(E-45) E> 45 MeV
r_{wv}=1.27
a_{wv}=0.768+0.021A**1/3

W_d=max(0;7.80+1.04A**1/3-0.712Wv)
r_{wd}=1.27
a_{wd}=0.768+0.021A**1/3

V_{so}= 6.00

a_{so}= 0.78+0.038A**1/3

The optical potential for tritons was taken with the parameters from [30]:

Table 3.

Optical potential parameters for tritons

V_r= 165.0 -0.17E -6.4(A-2Z)/A
r_v= 1.200
a_v= 0.720
r_{Coul}=1.30

W_v= 46.0 -0.33E -110(A-2Z)/A E < 40 MeV
W_v= 32.8 -110(A-2Z)/A E > 40 MeV
r_{wv}= 1.40
a_{wv}= 0.840
V_{so}= 2.5

r_{so}= 1.200
a_{so}= 0.720

The potential parameters for alpha-particles were taken in accordance with [31]:

Table 4.
Optical potential parameters for alpha-particles

V_r= 101.1-0.248E+D_{Coul}
r_v= 1.245
a_v= 0.817- 0.0085A**1/3

D_{Coul}= 6.051Z/A**1/3 r_{Coul}=1.245
W_d= 12.64+0.2E -1.706A**1/3 E<73 MeV
W_d= 26.82+0.006E -1.706A**1/3 E>73 MeV
r_{wd}= 1.57
a_{wd}= 0.692

Some shortcomings of the preequilibrium model used in the GNASH code were demonstrated in the analysis of production cross sections of deuterons and heavier charged particles[14,30,31]. To get more accurate evaluations of deuteron, triton and alpha-particle yields, use was made of the modified ALICE-IPPE code, which describes the cluster emission on the basis of the Ivamoto-Harada model [32] with parameters adjusted on the available experimental data of cluster yields and spectra in proton induced reactions [33]. A deuteron emission was calculated using the quasi-direct and pick-up mechanisms. For a triton emission the pick-up processes were taken into account, and for alpha-particles the knock-out, pick-up and multiple preequilibrium emission were included into consideration. Undoubtedly, uncertainties of such estimations of light cluster production cross sections are rather large, but we do not have enough experimental data to improve theoretical description essentially at the present time. On the other hand, all of these cross sections are much lower than the neutron production cross section and big uncertainties of less important cross sections seem acceptable for most applications related to the development of accelerator-driven systems.

The cross sections for the ^{238}U(n,xd), ^{238}U(n,xt) and ^{238}U(n,xα) reactions calculated in such an approach are shown in Figs. 16-18. The experimental data on the yields of the same charged particles in the proton induced reaction on ^{209}Bi are shown also.

To evaluate the spectra and angular distributions of emitted charged particles we returned, nevertheless, to the GNASH calculations, but the main parameter of the preequilibrium model was changed for each cluster channel to obtain the same production cross sections as with the ALICE-IPPE code. The calculated spectra of deuterons, tritons and α-particles are shown in Figs. 19, 20 and 21, respectively. The corresponding r-factors that define preequilibrium components of charged particle spectra are given in Fig. 22 for several energies of incident neutrons.

SUMMARY AND CONCLUSIONS

The major components of the intermediate-energy neutron data evaluations for ^{239}Pu have been described in the present work. Evaluations are based on the coupled-channels model and the statistical model of preequilibrium and equilibrium particle emission, with theoretical model parameters adjusted on the available experimental data. The recommended values are matched up with the well tested data below 20 MeV and have been used for preparation of the complete neutron data file of ^{239}Pu.

The same approach have been used for the creation neutron and proton data files for ^{238}U and ^{232}Th. These files were processed with NJOY and can be used for the investigations of the properties of various ADS facilities.

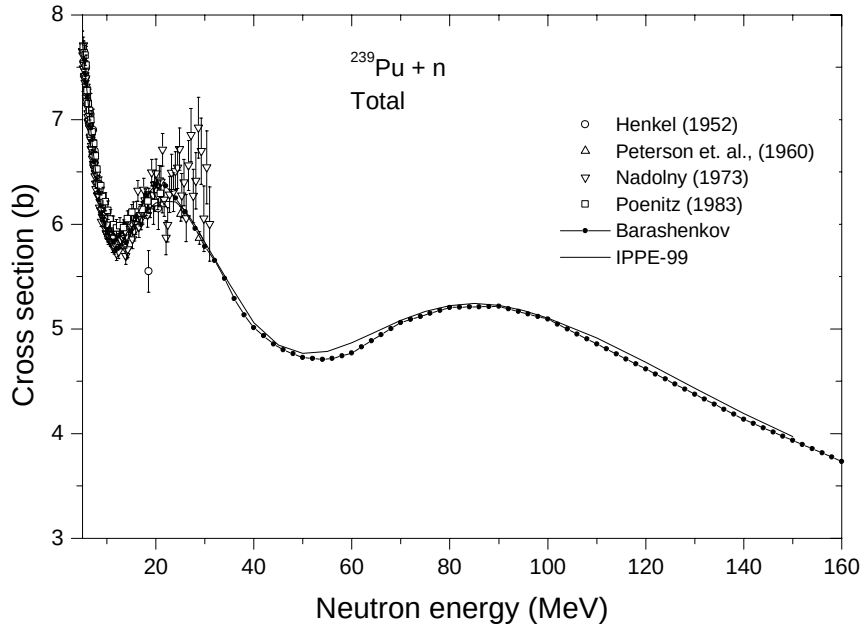

Fig. 1. Comparison of different evaluations of the total neutron cross section with experimental data

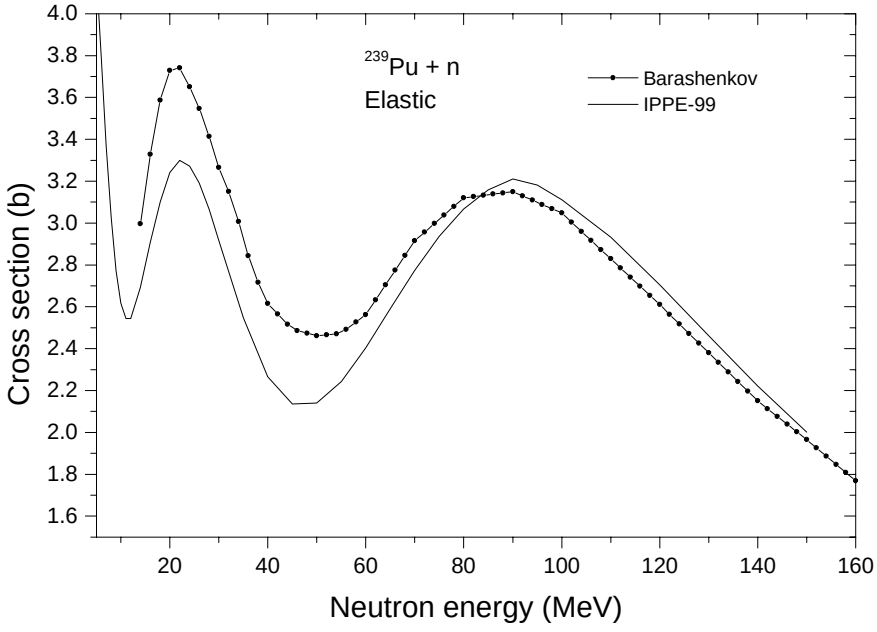

Fig. 2. Comparison of Barashenkov's systematics and evaluation of the elastic neutron cross section

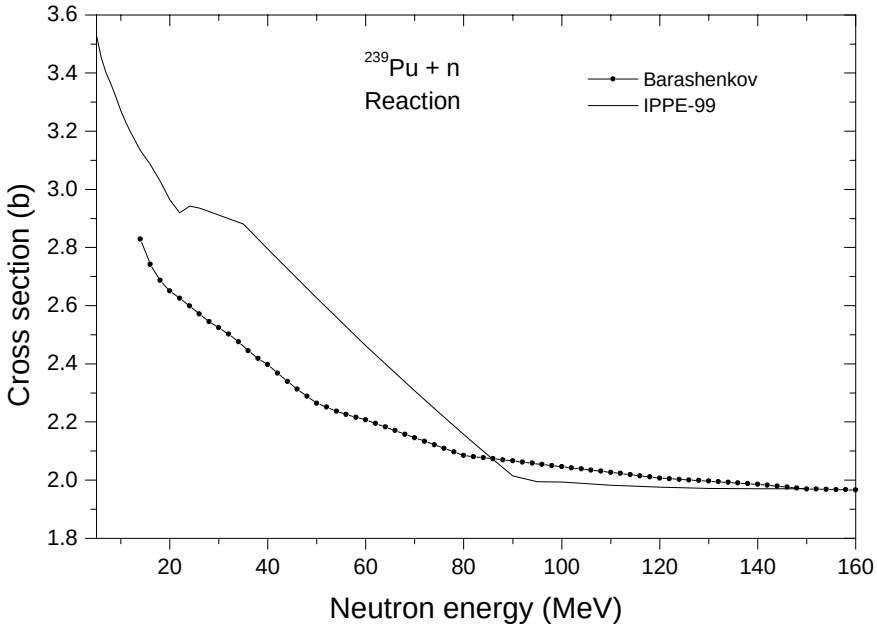

Fig. 3. Comparison of evaluated neutron reaction cross section and systematics

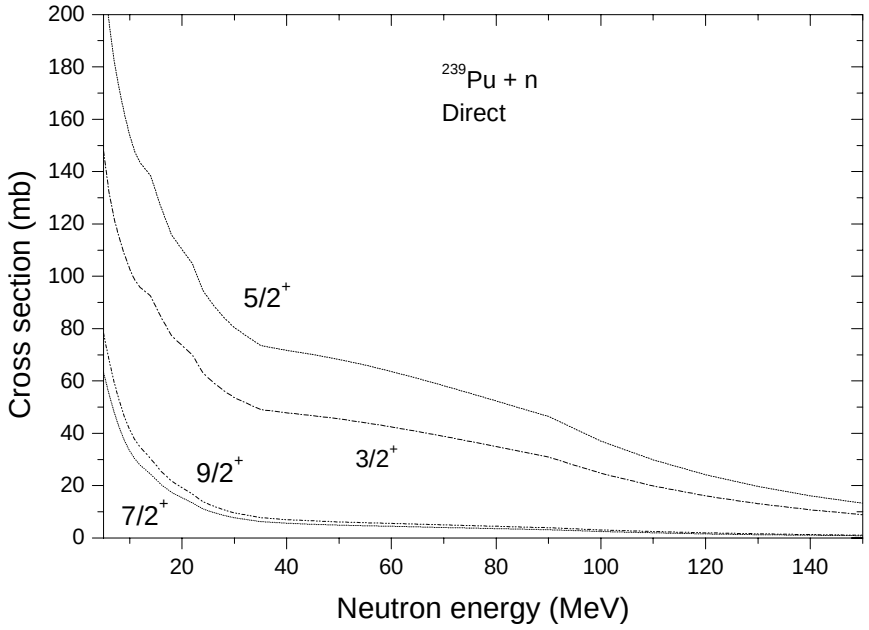

Fig. 4. Evaluated neutron inelastic scattering cross section to low-lying collective levels of ^{239}Pu

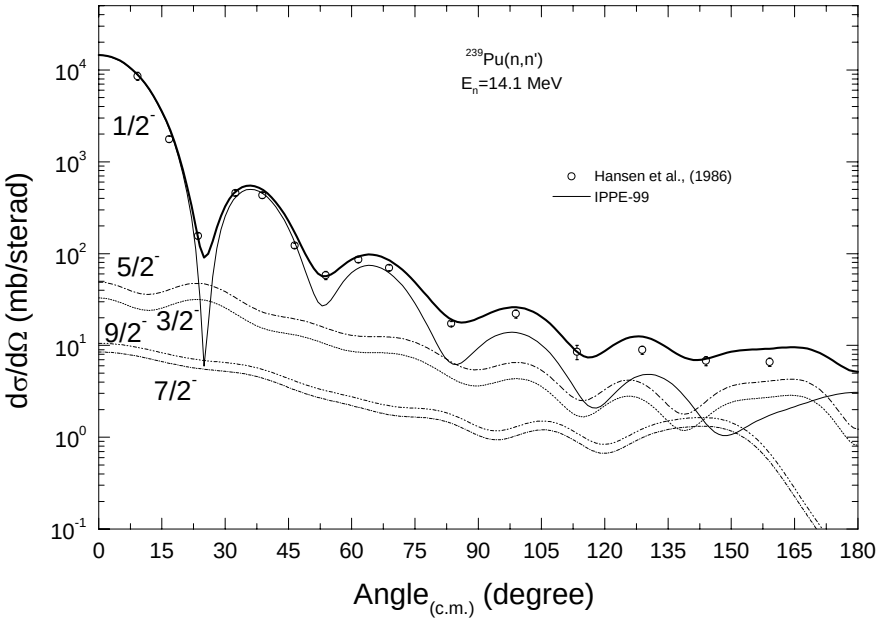

Fig. 5. Comparison of the calculated elastic scattering cross section at 14.1 MeV with experimental data. The scattering cross sections for the ground ($1/2^+$) and collective low-lying levels ($3/2^+$, $5/2^+$, $7/2^+$, $9/2^+$) are shown by solid, dotted, dashed-dotted, dash-dot-dot and short-dash-dot curves respectively. The thick solid curve is the sum of the cross sections for the ground and collective low-lying levels.

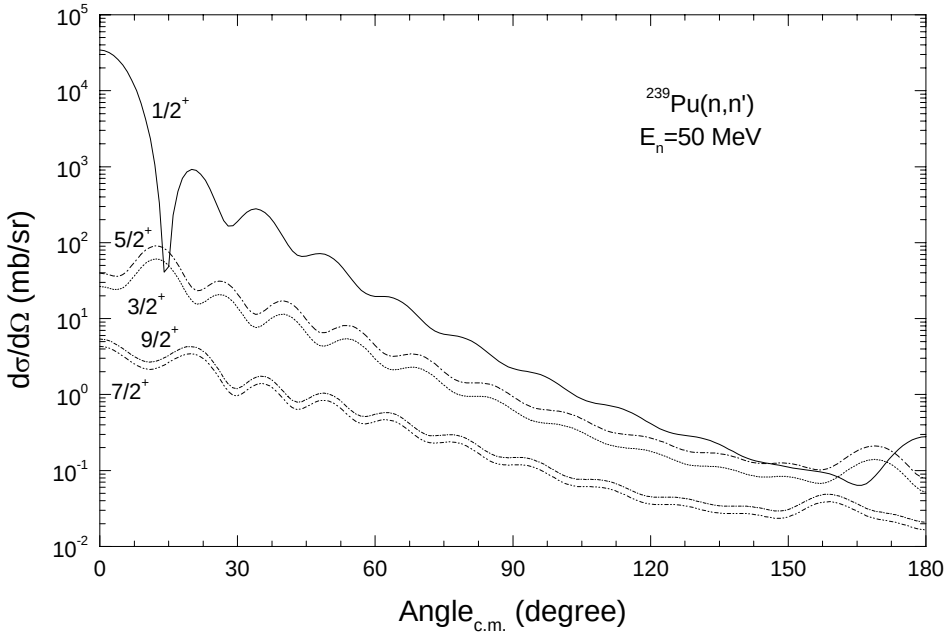

Fig. 6. Evaluated elastic and inelastic scattering cross sections for ^{239}Pu at 50 MeV

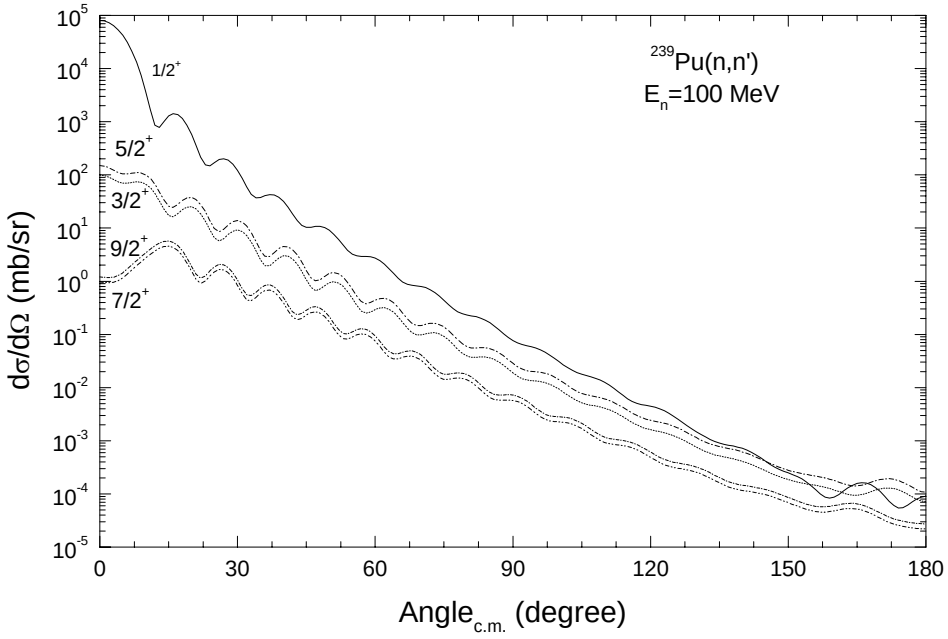

Fig. 7. Evaluated elastic and inelastic scattering cross sections for ^{239}Pu at 100 MeV

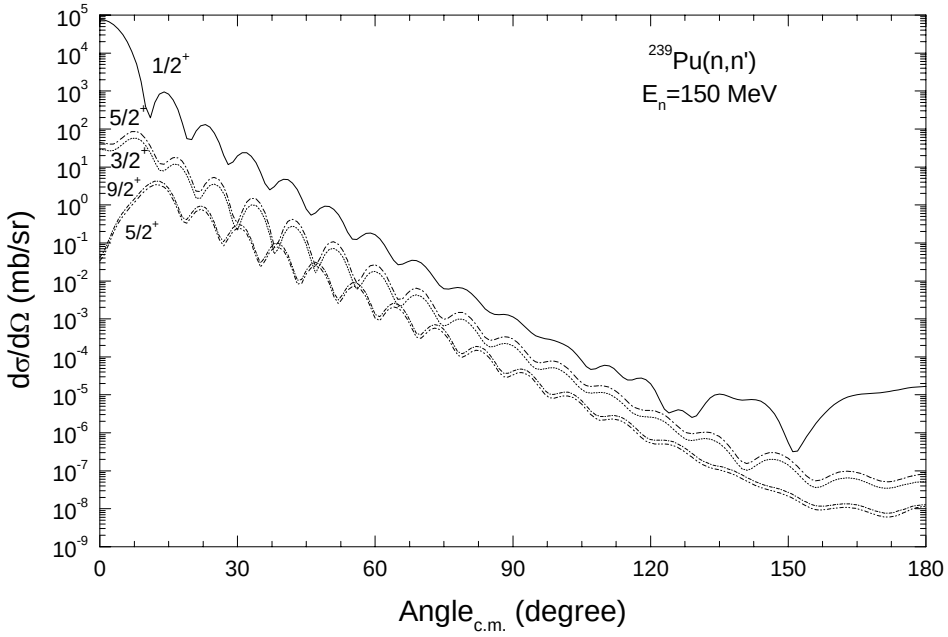

Fig. 8. Evaluated elastic and inelastic scattering cross sections for ^{239}Pu at 150 MeV

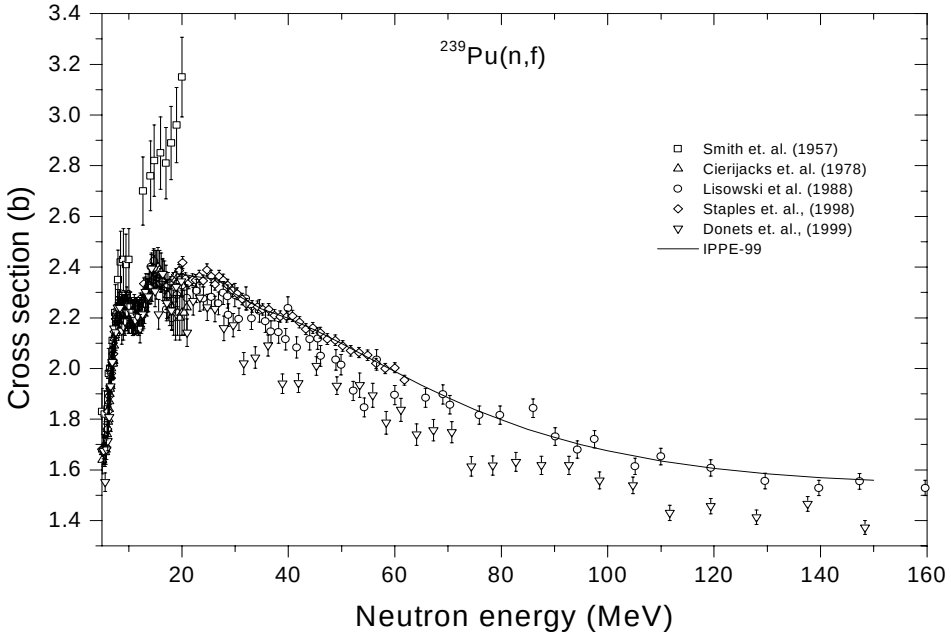

Fig. 9. Evaluated fission cross section in comparison with experimental data

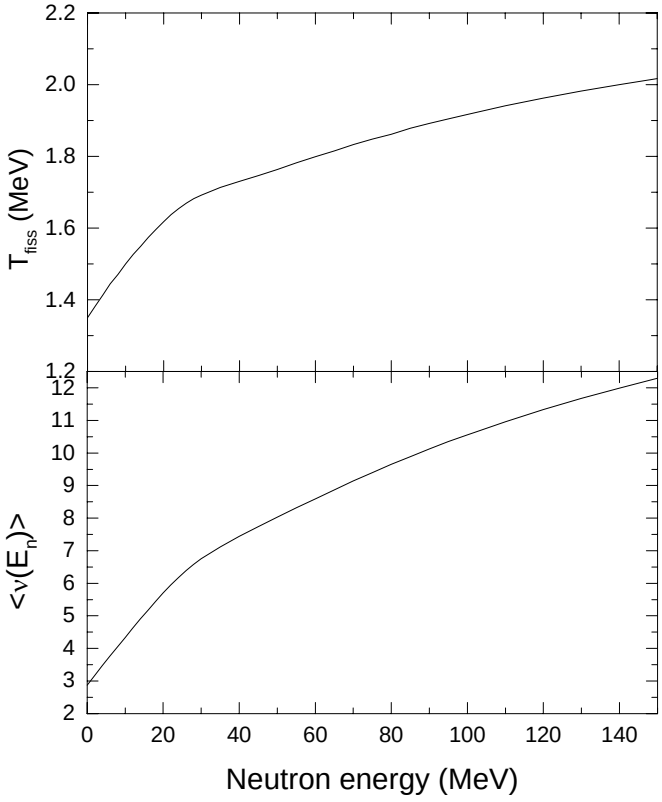

Fig. 10. Evaluated average prompt fission neutron number and fission neutron spectra temperature

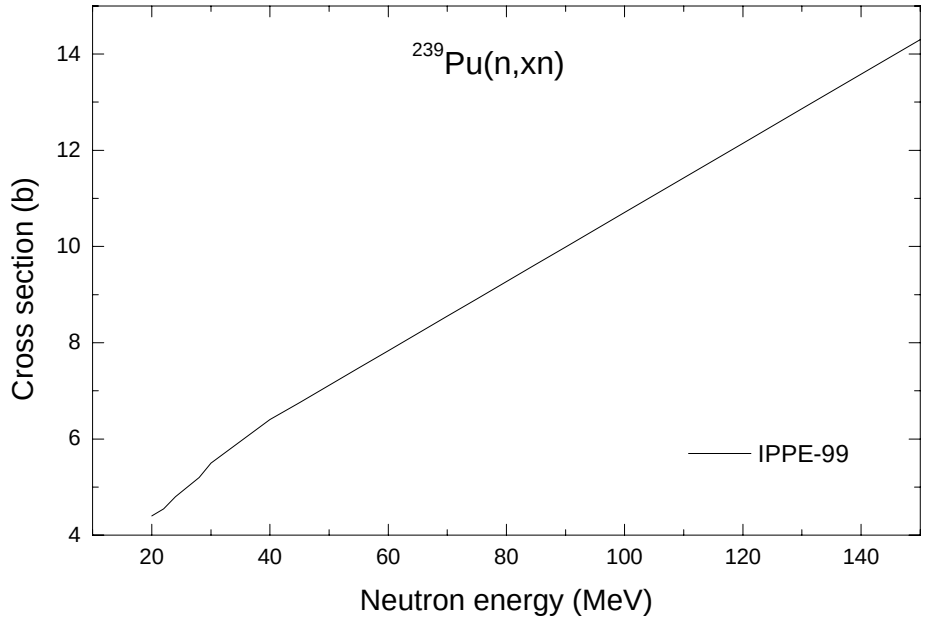

Fig. 11. Evaluated neutron production cross section

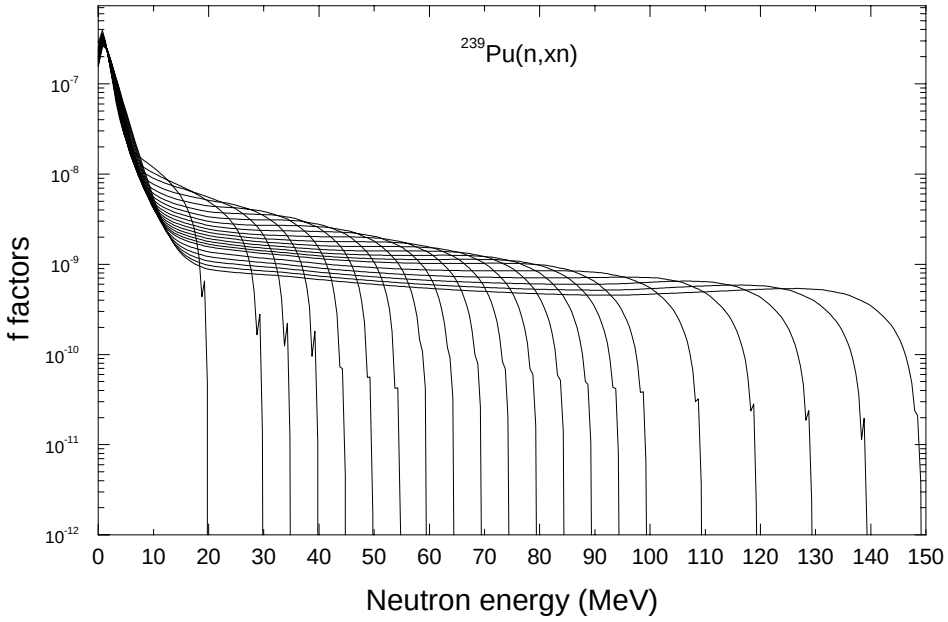

Fig. 12. Normalized secondary neutron spectra for the incident neutron energies from 20 to 150 MeV

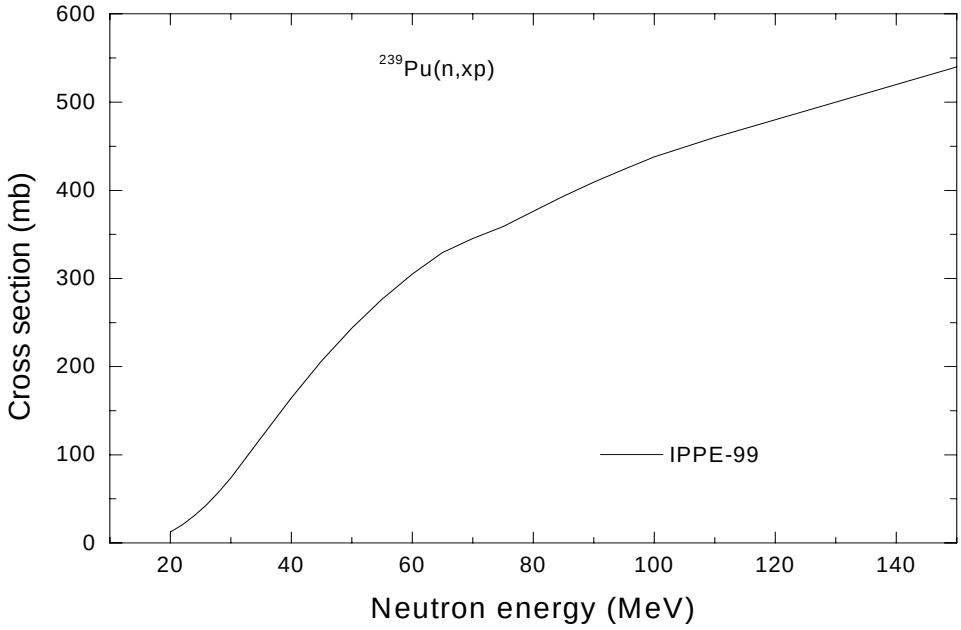

Fig. 13. The proton production cross section

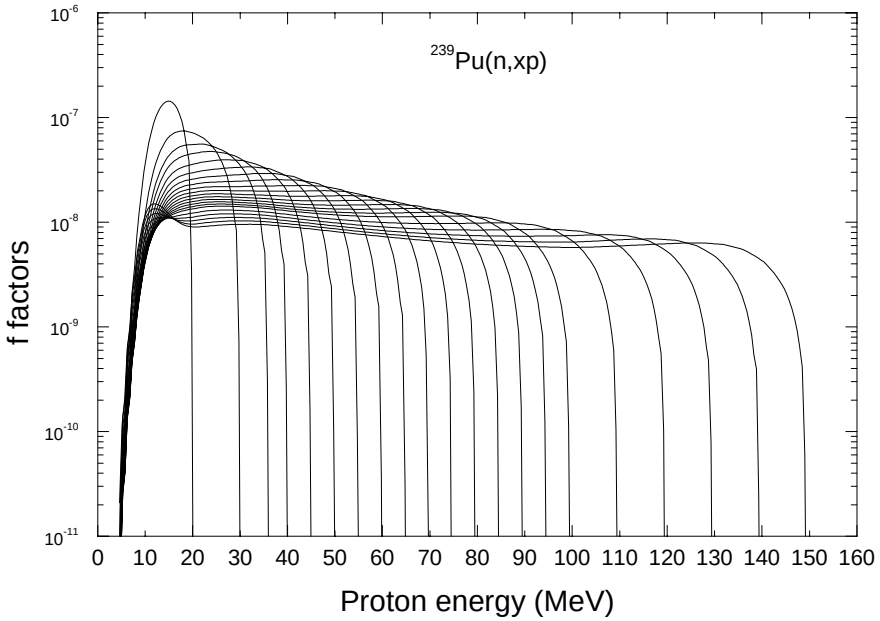

Fig. 14. Normalized secondary proton spectra for the incident neutron energies from 20 to 150 MeV

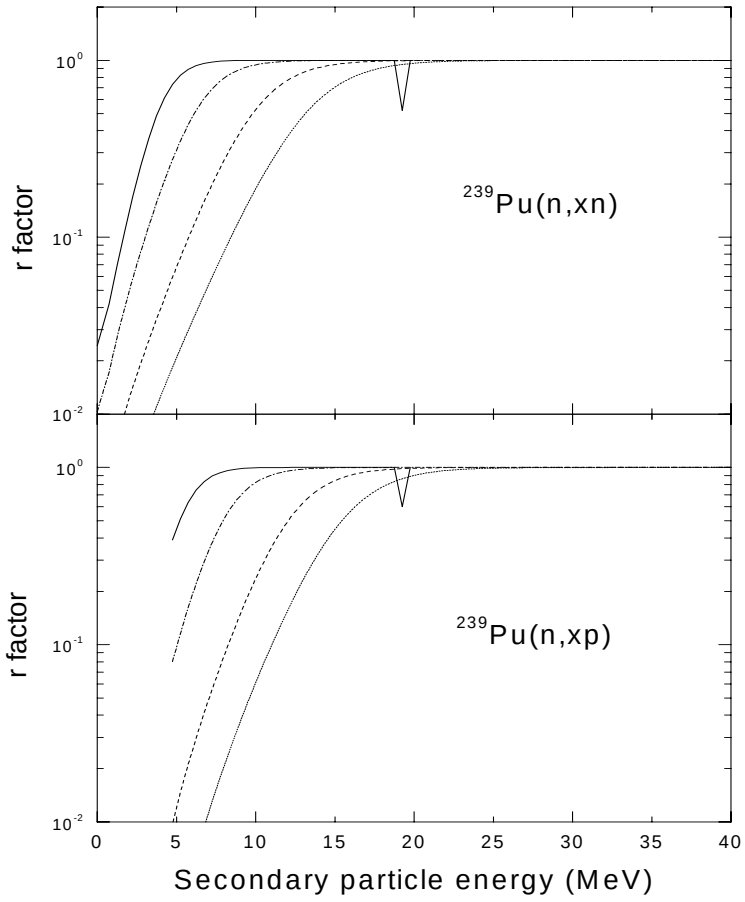

Fig. 15. Preequilibriuim components of the neutron and proton spectra for the incident neutron energies 20 MeV (solid), 50 MeV (dot-dashed), 100 MeV (dashed), and 150 Mev (dotted) curves

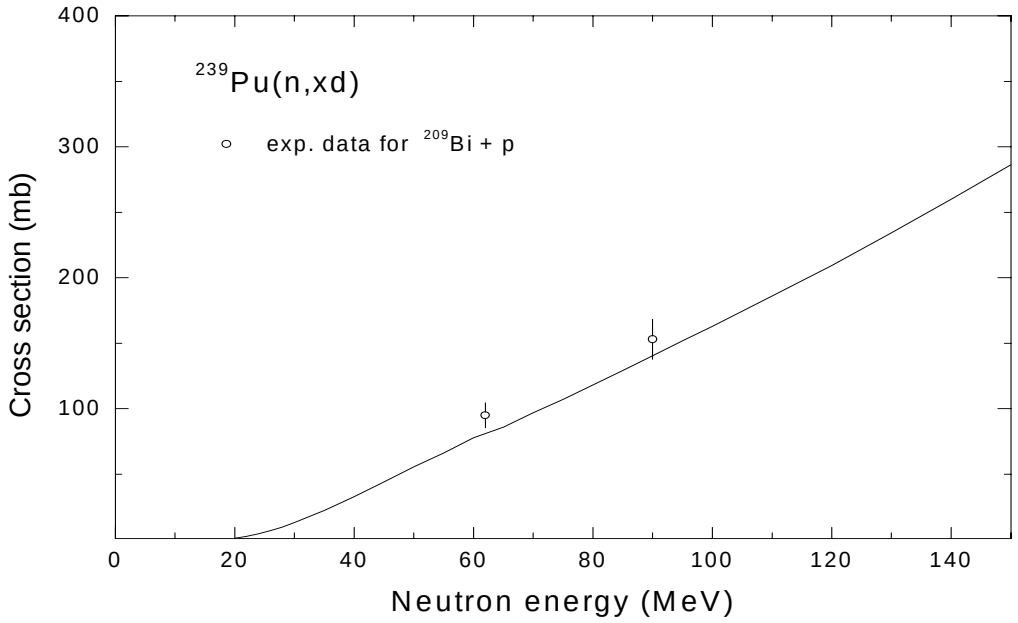

Fig. 16. The deuteron production cross section evaluated on the basis of statistical calculations and experimental data systematics

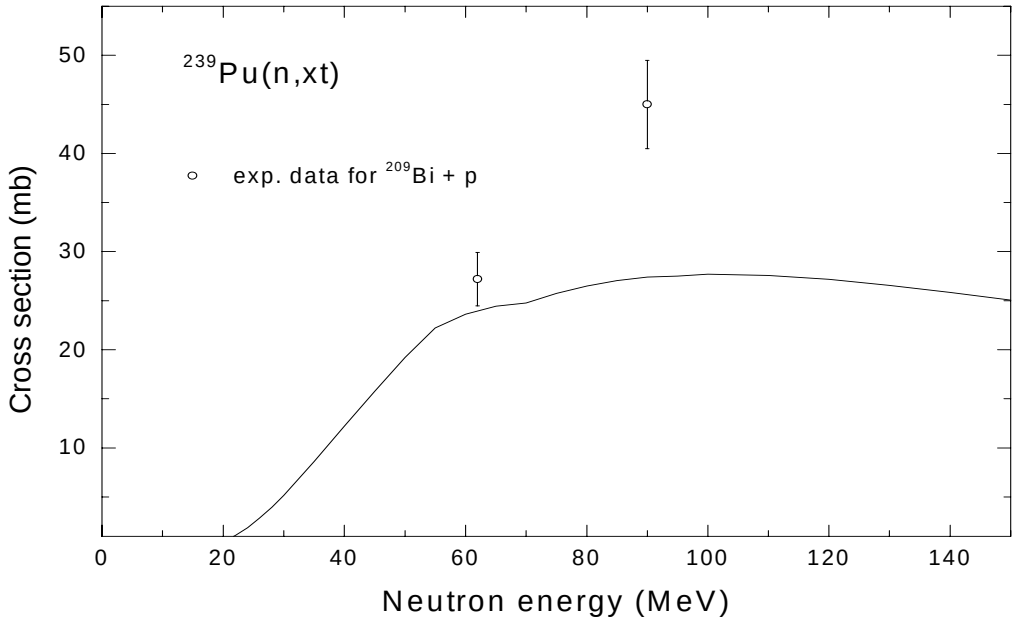

Fig. 17. The evaluated triton production cross section

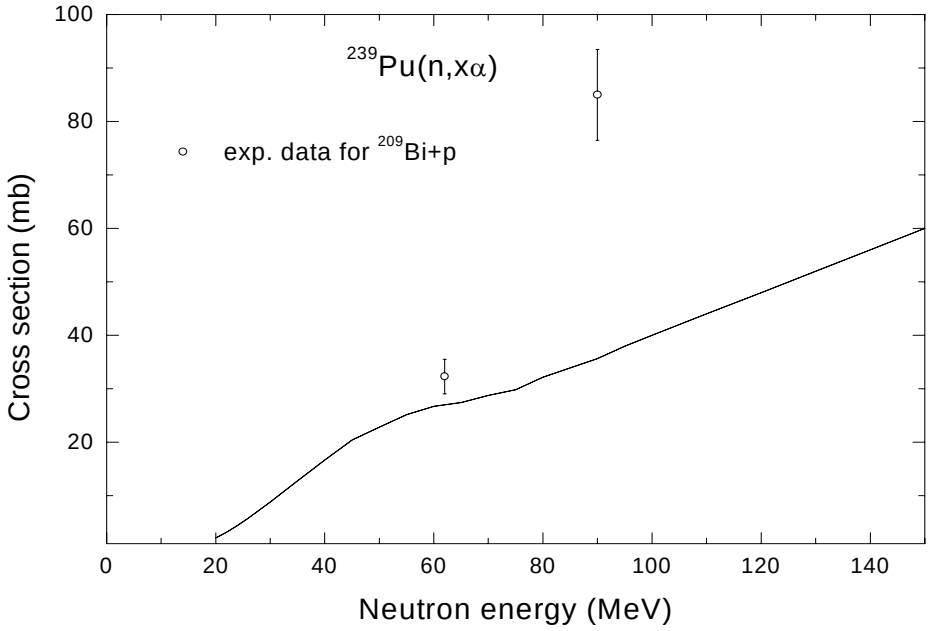

Fig. 18. The evaluated α-production cross section

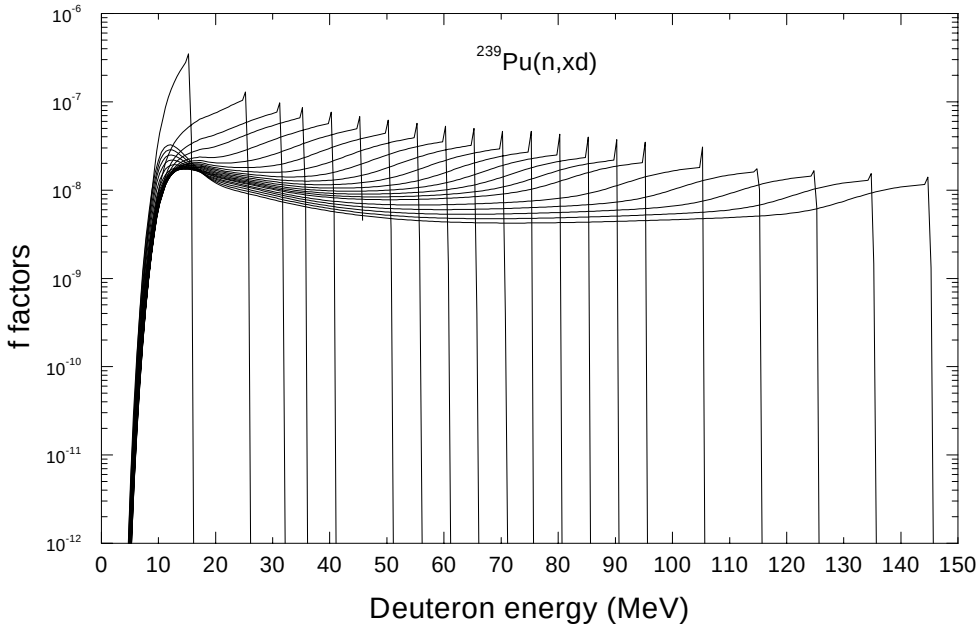

Fig. 19. Normalized secondary deuteron spectra for the incident neutron energies from 20 to 150 MeV

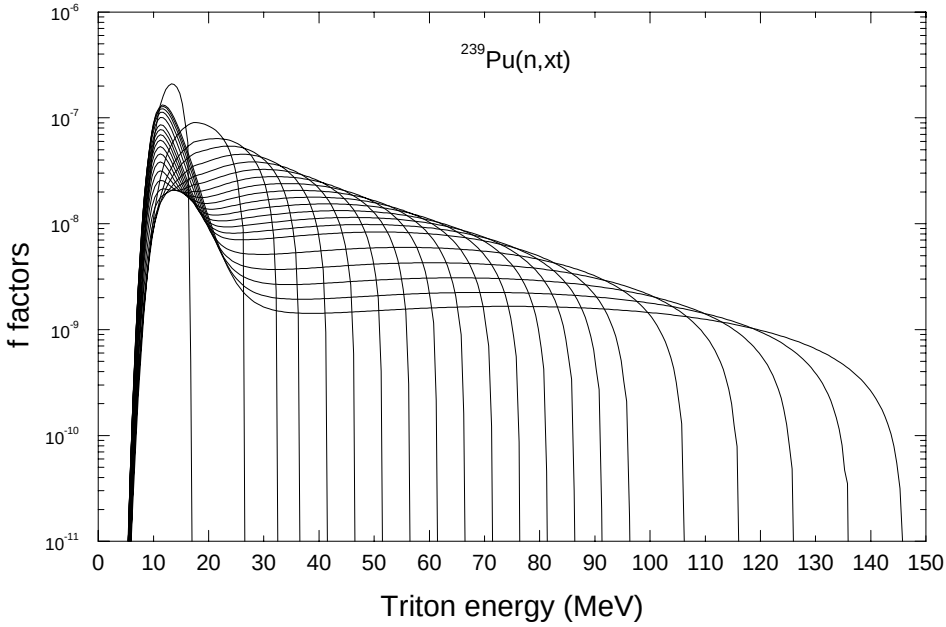

Fig. 20. Normalized secondary triton spectra for the incident neutron energies from 20 to 150 MeV

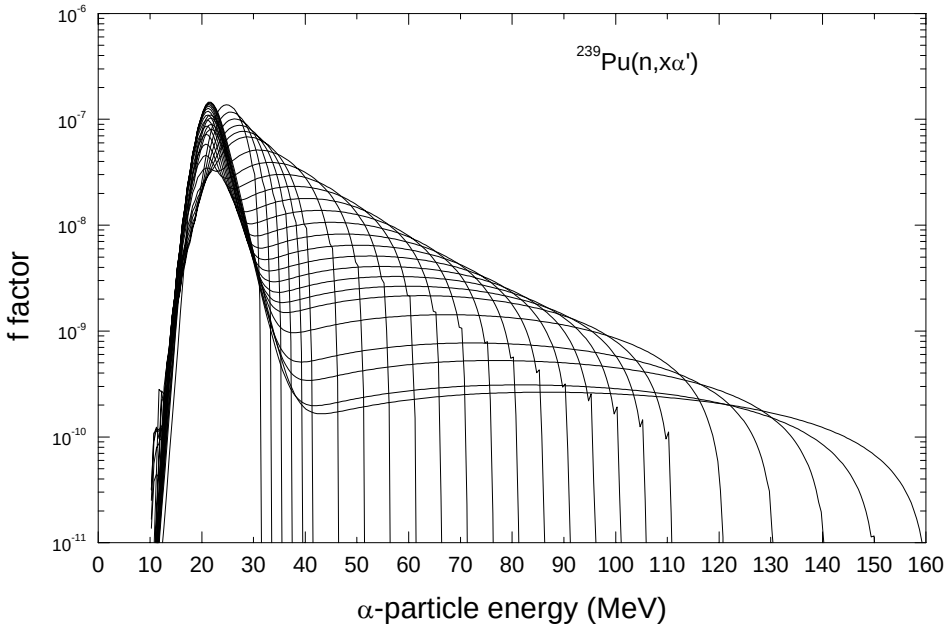

Fig. 21. Normalized secondary α-particle spectra for the incident neutron energies from 20 to 150 MeV

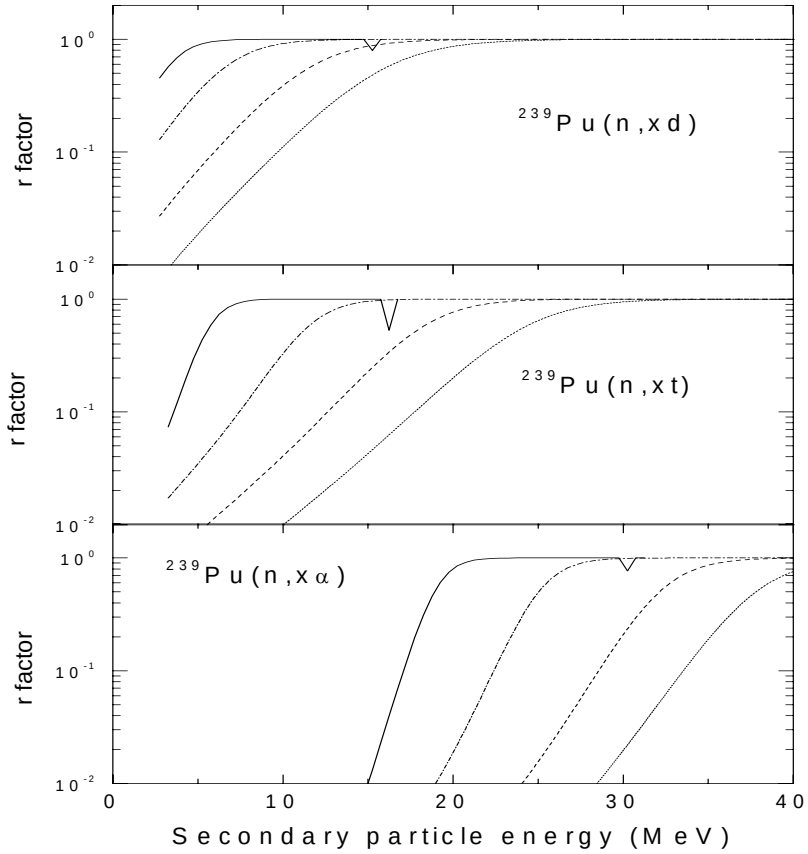

Fig. 22. Preequilibriuim components of the deuteron, triton and α-particle spectra for the incident neutron energies 20 MeV (solid), 50 MeV (dot-dashed), 100 MeV (dashed), and 150 MeV (dotted) curves.

REFERENCES

1. A.J.Koning, Requirements for an Evaluated Nuclear Data File for Accelerator Based Transmutation, Report NEA/NSC/DOC(93)6 and ECN-C-93-005; Nuclear Data Evaluation for Accelerator-Driven Systems, in Proc. Second International Conference on Accelerator-Driven Transmutation Technologies and Applications, Kalmar, Sweden, June 3-7, 1996, Vol. 1, p. 438, H. Condé, Ed., Gotab, Stockholm, Sweden (1997).
2. H.W.Bertini, Phys.Rev. 188, 1711 (1969).
3. T.W.Armstrong, K.C.Chandler, Nucl. Sci. Eng. 49, 110 (1972).
4. V.S.Barashenkov, V.D.Toneev, Interactions of High Energy Particles with Nuclei (Atomizdat, Moscow, 1972).
5. R.E.Prael, H.Lichtenstein, Users Guide to the LAHET Code System, Report LA-UR-89-3014, Los Alamos National Laboratory (1989).
6. M.B.Chadwick, P.G.Young, S.Chiba, S.C. Frankle, G.M. Hale, H.G. Hughes, A.J. Koning, R.C. Little, R.E. MacFarlane, R.E. Prael, and L.S. Waters, Nucl. Sci. Eng. 131, 293 (1999).
7. P.G.Young, E.D.Arthur, M.B.Chadwick, Comprehensive Nuclear Model Calculations: Theory and Use of the GNASH Code. in Proc.IAEA Workshop on Nuclear Reaction Data and Nuclear Reactors Trieste, Italy, 15 April - 17 May 1996, Vol. 1, p. 227, A.Gandini and G.Reffo Editors, World Scientific, Singapore (1998)
8. A.V.Ignatyuk, Level Densities. In: Reference Input Parameter Library for Nuclear Model Calculations - Handbook, IAEA - TECDOC-1034, Vienna, 1998, ch. 5.
9. L.F.Hansen, B.A.Pohl, C.Wong, R.C.Haight, Ch.Lagrange, Phys. Rev. C34, 2075 (1986).
10. V.A.Konshin, Calculations of Neutron and Proton Induced Reaction Cross Sections for Actinides in the Energy Region from 10 MeV to 1 GeV. Report JAERI-Research-95-036, Japan Atomic Energy Research Institute (1995).
11. P.G.Young, Optical Model Parameters. In Reference Input Parameter Library for Nuclear Model Calculations - Handbook, IAEA-TECDOC-1034, Vienna, 1998, ch. 4.
12. H.Vonach, A.Pavlik, M.B.Chadwick, R.C.Haight, R.O.Nelson, S.A.Wender, and P.G.Young, Phys. Rev. C50, 1952 (1994).
13. M.B.Chadwick, P.G.Young, GNASH Calculations of the Neutron and Proton Induced Reactions for Lead Isotopes and Benchmarking of Results. Report T-2-96, Los Alamos National Laboratory (1996).
14. V.S.Barashenkov, Cross Sections of Particle and Nucleus Interactions with Nuclei (Russian), JINR, Dubna, 1993.
15. F.Hansen, B.A.Pohl, C.Wong, R.C.Haight, Ch.Lagrange, Phys. Rev. C34, 2075 (1986).
16. R.L.Henkel, Report LA-1493, (1952)
17. K.A.Nadolny, K.A.Green, P.Stoler, Total Neutron Cross Section of 239-Pu. Preprint USNDC-9, 170 (1973)
18. J.M.Peterson, A.Bratenahl, J.P.Stoering, Phys.Rev. v.120 (1960) p.1252.
19. W.P.Poenitz, J.F.Whalen, Neutron Total Cross Section Measurements in the Energy Region from 47 keV to 20 MeV. Report ANL-NDM-80, (1983)
20. R.K.Smith, R.K.Henkel, R.A.Noble, BAP 2,(1957)
21. P.Staples, and K.Morley, Nucl.Sci.Eng. v.129 (1998) p.149.
22. K.,Kari and S.Cieriacks, Measurements of Neutron Induced Fission Cross Section Ratios at the Karlsruhe Isochronous Cyclotron. Report EANDC(E)-157, 8, BNL (1978)
23. P.W.Lisowski, J.L.Ullman, S.J.Balestrini, A.D.Carlson, O.A.Wasson, N.W.Hill, in: Proc. of Int. Conf. on Nuclear Data for Science and Technology. Mito, Japan, May 30-June 3. (Ed. I. Igarasi) (1988) p.97.
24. P.W.Lisowski et al., in Proc. Symp. on Neutron Cross-Sections from 10 to 50 MeV. Upton, 1980, Vol. 1, p.301; in Proc. Specialists' Meeting on Neutron Cross-Sections Standards for the Energy Region above 20 MeV (Uppsala, May 1991), NEANDC-305/U, p.177 (1991)
25. A.Yu.Donets, A.V.Evdokimov, A.V.Fomichev, T.Fukahori, A.B.Laptev, G.A.Petrov, O.A.Shcherbakov, Yu.V.Tuboltsev, A.S.Vorobyev, Neutron Induced Fission Cross-Sections of 233U, 235U, 238U, 232Th, 239Pu, and 237Np in the Energy Range 1 - 200 MeV. In: Proceedings of VII International Seminar on Interaction Neutrons with Nuclei, (Dubna, 1999, to be publ.)
26. A.V.Ignatyuk, G.A.Kudyaev, A.R.Junghans, M.deJong, M.G.Clerc, and K.H.Schmidt, Nucl. Phys. A593, 519 (1995).
27. J.Fréhaut, "Nu-bar Results at Bruyères-le-Châtel", Private communication to EXFOR-21685 (1976).
28. C.Kalbach, F.M.Mann. Phys. Rev. C23, 112 (1981).
29. J.Bojowald, H.Machner, H.Nann, W.Oelert, M.Rogge, and P.Turek, Phys. Rev. C38, 1153 (1988).
30. F.D.Becchetti Jr, and G.W.Greenlees, Ann. Rep. J.H. Williams Lab., Univ. Minnesota (1969).
31. V.Avrigeanu, P.E.Hodgson, and M.Avrigeanu, Phys.Rev. C49, 2255 (1994).
32. A.Iwamoto, K.Harada, Phys. Rev. C26, 1821 (1982).

33. A.I.Dityuk, A.Yu.Konobeyev, V.P.Lunev, Yu.N.Shubin, New Advanced Version of Computer Code ALICE-IPPE, Report INDC(CCP)-410, IAEA, Vienna (1998).
C.Kalbach, F.M.Mann, “Phenomenology of Continuum Angular Distributions. I. Syste-matics and Parameterization,” *Phys. Rev.* **C23,** 112 (1981).

UDC 539.173.84

SCISSION NEUTRON EMISSION AND PROMPT FISSION NEUTRON SPECTRUM.

Kornilov N.V.[*], *Kagalenko A.B.*
State Scientific Center of RF, Institute for Physics and Power Engineering,
Bondarenko Square 1, 249020 Obninsk, Russia

SCISSION NEUTRON EMISSION AND PROMPT FISSION NEUTRON SPECTRUM. The mass, energy and angular integrated spectra of prompt fission neutrons for ^{235}U induced fission in the energy range from thermal to 5 MeV were analyzed. It allows assume that about 0.362±0.025 neutrons per fission are emitted due to another mechanism then neutron emission from excited fragments after full acceleration. The spectrum of scission neutrons consists of two components with average energy 0.98 MeV and 2.74 MeV. The share of scission neutrons and their spectrum shape estimated in this work does not contradict to results of differential experiments analyzed in previous papers.

Introduction

In our papers [1,2] was shown that the experimental result of work [3] that was used as a main argument against existence of the scission neutrons (SCN), does not contradict to the experimental data of another works for ^{252}Cf [4-8] and for ^{235}U [9,10]. Analysis of the experimental results presented in last papers allows us to conclude that ~10–15% of SCN exist for thermal and spontaneous fission. In work [2] we estimated the properties of SCN for ^{252}Cf and ^{235}U as following:

- Total amount of SCN is ~0.4 n/fission;
- These neutrons have no isotropic distribution in the Laboratory System (LS);
- Angular integrated spectrum of SCN consists of two components which have different average energy.

In paper [2] from analysis of the experimental data of [9] it was fount that energy distribution of the SCN for ^{235}U at thermal energy can be described by equation 1:

$$\nu_{scn} N_{scn}(E) = \nu_{scn}\left[\omega_1 \frac{E}{T_1^{\,2}} \exp(-\frac{E}{T_1}) + (1-\omega_1)\frac{E}{T_2^{\,2}} \exp(-\frac{E}{T_2})\right], \qquad (1)$$

where ν_{scn}=0.38, ν_{scn}/ν=0.156, ω_1=0.657, T_1=0.49 MeV, T_2=1.37 MeV.

However, the experimental data for yield and spectrum shape of the SCN is rather scanty and cannot be applied for development of the detail model of SCN emission and for incorporation of this mechanism in neutron data evaluation. The energy spectrum and absolute yield of SCN for ^{235}U have been estimated on the basis work [9] only. So, the conclusion based on results of alone paper may be wrong due to some systematic errors. We do not know the dependence of SCN properties both on excitation energy of nucleus (neutron energy for induced fission) and on mass of fissile system. There is no theoretical model that may predict these properties.

[*] e-mail: kornilov@ippe.obninsk.ru

The SCN properties can be estimated for certain from differential experiments (see for example [3, 10]) in which the energy-angular distribution of fission neutrons have been measured in coincidence with fission fragments with selected mass and kinetic energy. However, these experiments can be carried out for limited amount of spontaneous and thermal induced fission. At the same time we have great amount of integral data for prompt fission neutron spectra (PFNS) for ^{235}U measured in the energy range from thermal point to the threshold of (n,nf) reaction. It seems that analysis of these data from this point of view (it never been done before) can be rather useful for estimation of the SCN emission existence. In any case it allow us to link differential and integral data and answer the question "does contradict the results of works [2, 9] (see eq.(1)) or not to the numerous integral spectra?". In addition, it may help to find any dependence of SCN properties on incident neutron energy and check new way for PFNS evaluation with an incorporation of the SCN emission.

1. Model used for experimental data evaluation

1.1 Neutron spectrum in the LS

The prompt fission neutron spectrum taking into account SCN emission can be described by the following equation:

$$\nu N(E) = \sum_i \nu_i Y_i F_i(E) + \nu_{scn} N_{scn}(E) \quad , \tag{2}$$

where $F_i(E)$ is the LS spectrum of neutrons emitted from moving fragment, Y_i is the yield of the fragment with mass A_i, and ν_i is total amount of emitted neutrons. The second term is connected with scission neutron emission. According to our assumption that should be checked, this term can be described by eq.(1).

If the hypothesis of Neutron Emission After Fragment Acceleration (NEAFA) is true, the $F_i(E)$ functions can be calculated with following relations:

$$F_i(E) = \int_{-1}^{1} F_i(E,\mu)d\mu, \; F_i(E,\mu) = \frac{\sqrt{E}}{2\sqrt{\varepsilon}}\Phi_i(\varepsilon), \;\; \varepsilon = E + E_{vi} - 2\mu\sqrt{EE_{vi}}$$
$$E_{vi} = TKE\frac{A - Ai}{A_i A} \tag{3}$$

where E_{vi} is fragment Center of Mass Energy (CMS) per nucleon, TKE – total kinetic energy of fragment after full acceleration, μ – cosine of angle between fragment and neutron, ε – neutron energy in CMS, and $\Phi(\varepsilon)$ – neutron spectrum in the CMS. Assuming that the neutrons are emitted isotropically and carrying out the variables transformation from μ to ε one can write the general formula for the LS spectrum calculation:

$$F(E) = \frac{1}{4\sqrt{E_v}} \int_{\left(\sqrt{E}-\sqrt{E_v}\right)^2}^{\left(\sqrt{E}+\sqrt{E_v}\right)^2} \Phi(\varepsilon)\frac{d\varepsilon}{\sqrt{\varepsilon}} \tag{4}$$

This formula is applied for the PFNS calculation in any theoretical models [11-14] that differ only by the methods and proper relations for $\Phi(\varepsilon)$ estimation.

1.2 CMS neutron spectrum.

As a rule the model of cascade neutron evaporation from excited fragment is used for the CMS spectrum calculation.

The very simple analytical relations for the LS spectrum shape can estimate if one assumes that $\Phi(\varepsilon)$ is:

$$\Phi(\varepsilon) = \frac{\varepsilon^{\lambda}}{\Gamma(\lambda+1)T^{\lambda+1}}\exp(-\frac{\varepsilon}{T}) \qquad (5)$$

The well-known Watt formula can be found if one assume that λ=0.5 (Maxwellian spectrum in the CMS). This assumption is supported by direct calculation presented in [15]. In frame of cascade evaporation model it was shown that λ=5/11.

In work [12] (see also references in this paper) used the assumption that the spectrum of each neutron in the cascade can be described by eq. (5) with λ=1 and multiple neutron emission can be simulated by an incorporation of triangle distribution of the fragment "temperatures":

$$P(T) = \begin{cases} 2T/T_m^2, T \le T_m \\ 0, \qquad T > T_m \end{cases}$$

In this case the CMS spectrum can be estimate by equation:

$$\Phi(\varepsilon, T_m) = \int_0^{T_m} P(T)\Phi(\varepsilon, T)dT = \frac{2}{T_m^2}\int_0^{T_m}\frac{\varepsilon}{T}\exp\left(-\frac{\varepsilon}{T}\right)dT. \qquad (6)$$

After the variable transformation $u=\varepsilon/T$, the following closed-form expression can be found:

$$\Phi(\varepsilon, T_m) = \frac{2\varepsilon}{T_m^2}\int_{u_m}^{\infty}\frac{e^{-u}}{u}du = \frac{2\varepsilon}{T_m^2}E_1(u_m), \quad u_m = \frac{\varepsilon}{T_m} \qquad , \qquad (7)$$

where $E_1(x)$ is the exponential integral. The mean energy is given by $<\varepsilon>=4/3T_m$.

As was shown in [12], the corresponding LS neutron spectrum of one of the fragments may be described as following:

$$F(E) = \frac{1}{3(E_v T_m)^{1/2}}\left[u_2^{3/2}E_1(u_2) - u_1^{3/2}E_1(u_1) + \Gamma(3/2, u_2) - \Gamma(3/2, u_1)\right], \qquad (8)$$

$$u_2 = \left(\sqrt{E}+\sqrt{E_v}\right)^2/T_m,\ u_1 = \left(\sqrt{E}-\sqrt{E_v}\right)^2/T_m$$

where $\Gamma(x,u)$ is the incomplete gamma-function.

In work [16] for ^{252}Cf it was shown that function (7) describes the experimental CMS spectra some better then Maxwellian. The similar conclusion was made for ^{235}U in [2] on the basis of experimental data from paper [9]. As one can see in Fig.1 function (7) some better agree with experimental data. In this study we used expression (7,8) for the experimental data analysis.

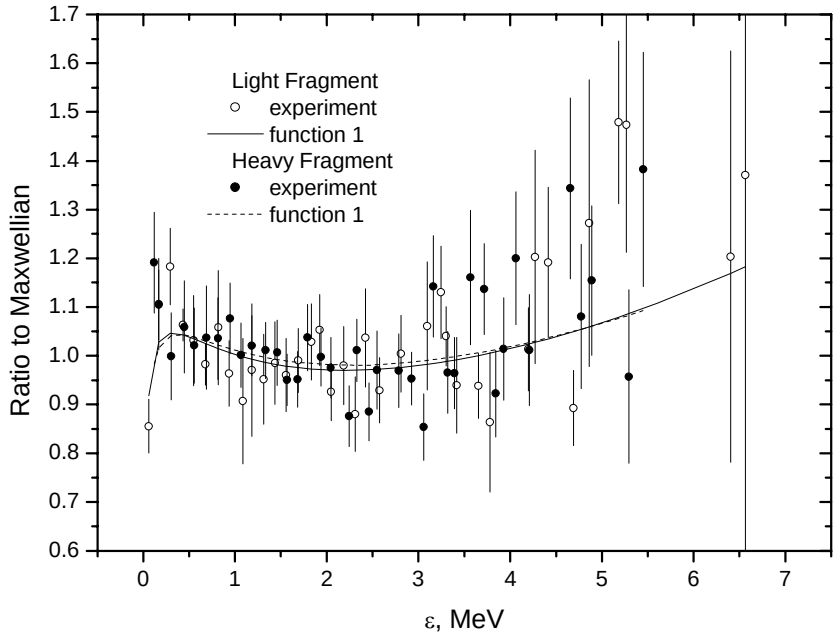

Fig. 1 Ratio of the CMS neutron spectra to Maxwellian. Points are experimental data, lines give the results calculated with eq. (7). Open symbols and solid line show the data for "light" fragment, filled circle and dashed line for "heavy" fragment.

1.3 Model parameters.

The detail description of the PFNS with eq. (2) requires too many parameters that complicate data evaluation. In the same time in several papers (see for example [17]) it was shown that application of the "two fragment model" did not change very much the spectrum shape. Having in mind this conclusion we used more simple expression for our study:

$$N(E) = (1-\omega_{scn})[\omega_l F_l(E) + \omega_h F_h(E)] + \omega_{scn} N_{scn}(E) \quad , \qquad (9)$$

where the indices *l,h* denote "light" and "heavy" fragments.

This simplification used in many papers for PFNS evaluation [12, 13, 16]. In our previous systematic of the experimental data we applied similar relation but assumed that contribution of the SCN is small ω_{scn}=0. In framework of this model we also could describe the experimental PFNS, but we be obliged to reduce the CMS energy (E_{vi} values) and incorporate different "temperature" for "light" and "heavy" fragment. So the proper adjusting of the model parameters may compensate the absence of an additional source of neutrons. To avoid ambiguity and reduce the influence of the model parameters on the final conclusion we carried out an additional evaluation of the average neutron energy from light and heavy fragments estimated from differential experiments.

The data for ^{233}U, ^{235}U and ^{252}Cf are collected in Table 1. Nucleus target masses and references are given in the first column. In the second one – masses for "light" and "heavy" fragments. The average neutron multiplicity, experimental mean neutron energy, and level

density parameter are given in the following columns. The total neutron multiplicity $\nu = \nu_l + \nu_h$ were re-normalized to standard values from [18]. The data from [9] for ^{235}U was also re-calculated in [2] taking into account the SCN emission. This data was denotes as (Skarsvag-Kornilov). The same procedure was applied for data from [3] and [4]. Level density parameter was taken from paper [7].

Table 1.

Experimental and evaluated data for the CMS mean neutron energies.

Ядро	$<A_{l,h}>$	$<\nu_{l,h}>$	$<\varepsilon>_{exp}$, MeV	a, 1/MeV	$C_{l,h}$	$<\varepsilon>_{cal}$, MeV
^{233}U	94	1.395	1.24	9.44	2.777	1.310
[19]	140	1.100	1.19	11.15	3.143	1.276
	94		1.17		2.605	r=1.03
^{233}U [20]	140		1.20		3.157	
^{235}U [21]	96	1.390	1.31	10.02	3.019	1.270
	140	1.047	1.43	11.15	3.830	1,278
^{235}U (Skarsvag - Kornilov)	96		1.18		2.708	r=1.01
	140		1.36		3.639	
^{252}Cf [3]	109	2.056	1.51	11.70	3.228	1.367
	143	1.710	1.31	13.01	3.179	1.390
^{252}Cf [3, 2]	109		1.45		3.112	r=0.98
	143		1.37		3.322	
^{252}Cf [4, 2]	109		1.29		2.762	
	143		1.31		3.181	
^{252}Cf [7]	109		1.49		3.183	
	143		1.46		3.531	

$<C_l>$=2.924±0.223 (7.7%), $<C_h>$=3.373±0.245 (7.3%)

The average energy uncertainties given in the references are ~30 keV. However, real data spread is much higher (see table 1) that complicate data evaluation. It is even not clear which fragment (“light” or “heavy”) does emit more energetic neutrons. The average value $<r>$ and mean-square spread for ratio of neutron energies emitted from “light” and “heavy” fragments is $<r>$=1.00±0.08. This simple comparison allows us to conclude that mean energies are equal. However, the data spread is rather high and it may be connected not only with data uncertainties. Fragment excitation energy is the main factor that provides the neutron energy and changes very much from uranium to californium isotopes. So, it seems reasonable to take into account this factor.

The mean neutron energy according to formula (5) is $<\varepsilon>=(1+\lambda)T$. Having in mind that “temperature” T is connected [12] with U excitation energy of fragment by formula $U=aT^2$ and U value with total amount of emitted neutrons as $U=B(\nu+0.5)$, (B – binding energy) one can re-write the equation for mean neutron energy as following:

$$<\varepsilon>=C\sqrt{(\nu+0.5)/a} \qquad (10)$$

One may assume also that λ и B are different for "light" and "heavy" fragments but the same for all fissile isotopes. This assumption allows us to calculate the average C - values separately for each fragment.

The calculated C_i values, their average values $<C_{l,h}>$ and mean-square spread are presented in the Table 1. The mean neutron energy calculated with eq. 10 on the basis of $<C_{l,h}>$ is given in last column of Table 1. The analysis given above reveals some tendency for neutron energy. But the difference between data for U and Cf is small. So, one may conclude that neutrons emitted from "light" and "heavy" fragments have the same average energy inside the ≤8% uncertainty.

Now we can estimate the model and its parameters:

- The PFNS spectrum is described by eq. (9) with equal "temperature" for both fragments $T_{ml}=T_{mh}=T_m$. The same assumption used in all model (see for example [12]) which was arrived if the fissile system is in statistical equilibrium;
- The spectrum of the SCN may be calculated by eq. (1) for any neutron incident energy;
- The contribution of neutron from fragments are ω_l=0.577, ω_h=0.423 and also were fixed for all input energies;
- The E_v parameters was calculated as it was given in work [16];
- Free parameters – T_m и ω_{scn} were adjusted by least square method.

2. Results and discussions.

In this paper we used practically the same data set as in our work [16]. For thermal point the spectra were taken from works [22-25]. According to [26], these data do not contradict to each other, so after the proper normalization [26] it was treated as one experimental spectrum at thermal energy. The data at higher incident energies were taken from papers [27-30]. All spectra were normalized to unity assuming that PFNS shape can be described by formula given in work [16].

The share of the SCN ω_{scn}, temperature parameter T_m and χ^2 values for one experimental point are presented in Table 2. Errors of fitted parameters were estimated by least square method assuming the independence of the experimental points.

Table 2.

Parameters of the SCN spectrum.

References	E_0, MeV	$\omega_{scn}\pm\delta\omega_{scn}$	$T_m\pm\delta T_m$, МэВ	χ^2
[22, 23, 24, 25]	0	0.152±0.003	0.924±0.001	1.28
[27]	0.53	0.135±0.016	0.949±0.005	0.38
[28]	0.5	0.199±0.023	0.955±0.016	0.52
[29]	0.5	0.033±0.022	0.955±0.005	0.46
[29]	1.5	0.112±0.024	0.955±0.006	0.49
[29]	2.5	0.124±0.030	0.988±0.007	0.64
[30]	2.9	0.110±0.009	0.974±0.009	0.42
[29]	3.5	0.095±0.045	1.027±0.008	0.80
[28]	5.0	0.123±0.020	1.025±0.013	0.55

The average value $<\omega_{scn}>$ and mean-square spread for share of the SCN emission is $<\omega_{scn}>=0.12\pm0.04$. It does not contradict (in the limits of the experimental errors) to the data estimated from differential experiments [2, 9].

The PFNS for thermal energy is given in Figs. 2,3. As one can see in these figures the incorporation of the SCN emission in the model improves the quality of the experimental data description and removes the typical disagreement between experiment and NEAFA model at low fission neutron energy <2 МэВ. The contribution of the SCN in the total PFN spectrum is as much as ~30% (see Fig.3). The some results for higher energy are shown in Figs. 4–7. All data in Fig. 1-7 are plotted as a ratio to Maxwellian with the same average energy.

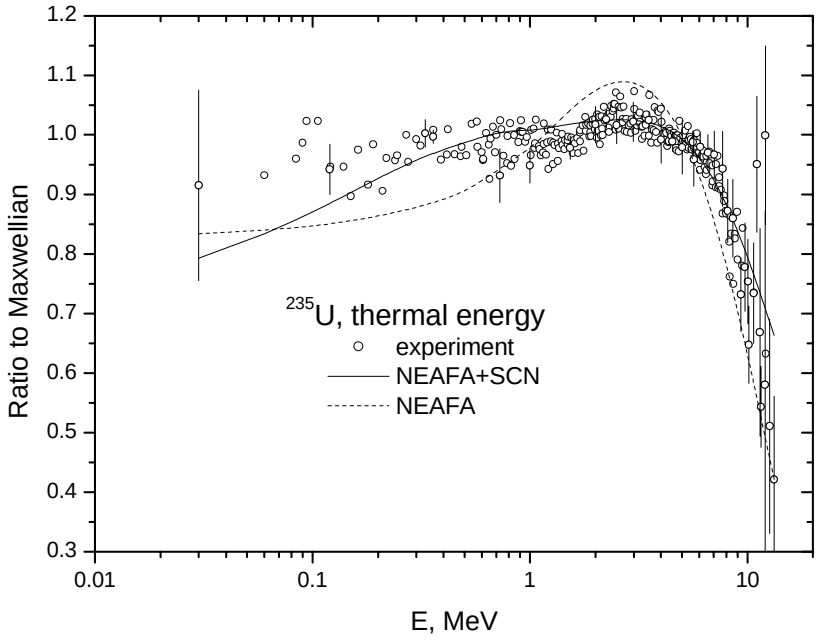

Fig 2. The PFNS for thermal energy. Points are experimental data from works [22–25]. Lines show the calculated results with the incorporation of the SCN emission (solid line, $\chi^2=1.28$) and without SCN (dashed line, $\chi^2=7.9$).

The dependence of the SCN yield (if it exists) was estimated by the following way. Two assumption have been studied: 1) the share of the SCN is constant $\omega_{scn}=\nu_{scn}/\nu=const$ and 2) absolute yield of the SCN is constant $\nu_{scn}=\omega_{scn}*\nu=$const. The weighted average values $<\omega_{scn}>$ and $<\nu_{scn}>$ were calculated for comparison. The weights were found from parameter uncertainties given in Table 2 as $1/\delta\omega^2$. The data of work [29] that deviates from bulk of the data was not taken into account. The total number of the PFN $\nu(E_0)$ was taken from ENDF/B–VI evaluation. It was found that $<\omega_{scn}>=0.145\pm0.015$ (11%), and $<\nu_{scn}>=0.362\pm0.025$ (7%). The second assumption ($\nu_{scn}=const$) it seems more realistic because of it reduces the data spread to ~1.5 times.

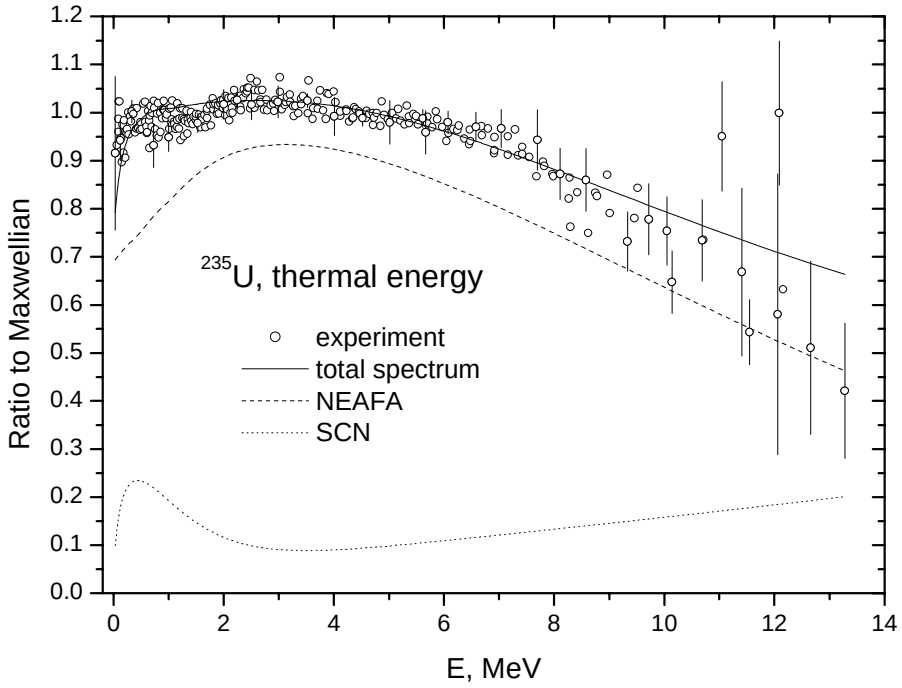

Fig.3. The same as in Fig.2. Solid line shows the total PFNS with the SCN emission. Dashed line gives the neutron spectrum from fragments only, dotted line shows the spectrum of the SCN.

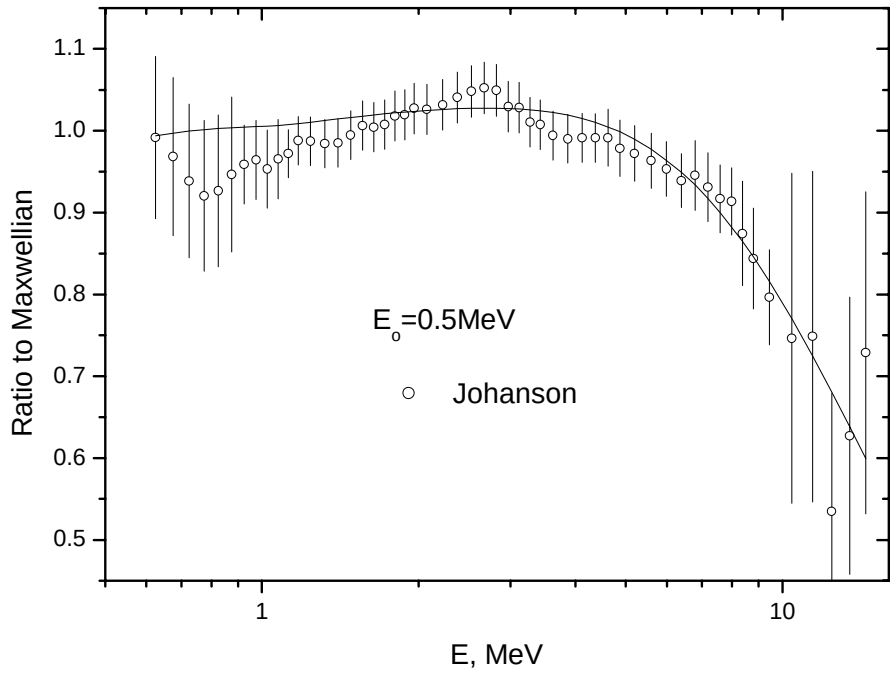

Fig.4 The ratio of the experimental data from work [27] (points) and calculated spectrum with fitted parameters from Table 2 (line) to Maxwellian.

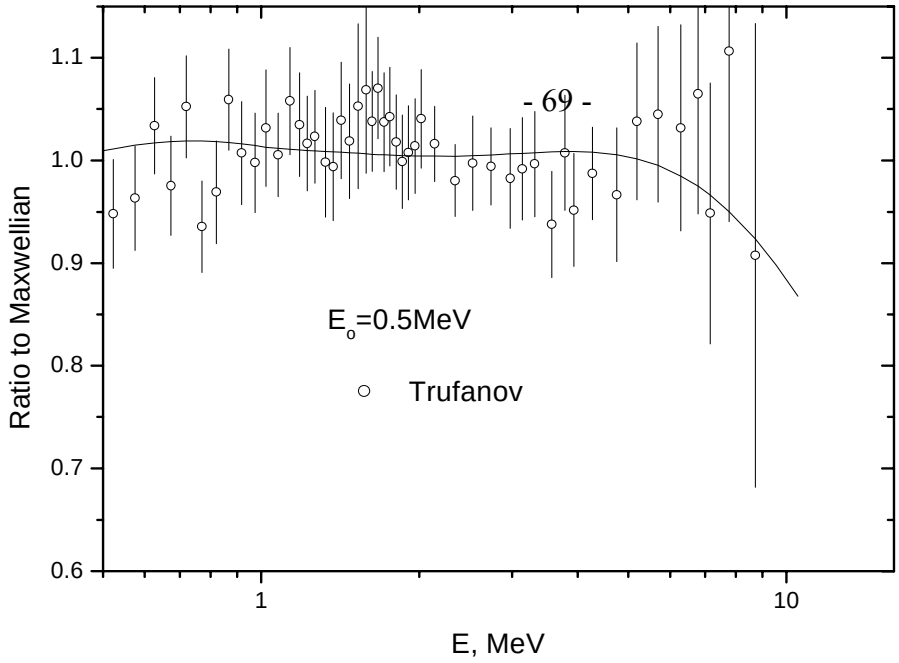

Fig. 5 The same as in Fig. 4 for data from work [28] at incident energy 0.5 MeV.

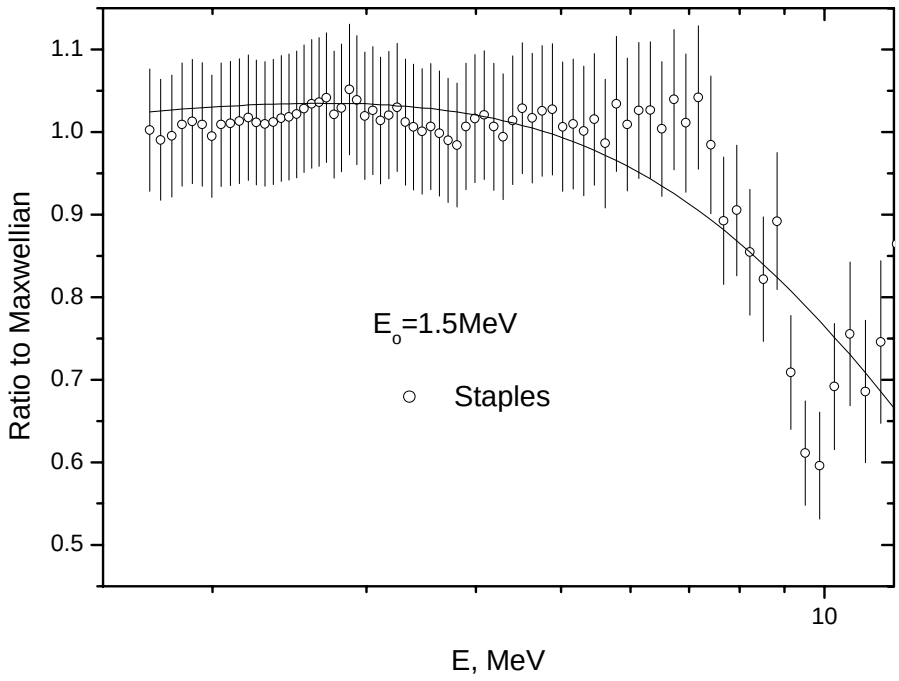

Fig. 6 The same as in fig. 4 for data from [29] at incident energy 1.5MeV.

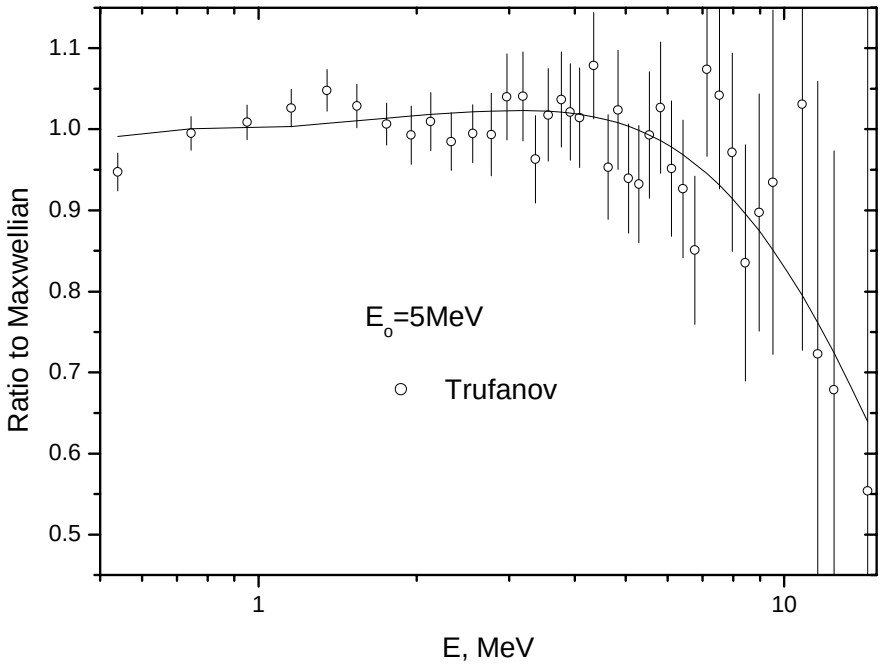

Fig. 7 The same as in fig. 4 for data from [28] at incident energy 5.0 MeV.

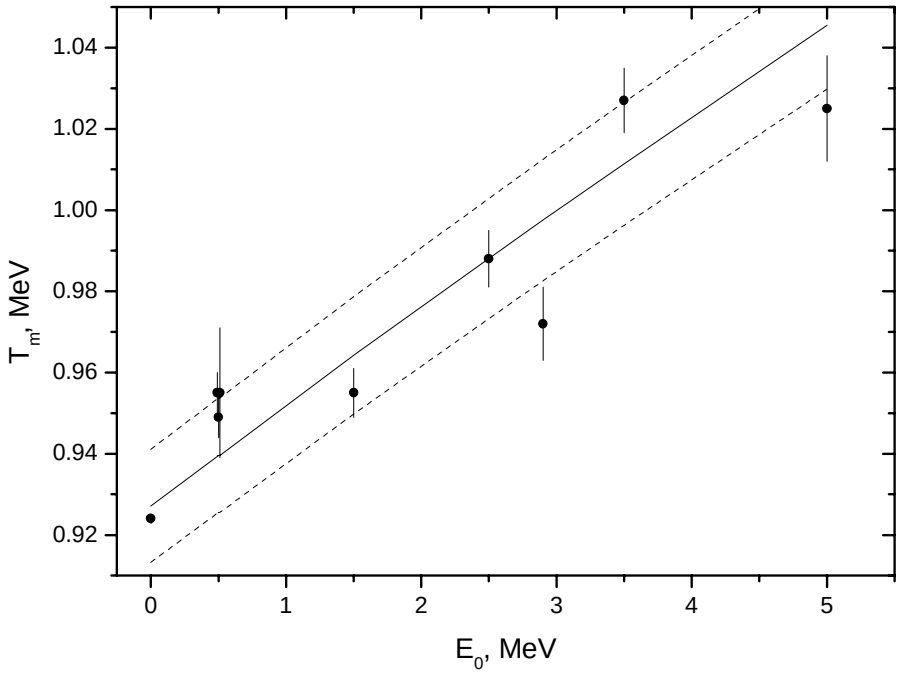

Fig.8 Fitted parameters T_m versus input energy of neutrons. Solid line shows the square root dependence. Dashed lines give uncertainty of the calculation of the curve (see text).

The Maxwellian shape was also applied for the PFNS calculation. In this case ω_{scn}=16.2% (χ^2=1.4) was found at the thermal point. This result may help to estimate the error for the SCN yield calculation due to the uncertainty of spectrum shape in the CMS as ~10%.

The assumption $T_{ml}=T_{mh}=T_m$ has very strong influence on the result. As one can see in Table 1, the spread of "temperature" ratio is ±15%. So, we fitted parameters ω_{scn} and T_m for $r=\langle\varepsilon_l\rangle/\langle\varepsilon_h\rangle$=1.15 and r=0.85. The values ω_{scn}=0.099 (χ^2=1.27) and ω_{scn}=0.193 (χ^2=1.46) were found for given before r parameters.

According to eq. (10), the T_m parameter should depends on excitation energy $U=E_r-TKE+B+E_0$ as the rood square. As one can see in Fig. 8 this dependence is valid with accuracy ~1.5%: $T_m = (0.201 \pm 0.003)\sqrt{U}$ for energy range from U ~ 21 MeV to U ~ 27 MeV.

The mean neutron energy for thermal fission estimated in framework of this model with fitted parameters ω_{scn} и T_m is $\langle E\rangle$=1.979±0.015 МэВ. Inside the estimated error this value is equal to experimental data $\langle E_{exp}\rangle$=1.977±0.008 МэВ evaluated in work [26].

So, on the basis of results presented in this paper one may conclude:

- The incorporation of an additional neutrons (scission neutrons) which have the energy spectrum described by eq. (1) with average energies 0.98 MeV и 2.74 MeV estimated from differential experiments does not contradict in total to the integral PFNS data for ^{235}U fission;

- There is some evidence that the SCN yield does not depends on incident neutron energy and is equal to 0.362±0.025 n/fission for ^{235}U in the energy range from thermal to 5 MeV.

We are grateful to I. Kimura and K. Nishio for supplying us with experimental data.

References

1. Kornilov, N.V., Kagalenko, A.B., Hambsch, F.-J. Preprint **FEI-2763**, Obninsk, Procceedings of **ISINN-7**, Dubna, p.241, (1999), Nuclear Physics **A686**, p.187, 2001.
2. Kornilov, N.V., Kagalenko, A.B., Hambsch, F.-J. Physics of Atomic Nuclei, **64(8)**, 1372, 2001.
3. Budtz-Jørgensen, C., Knitter, H.-H. Nuclear Physics **A490**, 307, 1988.
4. Bowman, H.R., Milton, J.C.D. et al. Physical Review **126**, 2120, 1962.
5. Riehs, P. Acta Phys. Austriaca **53**, 271, 1981.
6. Piksaikin, V.M. et al. Journal of Nuclear Physics **25(4)**, 723, 1977.
7. Seregina, E.A., Djatchenko, P.P. Journal of Nuclear Physics, 42, 6(12), (1985),1337; 43, 5, (1986), 1092.
8. Seregina, E.A. Measurements and Analysis of Angular-Energy Distribution for ^{252}Cf(SF) neutrons, PhD Thesis, 1985, Obninsk).
9. Skarsvag, K., Bergheim, K. Nuclear Physics **45**, 72, 1963.
10. Samant, M.S., Anand, R.P., et al. Physical Review **51(6)**, 3127, 1995.
11. Watt, B.E. Physical Review **52**, 1037, 1952.
12. Madland, D.G., Nix, J.R. Nuclear Science and Engineering **81**, 213, 1982.
13. Marten, H., Seeliger, D. Proceeding of the Advisory Group Meet. On Nuclear Standard Ref. Data, Geel, Belgium, 1984, **IAEA-TECHDOC-335**, Vienna, 255, 1985.
14. Gerasimennko, B.F., Rubchenia, V. A. Atomic Energy **59**, 335, 1985.
15. Le Couter, K.J., Lang, D.W. Nuclear Physics **13**, 32, 1959.
16. Kornilov, N.V., Kagalenko, A.B., Hambsch, F.-J. Journal of Nuclear Physics, **62(2)**, 173, 1999.
17. Madland, D., LaBauve, R.J., Nix, J.R. In: Lemmel, H.D. (Ed), Proceedings of Consultant Meeting., Mito City, Japan, 1988; **INDC(NDS)-220**, Vienna, p.259, 1989.
18. Nuclear Standards for Nuclear Measurements. In: Conde, H. (Ed.), NEANDC-311U, **INDC(SEC)-101**, OECD, 1992.
19. Kimura, I., Nishio, K., Nakagome, Y. J. Nuclear Science and Technology **35**, 631, 1998.
20. Milton, J.C.D., Frezer, J.S. Symposium on the Physics and Chemistry of Fission, IAEA, **2**, 39, 1965.
21. Nishio, K., Nakagome, Y. et al. Nuclear Physics **A632**, 540, 1998.
22. Starostov, B.I. Neutron Physics (6-th All Union Conference for Neutron Physics, Kiev, USSR, 1983), **2**, 285, 290, 294, (1984), EXFOR 40871, 40872, 40873.
23. Lajtai, A. et. al. **IAEA-TECDOC-335**, 312, 1985, EXFOR 30704,
24. Yufeng, W. et al. Chinese Journal for Nuclear Physics **11**, 47, 1989, EXFOR 32587.
25. Abramson, D. Neutron Physics (2-nd All Union Conference for Neutron Physics, Kiev, USSR, 1973), **3**, 47, (1974), EXFOR 20997.
26. Kornilov, N.V., Kagalenko, A.B., et al. Proceedings of **ISINN-6**, Dubna, p.242, 1998.
27. Johanson, P.I., Holmquist, B. Nuclear Science and Engineering, **62**, 695, 1977.
28. Trufanov, A.M., Lovchikova, G.N. et. al. Physics of Atomic Nuclei **57**, 572, 1994.
29. Staples, P., Egan, J.J. et al. Nuclear Physics **A591**, 41, 1995.
30. Boykov, G.S. et al. Journal of Nuclear Physics, **53**, 628, 1991, EXFOR 41110, 41094.

THE CONSTANTS AND PARAMETERS OF NUCLEAR STRUCTURE AND NUCLEAR REACTIONS

02-11288 (150) [2]
Translated from Russian

UDC 539.17

TRANSMUTATION OF ^{204}Pb IN AN INTENSIVE GAMMA-RAY FLUX

B.S. Ishkhanov, S.I. Pavlov

TRANSMUTATION OF ^{204}Pb IN AN INTENSIVE GAMMA-RAY FLUX. Transmutation chain formation during irradiation with various intensities of bremsstrahlung photon beam is analysed. The main features of transmutation chain formation by photons with energies corresponding to the giant dipole resonance are discussed.

Introduction

The study of the transmutation of atomic nuclei by intensive γ-radiation fluxes with an energy of up to 30 MeV is of interest for solving a wide range of fundamental and applied problems. The total cross-section for interaction of γ-rays with atomic nuclear in this energy region is determined as the sum of the cross-sections of the following main reaction channels:

$$\sigma(\gamma,tot) = \sigma(\gamma,p) + \sigma(\gamma,n) + \sigma(\gamma,2n).$$

For heavy nuclei (A > 150), the main reaction channels are (γ,n) and (γ,2n). The total contribution from the remaining reaction channels for heavy nuclei usually does not exceed a few percent. The (γ,n) and (γ,2n) reaction channels comprise 70-80% and 20-25% respectively of the total γ-ray absorption cross-section. The (γ,p) reaction channel does not exceed a few percent [1-4].

The aim of this paper is as follows:

- To investigate the roles of the (γ,2n) reaction channel in the formation of transmutation chains;
- To study the effect of the γ-ray flux intensity on the transmutation of atomic nuclei.

Increasing the intensity of the γ-ray flux should have the following two effects:

- As the γ-ray flux intensity increases, there should be more intensive burnup of the initial isotope and formation of a larger number of radioactive nuclei;
- As the γ-ray flux intensity increases, isotopes with a shorter half-life should become involved in the transmutation process.

However, it is practically impossible to predict in specific terms what the effect will be of increasing the γ-ray flux intensity, as this is heavily dependent on the relationship between the γ-ray flux intensity and the half-lives of the radioactive isotopes formed.

This study was performed using the numerical modelling method. A program package was developed which automatically constructs transmutation chains and calculates the evolution over time of the number of nuclei formed for exposure of an arbitrarily selected initial nucleus to an intensive γ-radiation flux [3].

The isotope ^{204}Pb was chosen as the initial isotope. This nucleus was chosen for the following reasons. It is the lightest stable isotope of lead (Z = 82). All lead isotopes formed by the (γ,n) and (γ,2n) reactions are β^+-radioactive, and therefore one can fairly reliably study the evolution of the transmutation chain relative to the γ-ray flux intensity.

1. Calculation method

The evolution over time of the quantity of each element in the transmutation chain (A,Z) is determined by its accumulation and decay processes. A reduction in the content of the isotope (A,Z) occurs in the α- and β-decay processes, and as a result of the (γ,n), (γ, 2n) and (γ,p) reactions. Accumulation occurs as a result of photonuclear reactions on neighbouring nuclei, and α- and β-decay of neighbouring nuclei from which the isotope in question (A,Z) may be formed (see Fig. 1).

The evolution over time of the number of nuclei *N(A,Z;t)* of the isotope (A,Z) is determined using the following equation:

$$\begin{aligned}\frac{dN(A,Z;t)}{dt} = -\big[&\lambda^{\beta^-}(A,Z) + \lambda^{\beta^+}(A,Z) + \lambda^{\alpha}(A,Z) + \\ &+ Y^{(\gamma,n)}(A,Z) + Y^{(\gamma,2n)}(A,Z) + Y^{(\gamma,p)}(A,Z)\big] \times N(A,Z;t) + \\ &+ \big\{\lambda^{\beta^-}(A,Z-1) \times N(A,Z-1;t) + \lambda^{\beta^+}(A,Z+1) \times N(A,Z+1;t) + \\ &+ \lambda^{\alpha}(A+4,Z+2) \times N(A+4,Z+2;t) + Y^{(\gamma,n)}(A+1,Z) \times N(A+1,Z;t) + \\ &+ Y^{(\gamma,2n)}(A+2,Z) \times N(A+2,Z;t) + Y^{(\gamma,p)}(A+1,Z+1) \times N(A+1,Z+1;t)\big\}.\end{aligned} \tag{1}$$

The term in square brackets in differential equation (1) describes the destruction of the isotope (A,Z) in α- and β-decay processes and in the photonuclear reactions (γ,n), (γ,2n) and (γ,p). The term in braces describes the formation of the isotope (A,Z) in α- and β-decay processes and in the (γ,n), (γ,2n) and (γ,p) reactions of the relevant nuclei.

The equation contains the following parameters:

$\lambda^i(A,Z)$ - decay constant of the nucleus (A,Z) for the channel *i*, where *i* stands for α, β^- and β^+ decays;

$Y^j(A,Z,E_{\gamma m})$ - yield of a photonuclear reaction on the isotope (A,Z) determined using the following equation:

$$Y^{j}(A,Z,E_{\gamma m}) = \Phi \int_{E_{\min}}^{E_{\gamma m}} W(E,E_{\gamma m})\sigma^{j}(E;A,Z)\,dE \quad , \qquad (2)$$

where *j* corresponds to the (γ,n), (γ,2n) and (γ,p) channels;

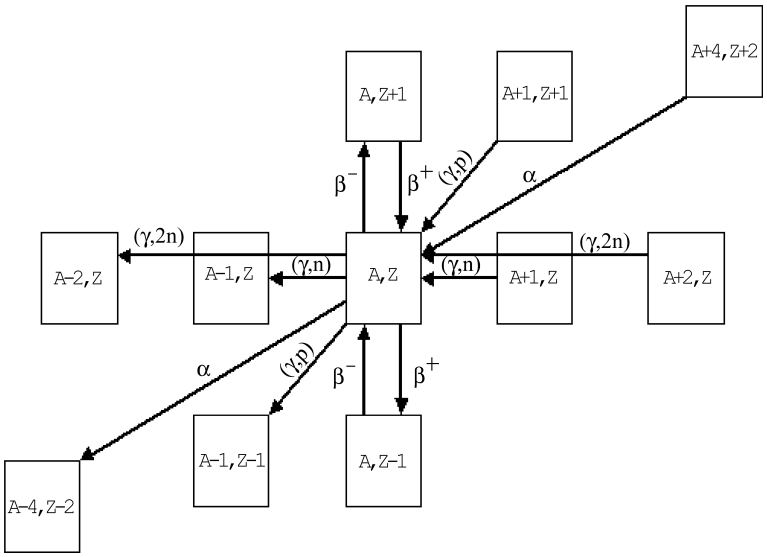

Fig. 1. Processes which determine the evolution over time of the isotope (A,Z)

$\Phi\left(\frac{\text{photon}}{\text{s}\times\text{cm}^2}\right)$ - flux density of the photons irradiating the target;

$\sigma^{j}(E;A,Z)$ - partial cross-section of the photonuclear reaction *j*, where *j* stands for the (γ,n), (γ,2n) and (γ,p) photonuclear reaction channels on the nucleus (A,Z);

$W(E,E_{\gamma m})$ - γ-bremsstrahlung spectrum normalized to 1:

$$\int_{E_{\min}}^{E_{\gamma m}} W(E,E_{\gamma m})\,dE = 1 \qquad (3)$$

Integration is performed in expressions (2, 3) in the nucleus excitation energy region from E_{min} (set at 5 MeV, which corresponds to the minimum photonuclear reaction threshold values) to the upper boundary of the gamma bremsstrahlung spectrum $E_{\gamma m}$.

The γ-bremsstrahlung spectrum formed when irradiating a substance with Z ~ 80 with 30 MeV electrons was used in the calculations. The shape of the bremsstrahlung was calculated using the GEANT 3.21 program package [5].

The radioactive decay constants $\lambda^{i}(A,Z)$ were taken from Ref. [6]. One serious problem in using the approach developed is determining the cross-sections of the photonuclear

reactions for the various isotopes in the transmutation chain, as the majority of the isotopes formed as a result of photonuclear reactions are radioactive and there are no experimental reaction cross-section data for them. In this paper, the cross-sections of the (γ,n), (γ,2n) and (γ,p) reactions have been described using the phenomenological model developed in Refs [1-4]. This model takes account of the basic mechanisms for formation and decay of the giant dipole resonance for nuclei with 10 < A < 210 using all available experimental data [7, 8] on photodisintegration of atomic nuclei in the giant dipole resonance excitation energy region.

We used the following approximations in our calculations which proved fairly accurate:

1. The position of the centre of mass of the giant dipole resonance E^m was determined using the equation:

$$E^m = 31.2A^{-1/3} + 20.6A^{-1/6} \text{(MeV)}. \quad (4)$$

2. The total integrated photoabsorption cross-section $\sigma_{\text{int}}(\gamma, tot)$ was determined using the equation:

$$\sigma_{\text{int}}(\gamma, tot) = 60\frac{NZ}{A} \text{(MeV mbarn)}. \quad (5)$$

3. In line with the experimental data on photonuclear reaction cross-sections in the A ~ 150-180 mass number region:

   - The (γ,n) channel comprised ~70% of the total absorption cross-section;
   - The (γ,2n) channel comprised ~25% of the total absorption cross-section;
   - The (γ,p) channel comprised ~5% of the total absorption cross-section [5, 8].

The relative cross-section values for the different reaction channels were taken to be identical for all isotopes formed irrespective of A and Z.

4. The more complex giant dipole resonance channels were not taken into account.

2. Calculation results

2.1 Role of the (γ,2n) channel in the transmutation process

Irradiation of the initial isotope ^{204}Pb over 30 months with a γ-ray flux of intensity $\Phi = 10^{18}\left(\frac{\text{particles}}{\text{s}\times\text{cm}^2}\right)$ was modelled. The initial number of nuclei of the isotope ^{204}Pb was set at 10^{22}. Monitoring continued for 90 months after irradiation ceased. This lengthy "waiting" period was necessary for all the short-lived nuclides to decay. The calculation results are given in Table 1. The first, second and third columns of Table 1 give the chemical element, the charge and the mass number of the isotopes formed respectively. The fourth column gives the number of nuclei of the isotopes formed taking into account the (γ,n), (γ,2n) and (γ,p) channels. The fifth column gives the number of nuclei of the isotopes formed taking into account only the (γ,n) and (γ,p) channels (i.e. the (γ,2n) channel was excluded). Table 1 includes all isotopes where the number of nuclei formed at the point of monitoring exceeded 10^{19}.

Table 1

Number of nuclei formed as a result of irradiation of the initial isotope ^{204}Pb with a γ-ray flux of intensity $\Phi = 10^{18}\left(\frac{\text{particles}}{\text{s}\times\text{cm}^2}\right)$

Chemical element	Charge Z	Mass number A	Number of nuclei formed	
			(γ,n)+ (γ,2n)+ (γ,p)	(γ,n)+ (γ,p)
Ir	77	191	6.09E+19	
	77	193	2.79E+19	
Pt	78	190	1.19E+19	
	78	192	1.15E+20	
	78	193	1.81E+20	
	78	194	3.09E+20	
	78	195	5.58E+20	5.23E+19
	78	196	5.26E+20	1.39E+20
Au	79	197	1.11E+21	3.64E+20
Hg	80	194	4.33E+19	
	80	196	2.93E+20	1.49E+19
	80	198	1.35E+21	7.47E+20
	80	199	1.49E+21	1.31E+21
	80	200	1.44E+21	1.90E+21
	80	201	1.18E+21	2.19E+21
	80	202	6.63E+20	1.87E+21
Tl	81	203	3.76E+20	1.07E+21
Pb	82	202	1.17E+20	1.13E+19
	82	204	**1.05E+20**	**3.00E+20**

The isotopes ^{203}Pb and ^{202}Pb are formed by irradiation of the initial isotope ^{204}Pb in the (γ,n) and (γ,2n) photonuclear reactions. The isotope ^{203}Pb has a half-life of 51.9 hours and therefore, forming in the (γ,n) reaction, it quickly transforms into the stable isotope

^{203}Tl (Z = 81). The isotope ^{202}Pb, which has a half-life of 5×10^4 years, is formed principally in the (γ,2n) reaction, as excluding the (γ,2n) reaction channel causes a drop in the formation of this isotope by one order of magnitude, as can be seen clearly from the data in the table.

The isotope ^{203}Tl, which is formed through β^+-decay of ^{203}Pb, is the lightest stable isotope with Z = 81, and its photodisintegration when exposed to the photon beam, and the subsequent β^+-decay of the radioactive isotopes with Z = 81 (A < 203), leads to the formation of a large number of stable isotopes of mercury (Z = 80), starting from the lightest stable isotope A = 196 up to A = 202. In addition, the radioactive isotope ^{194}Hg (Z = 80) is formed which has a half-life of 367 years. It should be noted that the heaviest stable isotope ^{204}Hg cannot be formed in photonuclear reactions where ^{204}Pb is irradiated as the initial isotope. Fig. 2 shows the number of different stable isotopes of mercury formed by irradiation of the initial isotope ^{204}Pb relative to the photodisintegration channels taken into account in the calculation.

The dots in Fig. 2 show the number of nuclei of this isotope formed taking into account the (γ,n), (γ,2n) and (γ,p) reactions. The circles in Fig. 2 show the calculation results not taking into account the (γ,2n) channel. There is a clear shift in the mass distribution of the number of mercury isotopes formed towards the lighter isotopes when the (γ,2n) reaction channel is taken into account. Thus, the data in Fig. 2 clearly show that the (γ,2n) reaction channel plays a major role in the formation of the light stable isotopes of mercury.

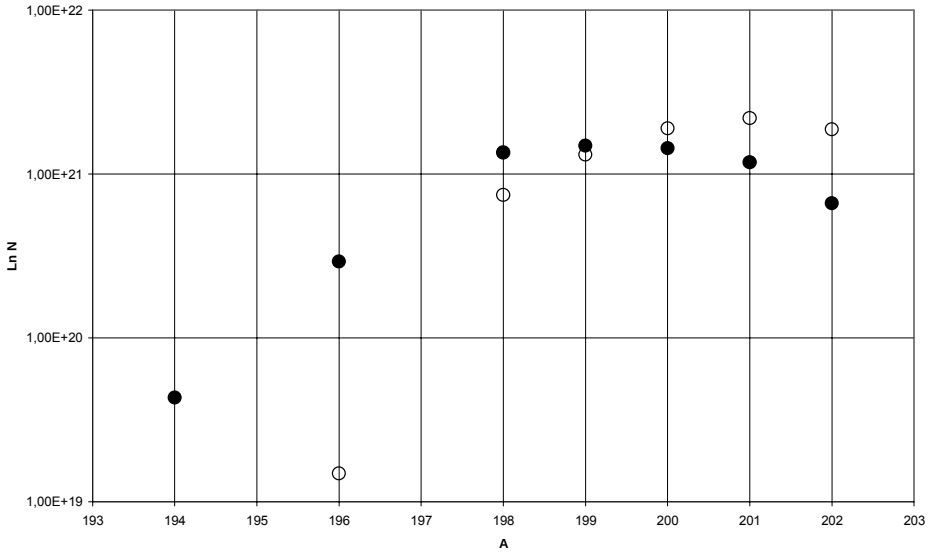

Fig. 2. Number of different stable isotopes of mercury (Z = 80) relative to the photodisintegration channels taken into account in the calculation. The dots show the number of nuclei of this isotope formed taking into account the (γ,n), (γ,2n) and (γ,p) reaction channels; the circles show the calculation results taking into account the (γ,n) and (γ,p) reaction channels.

The isotope ^{194}Hg, which has a half-life of 367 years, can only be formed through the (γ,2n) reaction, as the isotope ^{195}Hg has a half-life of 9.5 hours and blocks almost entirely the formation of ^{194}Hg through the (γ,n) reaction chain. A similar result was obtained for the isotopes of platinum (Z = 78). Only the relatively heavy isotopes ^{195,196}Pt are formed in the (γ,n) reaction, whereas including the (γ,2n) channel leads to the formation of all the light

stable isotopes of platinum. As in the case of mercury (Z = 80), the lightest stable isotope ^{190}Pt is only formed through the (γ,2n) reaction as the isotope ^{191}Pt has a half-life of 2.8 days. The isotopes ^{191,193}Ir (Z = 77) are also only formed when the (γ,2n) reaction channel is included in the calculation.

2.2 Effect of the γ-ray flux intensity

Using the method described above, calculations were performed for two different photon beam intensities. In the first case, irradiation of the initial isotope ^{204}Pb in a 30 MeV γ-bremsstrahlung flux with an intensity of $\Phi = 10^{18}\left(\frac{\text{particles}}{\text{s}\times\text{cm}^2}\right)$ over 30 months was modelled. In the second case, the intensity of the bremsstrahlung flux was $\Phi = 10^{19}\left(\frac{\text{particles}}{\text{s}\times\text{cm}^2}\right)$; the irradiation time was 30 months, as in the first case. The "waiting" time after irradiation was 90 months in both cases, which was necessary for decay of the short-lived isotopes ($T_{1/2}$ < 1 year). The number of nuclei of the initial isotope ^{204}Pb was the same in both cases: 10^{22}.

The calculation results are shown in Table 2 and Fig. 3. The first, second and third columns of Table 2 give the chemical element, the charge and the mass number of the isotopes formed respectively. The fourth column gives the number of nuclei of the isotopes formed for a γ-ray flux intensity of $\Phi = 10^{18}\left(\frac{\text{particles}}{\text{s}\times\text{cm}^2}\right)$. The fifth column gives the number of nuclei of the isotopes formed for a γ-ray flux intensity of $\Phi = 10^{19}\left(\frac{\text{particles}}{\text{s}\times\text{cm}^2}\right)$. Table 2 includes all isotopes where the number of nuclei formed at the point of monitoring exceeded 10^{19}.

The dots in Fig. 3 show the calculation results for $\Phi = 10^{18}\left(\frac{\text{particles}}{\text{s}\times\text{cm}^2}\right)$ and the circles those for $\Phi = 10^{19}\left(\frac{\text{particles}}{\text{s}\times\text{cm}^2}\right)$.

Comparing the calculation results for the two different γ-ray flux intensities reveals the following. As the intensity of the γ-radiation flux increases, there is a marked shift in the mass distribution of the isotopes towards lower values of A, and the distribution becomes broader. Thus, at a bremsstrahlung flux intensity of $\Phi = 10^{18}\left(\frac{\text{particles}}{\text{s}\times\text{cm}^2}\right)$, the stable isotopes formed have a relatively narrow distribution of A ~ 190-204, with a maximum of A ≈ 200. The shift in the centre of mass of the mass distribution comprises ~4 units relative to the mass distribution for the initial isotope ^{204}Pb. Increasing the γ-ray flux intensity to $\Phi = 10^{19}\left(\frac{\text{particles}}{\text{s}\times\text{cm}^2}\right)$ causes significant broadening of the mass distribution from A ≈ 125 to A ≈ 170. The shift in the centre of mass of the mass distribution comprises ~56 units relative to the mass distribution for the initial isotope ^{204}Pb.

Table 2

Number of nuclei formed as a result of irradiation of the initial isotope ^{204}Pb with a γ-ray flux of intensity

$$\Phi = 10^{19}\left(\frac{\text{particles}}{\text{s}\times\text{cm}^2}\right) \text{ and } \Phi = 10^{18}\left(\frac{\text{particles}}{\text{s}\times\text{cm}^2}\right)$$

	Z	A	Number of nuclei (Φ=10E19)	Number of nuclei (Φ=10E18)
I	53	127	2.60E+19	
Xe	54	126	1.33E+19	
	54	128	3.62E+19	
	54	129	4.98E+19	
	54	130	6.13E+19	
	54	131	8.85E+19	
	54	132	8.14E+19	
Cs	55	133	1.45E+20	
Ba	56	132	3.32E+19	
	56	134	1.81E+20	
	56	135	2.21E+20	
	56	136	2.29E+20	
	56	137	3.13E+20	
	56	138	1.74E+20	
La	57	139	3.86E+20	
Ce	58	136	3.75E+19	
	58	138	1.92E+20	
	58	140	5.56E+20	
Pr	59	141	4.34E+19	
Nd	60	142	4.85E+19	
	60	143	5.75E+19	
Sm	62	149	2.79E+20	
	62	150	3.05E+20	
	62	152	3.05E+20	
Eu	63	151	3.40E+20	
	63	153	5.59E+20	
Gd	64	154	5.65E+20	
	64	155	5.72E+20	
	64	156	5.14E+20	
	64	157	5.30E+20	
	64	158	3.27E+20	
Tb	65	159	4.47E+20	
Dy	66	156	4.20E+19	
	66	158	1.65E+20	
	66	160	3.96E+20	
	66	161	3.44E+20	
	66	162	2.63E+20	
	66	163	2.43E+20	
	66	164	9.93E+19	
Ho	67	165	1.54E+20	
Er	68	162	2.89E+19	
	68	164	9.61E+19	
	68	166	1.18E+20	
	68	167	8.87E+19	
	68	168	5.33E+19	
Tm	69	169	4.58E+19	
Yb	70	168	1.14E+19	
	70	170	3.17E+19	
	70	171	2.08E+19	
	70	172	1.36E+19	

	Z	A	Number of nuclei (Φ=10E19)	Number of nuclei (Φ=10E18)
Ir	77	191		6.09E+19
	77	193		2.79E+19
Pt	78	190		1.19E+19
	78	192		1.15E+20
	78	193		1.81E+20
	78	194		3.09E+20
	78	195		5.58E+20
	78	196		5.26E+20
Au	79	197		1.11E+21
Hg	80	194		4.33E+19
	80	196		2.93E+20
	80	198		1.35E+21
	80	199		1.49E+21
	80	200		1.44E+21
	80	201		1.18E+21
	80	202		6.63E+20
Tl	81	203		3.76E+20
Pb	82	202		1.17E+20
	82	204		**1.05E+20**

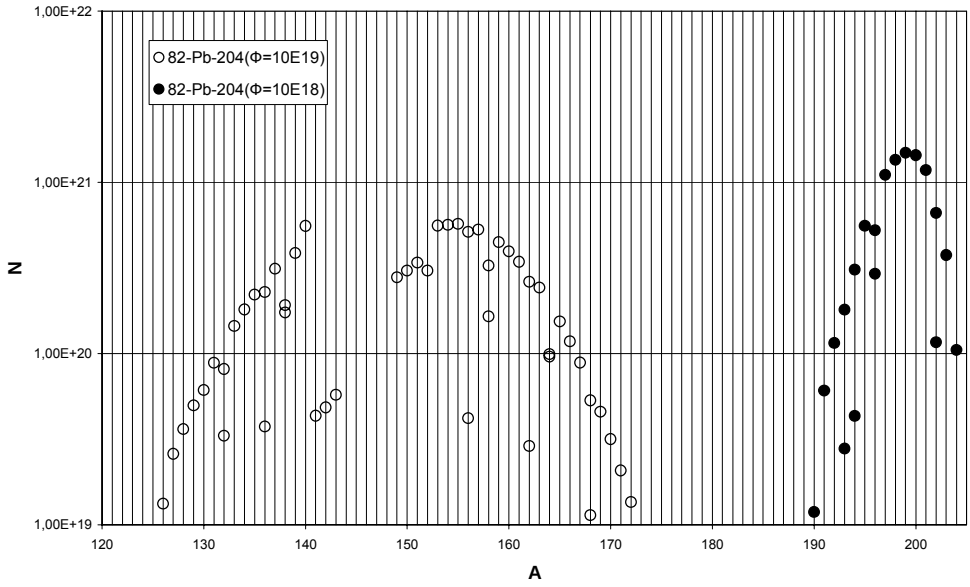

Fig. 3. Mass distribution of isotopes

Analysis of the mass distribution of the isotopes formed at a flux intensity of $\Phi = 10^{19}\left(\frac{\text{particles}}{\text{s}\times\text{cm}^2}\right)$ reveals a series of interesting patterns. For isotopes with large Z values (64-69), almost all the stable isotopes of the element in question are formed. The only exception for this group of isotopes are the heaviest stable isotopes ^{170}Er (Z = 68) and ^{160}Gd (Z = 64) which only form in mono-particle reactions, for instance in the reactions:

$$^{172}\text{Yb}(\gamma,\text{pn})^{170}\text{Er} \qquad\qquad ^{162}\text{Dy}(\gamma,\text{pn})^{160}\text{Gd}.$$

As is mentioned above, for the heavy nuclei the cross-sections of these reactions are small - at most a few percent of the total cross-section. For the lighter elements (Z = 53-56), again almost all the stable isotopes are formed, except for the lightest isotopes ^{130}Ba (Z = 56) and ^{124}Xe (Z = 54) and the two heaviest isotopes ^{134,136}Xe (Z = 54).

It is clear why this is the case for the heavy isotopes of xenon. The isotopes ^{134,136}Xe are too far from the main stability band and are separated from it by the short-lived isotopes ^{137}Xe ($T_{1/2}$ = 5.25 days) and ^{135}Xe ($T_{1/2}$ = 9.1 hours).

The situation near the maximum of the mass distribution for irradiation with a γ-ray flux of intensity $\Phi = 10^{19}\left(\frac{\text{particles}}{\text{s}\times\text{cm}^2}\right)$ is interesting. There are no stable isotopes among the isotopes of Pm (Z = 61). All the isotopes of promethium (Z = 61) with A < 146 are β^+-radioactive, and all the isotopes with A > 146 are β^--radioactive. The isotope ^{146}Pm decays through both β^+- and β^--decay. There is a characteristic feature in the mass distribution of the isotopes reflecting this fact: the number of nuclei with mass numbers of A ≈ 144-147 is less than 10^{19}, and the number of nuclei with mass numbers of A = 141-143 is less than 10^{20}.

Only the two lightest isotopes of neodymium ^{142,143}Nd are formed in photonuclear reactions. These isotopes can be formed by β^+-decay of the long-lived isotopes $^{144\text{-}146}$Pm,

forming the stable isotopes $^{144\text{-}146}$Nd which are then destroyed in (γ,n) and (γ,2n) reactions to form the stable isotopes $^{142\text{-}143}$Nd. The complex formation mechanism explains the small number of nuclei (~5×10^{19}) of these isotopes. ^{141}Pr is a similar case. This isotope forms through the ^{142}Nd(γ,n)^{141}Nd and ^{143}Nd(γ,2n)^{141}Nd reactions. The isotope ^{141}Nd is β^+-radioactive with a half-life of 2.5 hours and is transformed almost immediately into the stable isotope ^{141}Pr. Therefore the isotopes ^{142,143}Nd and ^{141}Pr are formed in comparable quantities (4-6 $\times 10^{19}$).

The β^+-radioactive isotope ^{152}Eu, which has a half-life of 9.3 hours, plays a significant role in the formation of ^{151,153}Eu and ^{149,150,152}Sm. This group of isotopes is formed in (γ,n) and (γ,2n) reactions in comparable quantities (~3×10^{19}).

The isotopes of gadolinium $^{154\text{-}158}$Gd (Z = 64) are at the top of the mass distribution. Each isotope in this group of nuclei is formed in practically identical numbers (~3-5 $\times 10^{20}$). The stable Gd (Z = 64) isotopes formed do not include the lightest isotope ^{152}Gd and the heaviest isotope ^{160}Gd. Both these stable isotopes are separated from the main group of stable isotopes by the short-lived isotopes ^{153}Gd ($T_{1/2}$ = 241 days) and ^{159}Gd ($T_{1/2}$ = 19.6 hours) and their formation is therefore strongly suppressed.

Conclusion

The transmutation of atomic nuclei by intensive γ-ray fluxes leads to the formation of chemical elements with a charge Z less than the charge of the initial isotope irradiated ^{204}Pb. The presence in the isotope mixture of nuclei with Z < 82 is due to the fact that the atomic nuclei formed in the (γ,n) and (γ,2n) photonuclear reactions are stable as a rule, or β^+-radioactive. The (γ,2n) reaction channel, despite its relatively small cross-section by comparison with the (γ,n) reaction channel, plays a significant role in the formation of the lightest isotopes of the chemical element in question. The (γ,2n) reaction channel is the only photonuclear reaction channel where the light isotopes of the chemical element can form when the lightest isotope of the element in question is blocked by a heavier radioactive isotope with a mass number one higher and a short half-life. The (γ,2n) channel is the main channel where bypassed nuclei can form in reactions induced by intensive photon beams.

Increasing the intensity of the γ-bremsstrahlung causes a significant shift in the mass distribution of the stable isotopes formed towards lower values of A, and the distribution becomes broader.

The number of different isotopes formed by the transmutation of the initial nucleus is heavily dependent on the radioactive characteristics of the isotopes, the reaction chains and the decays in which they form.

The conclusions drawn are based on model calculations performed for the initial isotope ^{204}Pb. However, they have more general significance and are not dependent on the initial isotope selected. Similar results were obtained when the isotopes ^{202}Hg and ^{205}Tl were selected as the initial isotopes.

In a real situation, the cross-sections of the photonuclear reactions are different from those we used. The number of isotopes formed is dependent on the relation between the cross-sections of the photonuclear reactions and the shape of the γ-ray spectrum. These differences

from the calculation can result in a difference in the yields of individual isotopes, but they do not affect the principal conclusions drawn from the analysis using the initial isotope ^{204}Pb.

References

1. Borodina, S.S., Ishkhanov, B.S., Mokeev, V.I., Pavlov, S.I., Vestn. Mosk. un-ta, Fiz. Astron., 6 (2000) p. 30.
2. Borodina, S.S., Ishkhanov, B.S., Mokeev, V.I., Vestn. Mosk. un-ta, Fiz. Astron., 1 (1998) p. 22.
3. Borodina, S.S., Ishkhanov, B.S., Mokeev, V.I., Pavlov, S.I., Preprint NIIYaF MGU-99-32/950, Moscow (1999).
4. Borodina S.S., Ishkhanov B. S., Mokeev V.I., Intern. Nucl. Phys. Conf. (INPC/98), August 24-28 1998, Paris, p. 794.
5. Brun R., Bruyant F., Maire M. et al., GEANT 3.21 (User's Guide). CERN, Geneva, Switzerland, 1987.
6. Nuclear Wallet Cards N.Y., 2000 (http://www.nndc.bnl.gov).
7. Varlamov A.V., Varlamov V.V., Rudenko D.S., Stepanov M.E., Atlas of Giant Dipole Resonance, IAEA, Nuclear Data Section, Austria, Vienna, 1999.
8. Dietrich S., Berman B.L., Atomic Data and Nuclear Data Tables, 38 (1998) p. 199.

NUCLEAR REACTOR DATA

UDC 539.17

EVALUATION AND BENCHMARKING OF NUCLEAR DATA OF VANADIUM IN INTEGRAL EXPERIMENTS WITH 14-MeV NEUTRONS

A. Blokhin, V. Manokhin
The State Scientific Centre of the RF - Institute of Physics and Power Engineering, Obninsk, Russia

A. Livke, A. Shvetsov, V. Nagorny, A. Zhitnik, V. Chirkin, Y. Nefedov, V. Semenov, A. Shmarov, R. Orlov, M. Savin
Russian Federal Nuclear Center – VNIIEF, Sarov (Arzamas-16), Russia

D. Markovskij, D. Chuvilin, V. Zagryadsky
The Russian Research Centre "Kurchatov Institute", Moscow, Russia

The measurements of the gamma-ray and neutron leakage spectra from three vanadium spheres with diameter 10, 24 and 34 cm at their internal irradiation by 14-MeV neutrons were carried out in frame of the ISTC Project #910 in collaboration with FZK. All the spheres have the same geometry of the central hole of 3 cm in diameter. The neutron leakage spectra were measured by a scintillation detector, and by a gas proportional counter. The gamma-ray leakage spectra were measured with help of a crystal NaI(Tl). Analysis of these experiments is performed with the new evaluated nuclear data files prepared in frame of the project activities. A comparison of experimental and calculated neutron and gamma-ray leakage spectra from three vanadium spheres is given.

I. Introduction

The perspective of using the vanadium in fusion reactor leads to high requirements to accuracy of its nuclear data, which, in turn, is followed by the necessity of testing the recommended evaluated data library (FENDL-2) with integral experiments. Previously the measurements were carried out with 100-mm vanadium sphere having 14-MeV neutron source in a center (IPPE-FZK[1)]) and with a cubic sample 250 mm thick under external irradiation with 14-MeV neutrons (JAERI[2)]), however there is a need for experiments both with thicker sample and at lower energies of neutron leakage.

To meet these demands, the ISTC project "Execution of the complex of benchmark-experiments for testing the nuclear data of vanadium - main component of low-activation structural materials for advance nuclear energy" was proposed by the Russian Research Centre ”Kurchatov Institute” (RRC ”KI”), Moscow as Contracting Institute with two Participating Institutes: the Russian Federal Nuclear Center VNII of Experimental Physics (VNIIEF), Sarov, Nizhny Novgorod region and the State Scientific Centre of the RF - Institute of Physics and Power Engineering (IPPE), Obninsk, Kaluga region.

In this report a set of benchmark-experiments with the 14 MeV-neutron generator is presented for three spherical samples (radius of 5, 12 and 17 cm). Comparison with calculated data is also given.

II. Manufacturing the Vanadium Spherical Sample

The vanadium ingots (∅115 mm) were realized in an electron-beam furnace in a crystallize tank. After melting the ingots of 800-mm height were annealed in vacuum at a temperature interval of 900-1100°C. For reshaping of ingots to the shape of a hemisphere a 2000 ton press was used. After that a forging was again annealed for taking out of stresses. Three spheres were made from the obtained blanks 10, 24 and 34 cm in diameter (each of two semi-spheres) with 3-cm central cavity. In Table 1 the chemical impurities in vanadium sample measured by a laser mass-spectrometric method are given.

Table 1.

Chemical impurity of the sample material (ppm)

C-100; N-100; O-200; Na<9.5; Mg–7.2; Al-400; Si-250; P<9.3; S-14; Ti-27; Cr–5.7; Mn–0.95; Co–0.7; Fe-150; Cu–3.6; Ni–5.7; Mo <1

III. Setting of measurements

III.1. Neutron generator and measurement geometry

The measurements were done with a standard D-T neutron source OI-G-18[3)] created on the basis of high-current neutron generator NG-150M. An uncertainty of neutron fluency determination is ~2.5%. The generator is operated in a pulsed mode.

The neutron detector is shielded from the generator by 300 cm concrete wall thick and placed in an experimental hall at the height of ≈150 cm from a floor.

The neutron source is located in a separate hall behind the concrete wall. The gamma and neutron radiation from the vanadium assembly penetrates to the experimental hall through a radiation channel (RC) of inner diameter 300 mm. As the diameter of the vanadium assembly (340 mm) is larger than that of the collimator (300 mm), for ensuring the direct visibility of the assembly from all the points of the detector working surface, the distance from the neutron target to the RC entrance was 3 m.

III.2. Neutron yield monitoring

For a neutron yield measurement two α-counters (monitors) registering alpha-particles from the $T(d,n)^4He$ reaction are placed in an ion drift tube. The α-monitors are calibrated with the help of a certified proton telescope, placed on a deuteron beam axis at a distance of L=30 cm from the tritium target. The neutron effective energy was E_{eff}=14.75 MeV. The counting efficiency of the telescope to these neutrons is known with an uncertainty of ±1.5% (confidence probability P=0.95).

III.3. Determination of γ-ray and neutron spectra from target unit

The yield and spectrum of γ-rays generated in a target unit under the incident DT-neutrons were determined in measurements without vanadium assembly. The yield and spectrum of secondary neutrons generated in a target unit in inelastic interactions of the DT-neutrons are calculated by the Monte-Carlo method. Because of small output of these neutrons (their fraction in a total neutron spectrum is ~5%) such approximation is quite justified.

IV. Measurement of neutron leakage spectra from vanadium spheres

For the measurements the neutron leakage spectra two detectors were used: a proportional gas counter and a scintillation detector. The proportional counter has low threshold and wide energy range of neutron detection (0.05-14 MeV). A counter with such characteristics is firstly used in such experiments. To provide a control the measurements were additionally performed with a scintillation detector, having the high neutron registration efficiency.

IV.1. Measurement by proportional counter

The proportional counter has a cylindrical shape manufactured from stainless steel. The cylindrical cathode has a length of 1 m, inner diameter of 75 mm, wall thickness and end flanges of 1 mm. The energy calibration and determination of an energy resolution of the counter was done by the $^3He(n,p)T$ reaction (Q=0.764 MeV) using the thermal neutrons. With this purpose the 0.4% volumetric ^3He was added in the working gas. Energy resolution of counter was determined as 3.5%.

The systematic uncertainty of the unfolded neutron spectra includes uncertainties of cross sections and tracks (~3%), energy calibration of the analyzer scale (~2%), corrections for γ-background (~5% for neutron energies less than 0.4 MeV). Thus the total systematic uncertainty in the energy range E_n<0.4 MeV can be ≈6.2% and for an interval $0.4 \le E_n \le 14.7$ MeV - ≈4.0%.

IV.2. Measurements by scintillation detector

The time-of-flight method and scintillation detectors were used for the measurements of neutron leakage spectra from vanadium spherical samples. The neutron generator was operated in pulsed mode with duration of pulse equal to 25 ns.

The energy threshold of registration by the scintillation detector is E_n=0.5 MeV. At energies E_n<1.5 MeV the efficiency of neutron registration by the scintillation detector drops sharply, and the uncertainty of measured spectra increases. That is why the measurement was performed for neutron energy range from 1.5 to 10.0 MeV.

V. Measurement of γ-ray leakage spectra

The measurement technique of γ-ray leakage spectra is based on one-crystal scintillation spectrometer and time-of-flight (TOF) technique for separation of γ-quanta from neutrons.

The scintillation detector consists of the NaI(Tl) crystal of diameter 150 mm and height 100 mm. For reducing the background, the detector is located in a massive lead shield with a conic collimator of diameter 98.9 mm and 268 mm long. With the purpose of increasing the fraction of pulses corresponding to total absorption of γ-ray energy, the lead collimator is installed in front of the crystal, which limits its working surface up to diameter of 98.9 mm. The linear

range of γ-rays registration by a spectrometer is (0.35-14) MeV with the energy resolution of 9% for the γ-line of ^{65}Zn (E_γ=1.15 MeV).

The detection efficiency and its response function are calculated by the Monte-Carlo method in real geometry of the detector, collimator and shield for the source-detector distance of L=9.11 m.

The accuracy of the measurements for the gamma-rays emission spectra is estimated to be about (6–6.5)% for E_γ=0.5-5 MeV, (6.5–9.0)% for E_γ=5-8 MeV and more than 20% for E_γ>8 MeV.

VI. Evaluation of vanadium neutron data

The evaluation of neutron data for isotopes ^{51}V and ^{50}V was performed in the energy range from thermal to 20 MeV. The evaluated nuclear data include the total, elastic and inelastic scattering, capture, (n,2n), (n,p), (n,d) and other reaction cross-sections, resonance parameters and angular-energy distributions of emitted secondary particles and γ-rays. The resonance parameters are recommended below 200 keV. Both experimental data and theoretical calculations were used in evaluation of the different partial cross sections. The measured total cross sections and elastic neutron angular distribution data extended from 200 keV up to 30 MeV were used to adopt the optical model parameters. Below 200 keV the total, elastic and capture cross sections are presented by resonance parameters. For theoretical description of neutron cross sections the traditional optical-statistical method was used with taking into account consistently the contribution of the direct, pre-equilibrium and statistical equilibrium processes into different reaction channels. The practical calculations were made on the basis of the STAPRE[4] and GNASH[5] codes. The gamma-ray production cross sections and energy distributions for neutron capture and the (n, xγ) reactions were evaluated on the basis of the GNASH calculations and experimental data.

On Figs. 1-2 the results of our description of different neutron reaction channels for vanadium isotopes are shown. It can be seen that experimental information is rather limited and the evaluations disagree essentially even for dominant reaction channels. So the test of evaluations plays an important role in a choice of data recommended for practical applications.

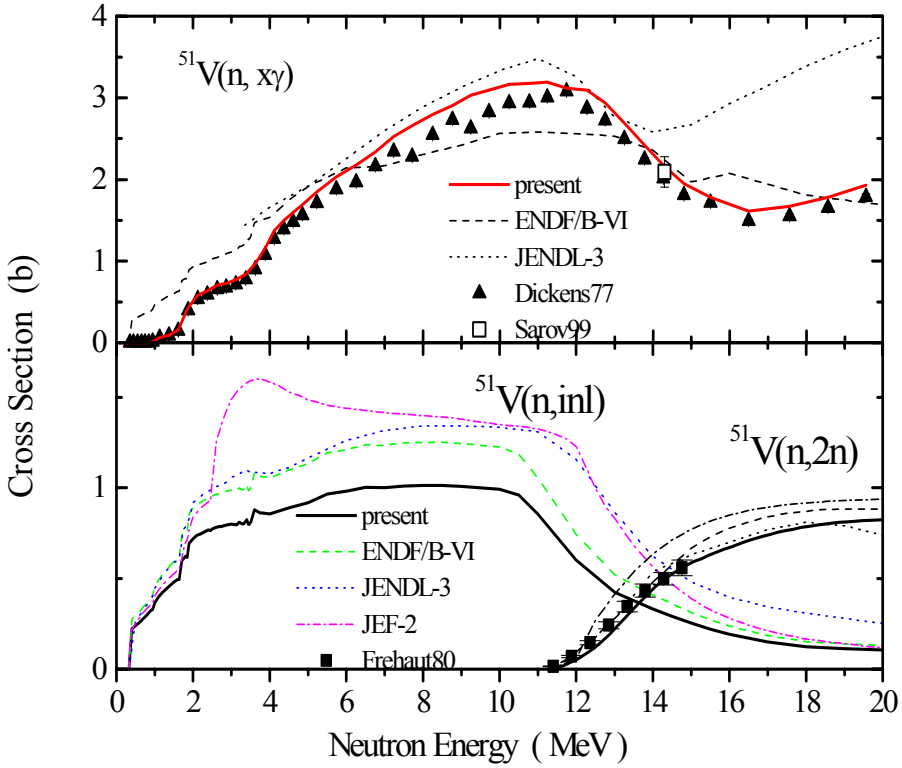

Fig. 1 (Top) Integral gamma-ray production cross sections as a function of the incident neutron energy. Curves: the present work (solid for E_γ>0.7 MeV), ENDF/B-VI (dashed) and JENDL-3.2 (short-dashed). Points: experimental data for E_γ>0.7 MeV.

Fig. 1 (Bottom) (n,inel) and (n,2n) cross sections as a function of the incident neutron energy. Curves: the present work (solid), ENDF/B-VI (dashed), JENDL-3.2 (short-dashed) and JEF-2 (dash-dotted). Points: experimental data from EXFOR library.

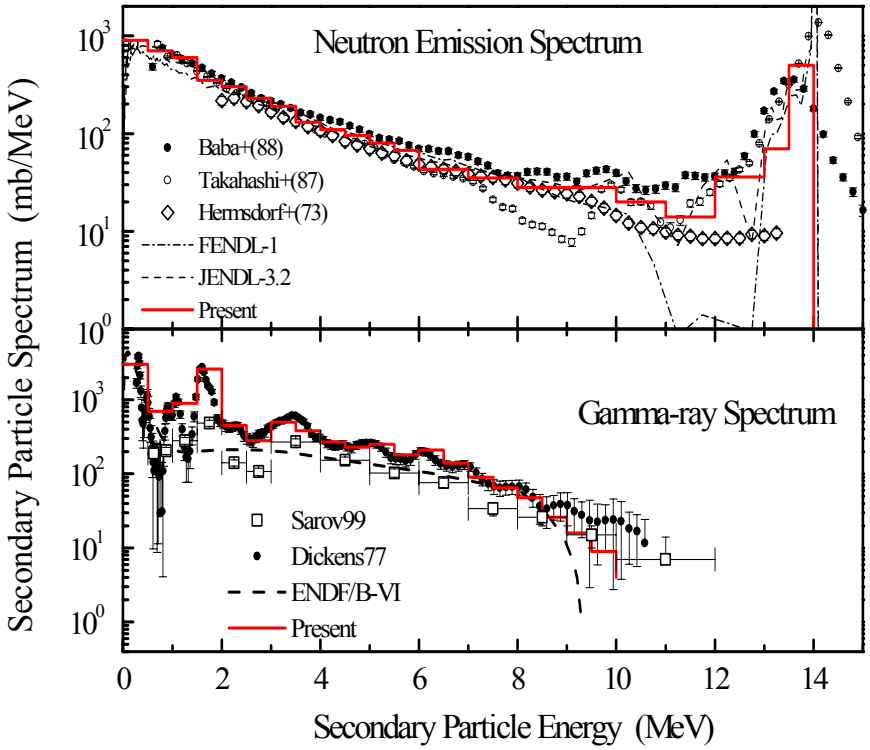

Fig. 2 (Top) Neutron emission spectra at the neutron energy about 14.3 MeV. Curves: the present calculations (solid), ENDF/B-VI (dashed). Points: experimental data from EXFOR library.

Fig. 2 (Bottom) Gamma-ray production spectra at the neutron energy about 13.02 MeV. Curves: the present calculations (solid), ENDF/B-VI (dashed). Points: experimental data from EXFOR library and Sarov-99 experiment for E_n=14.3 MeV.

VII. Transport calculations

To test the evaluated neutron data the transport calculations for the materials considered were performed with the Monte-Carlo code MCNP-4A. Transport cross sections for the MCNP calculations were prepared by using the NJOY system. The photon-interaction cross sections were taken from the photo-interaction ENDF/B-VI library.

VIII. Results and discussion

The gamma-ray emission and neutron leakage spectra from vanadium spheres of 10, 24 and 34 cm diameter with a 14-MeV neutron source in the center were measured and the results in comparison with the calculated data are shown in Figs. 3 and 4. Both the measured and calculated spectra are normalized to the neutron source. The comparison of experimental and calculated data for the gamma-ray leakage multiplication is given in Table 2. From the results presented on Fig. 4 we can make the following conclusions:

- a good agreement between a slope of experimental and calculated gamma-ray leakage spectra in the gamma-ray energy above 2.5 MeV is obtained;
- a good agreement between absolute value of experimental and calculated gamma-ray leakage spectra in the gamma-ray energy above 2.5 MeV are obtained;
- the agreements are bad in the range of low gamma-ray energy below 2.5 MeV where we have a lot of discrete gamma-rays. We see underestimations in the energy range 1.0–1.5 MeV and overestimations for gamma-ray energy range 1.5–2.5 MeV;
- the measured integral yields of gamma-rays from the surface of spheres have the large disagreements with calculated data obtained with the ENDF/B-VI, FENDL, JENDL-FF, JEF-2 and Present evaluated nuclear data. Only for experiments with two vanadium spheres with diameters of 10 and 24 cm we obtained the agreement around 7%. For third spheres with D=34 cm it is obtained a large disagreement up to 25%.

Table 2.

Comparison of experimental and calculated gamma-ray multiplication K_γ for three vanadium spheres

K_γ		D_{out}=10 cm	D_{out}=24 cm	D_{out}=34 cm
Experiment		0.285±0.0162	0.361±0.0217	0.279±0.0167
Calc.:	Present	0.263 (-7.7%)	0.387 (+7.2%)	0.345 (+23.6%)
	FENDL-1	0.251	0.368	0.336
	JENDL-FF	0.283	0.392	0.367
	JEF-2.2	0.312	0.411	0.389

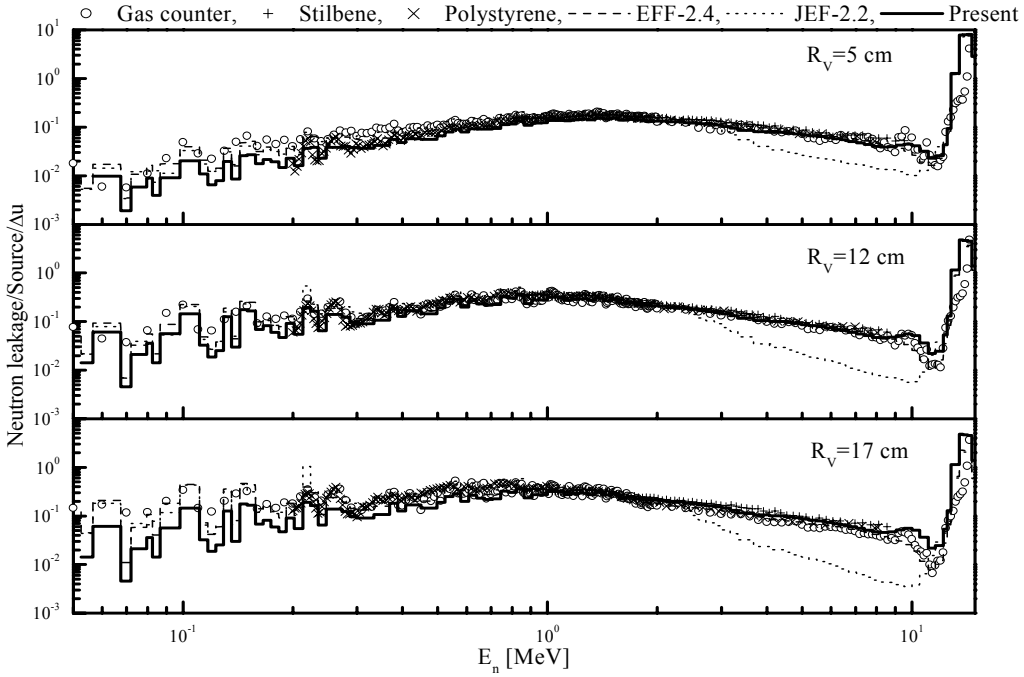

Fig. 3 Neutron leakage spectra for the vanadium spheres with D=10, 24 and 34 cm in a comparison with the Sarov's measurements (symbols). Curves: MCNP calculations with evaluated data from the present work (solid), EFF-2.4 (dashed), JEF-2.2 (dotted).

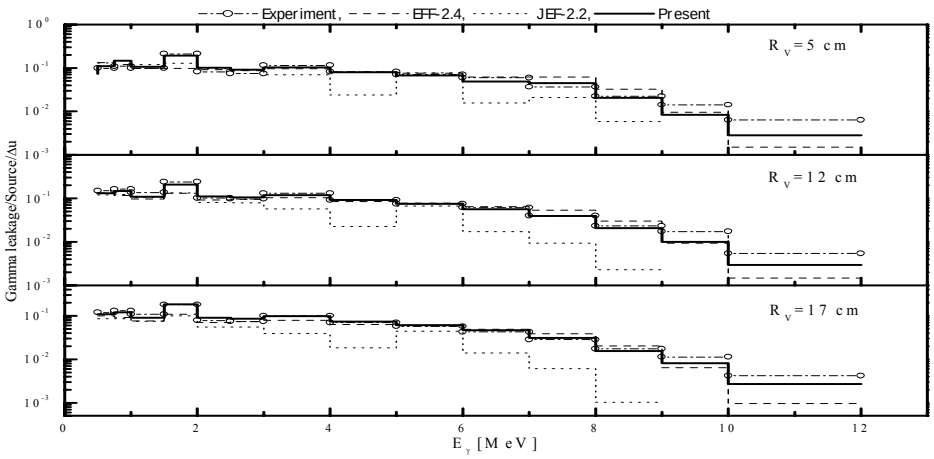

Fig. 4 Gamma-ray emission spectra for the vanadium spheres with D=10, 24 and 34 cm in a comparison with the Sarov's measurements (symbols). Curves: MCNP calculations with evaluated data from the present work (solid), EFF-2.4 (dashed), JEF-2.2 (dotted)

IX. Conclusion

Neutronics benchmark experiments on vanadium spheres were performed in the frame of the ISTC project "Execution of the complex of benchmark-experiments for testing the nuclear data of vanadium - main component of low-activation structural materials for advance nuclear energy" by the Russian Federal Nuclear Center VNII of Experimental Physics (VNIIEF).

The modern experimental and calculational results together with those reported in the literature and the EXFOR library were used to construct a comprehensive evaluated neutron data files in the ENDF-6 format for ^{50}V and ^{51}V isotopes. Some results of these evaluated nuclear data in comparison with similar results are presented. The following testing of these files on the basis of available macro-experiments is necessary.

First experimental results of neutron and gamma-ray leakage spectra from three spherical shells of vanadium were obtained and were analyzed with the ENDF/B-VI, FENDL, JENDL-FF, JEF-2 and present evaluated nuclear data.

References

1. S.P. Simakov, B.V. Devkin, B.I. Fursov, *et al*., "Benchmarking of Eevaluated neutron data for vanadium by a 14 MeV spherical shell transmission experiment," INDS(CCP)-417, IAEA Nuclear Data Section, (1998).
2. F. Maekava, Y. Kasugai, C. Konno, *et al*., "Benchmark experiment on vanadium with D-T neutrons and validation of evaluated nuclear data libraries by analysis of the experiment", *J. Nucl. Sci. Technol.*, vol.**36**(3), p.242 (1999).
3. G.A. Borisov, V.D. Sevastyanov, Yu.A. Nefedov, *et al*., "Creating of branch metrology basis of neutron measurements," *Proc. All-Union Counsel on a Metrology of Neutron Measurements in Reactors and Accelerators,* - Abstracts of the VNIIFTRI reports. - M., 1990. - p 3 (in Russian).
4. M. Uhl, B. Strohmaier, "STAPRE A Computer Code for Particle Induced Activation Cross Sections and Related Quantities," Report IRK 76/01, Vienna, 1976.
5. P.G. Young, E.D. Arthur, M.B. Chadwick. "Nuclear Reaction Data and Nuclear Reactors" (Trieste, 1996). Ed. A.Gandini, G.Reffo, World Sci., Singapore, 1998, v. 1, p. 227.

02-11288 (151) [3]
Translated from Russian

UDC 621.039.51

BURNUP CALCULATIONS USING THE ORIGEN CODE IN THE CONKEMO COMPUTING SYSTEM

S.V. Zabrodskaya, Yu.S. Khomyakov, A.A. Tsibulya
Russian Federation National Research Centre Institute for Physics and Power Engineering (IPPE), Obninsk

BURNUP CALCULATIONS USING THE ORIGEN CODE IN THE CONKEMO COMPUTING SYSTEM. This article describes the CONKEMO computing system for kinetic multigroup calculations of nuclear reactors and their physical characteristics during burnup. The ORIGEN burnup calculation code has been added to the system. The results of an international benchmark calculation are also presented.

The CONKEMO computing system [1] has been developed to perform reference multigroup calculations of nuclear reactors and changes in their physical characteristics as the nuclide composition of their fuel changes during burnup. Its main sphere of application is in calculations for water-cooled and -moderated (WWER) reactors with uranium and MOX fuel. It is based on a number of independently developed codes and nuclear data libraries. To ensure that its various components are consistent, the authors have developed several additional elements, including specialized exchange files. The basic flow diagram for how the various modules in the CONKEMO system interact is shown in Fig. 1. In it, codes are depicted as rectangles and libraries and exchange files as ellipses.

The nuclear data underlying the CONKEMO system is the ABBN-93 [2] system of group data and is used in conjunction with the basic CONSYST [2] code for preparing data for calculation. The neutron fields can be calculated using one of the Monte Carlo codes: KENO-Va [3], KENO-VI [4], MMKKENO [5], MCNP [6], or using the TWODANT [7] deterministic code. The MAYAK code [1] computes a number of the system's physical characteristics, and also fulfils dispatcher functions to ensure that all parts of the system are co-ordinated. The isotope kinetics are computed using the ORIGEN-S [8] or CARE [9] codes. The burnup calculation is modelled using a step-by-step algorithm. Each step recalculates the data, neutron fields, various physical characteristics and the isotope concentrations in the regions under calculation.

It should be noted that the CONKEMO system has already helped to solve a number of important practical problems: [1] and [10-12]. This paper describes how the neutron physics computation codes for reactors are linked to the ORIGEN burnup code, and presents some results of international benchmark calculations to verify it.

1. COR code

The ORIGEN code [13] was developed at the Oak Ridge National Laboratory, USA, to calculate changes in the composition and radioactivity of fuel elements, fission products and structural materials in nuclear reactors. This code's main advantage compared with other burnup codes was that it can represent the full matrix of isotope transmutations with no limit on the number of transmutation chains. This was achieved thanks to rational application of the matrix exponential method by retention of only the non-zero elements of the matrix and by the expansion method using recursive correlation, which requires only two vectors in addition to the solution vector.

CONKEMO uses the ORIGEN-S [13] version, taken from the American SCALE4.3 [14] system. This version is the successor to the original ORIGEN code, and has enhanced characteristics and new features (for brevity's sake ORIGEN-S is referred to hereafter as ORIGEN). These new features include: the introduction of a free format for input and output data, a flexible dynamic memory distribution, the ability to calculate gamma- and neutron-source spectra in any energy representation, a new algorithm for preparing and representing nuclear data, and many others.

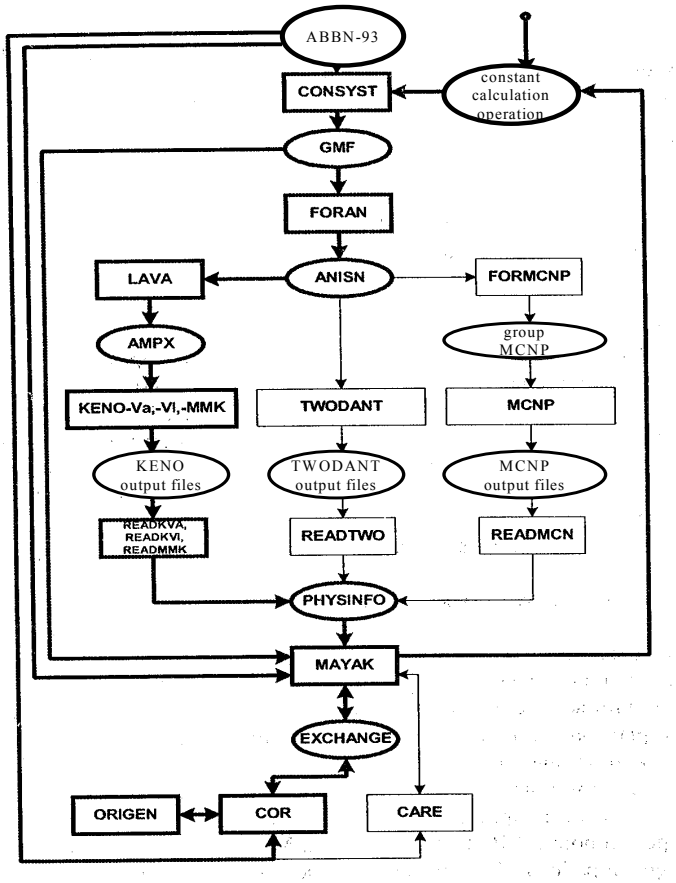

Fig. 1. Basic flow diagram showing how the modules in the CONKEMO system interact. The main "branch" of the system, giving it its name (CONsyst-KEno-Mayak-Origen) is highlighted.

ORIGEN solves the standard isotope kinetics equation for determining the concentration of the N_i nuclide with respect to time [13]:

$$\frac{Ni}{dt} = \sum_j \gamma_{ji}\sigma_{f,j}N_j\Phi + \sigma_{c,i-1}N_{i-1}\Phi + \lambda_i' N_i' - \sigma_{f,i}N_i\Phi - \sigma_{c,i}N_i\Phi - \lambda_i N_i \,, \tag{1}$$

where $i=1,...I$ and

$\sum_j \gamma_{ij}\sigma_{f,j}N_i\Phi$ - is the rate of formation of an N_i-nuclide as a result of fission of all the N_j;

$\sigma_{c,i-1}N_{i-1}\Phi$ - is the rate of transmutation into an N_i-nuclide as a result of radiative capture on the N_i-nuclide;

$\lambda_i' N_i'$ - is the rate of formation of an N_i-nuclide as a result of decay of the N_i-nuclide;

$\sigma_{f,i}N_i\Phi$ - is the rate of disappearance of an N_i-nuclide as a result of fission;

$\sigma_{c,i}N_i\Phi$ - is the rate of disappearance of an N_i-nuclide as a result of neutron absorption in the (n,γ), (n,α), (n,p), (n,2n) and (n,3n) neutron reactions;

$\lambda_i N_i$ - the rate of decay of an N_i-nuclide.

Equation (1) is written for a homogeneous medium with a space and energy averaged flux Φ and spectrum weighted cross-sections σ_f, σ_c. In actual fact, the flux - as a function of space, energy and time - is dependent on the nuclide concentration. In ORIGEN, it is assumed that the space and energy averaged flux can be considered constant during time interval Δt. A similar assumption is also made for the single set of weighted cross-sections for representing the fuel composition. For the given time step these assumptions are essential if equation (1) is to be considered a linear differential expression of the first order in the form $\overset{\circ}{\underset{-}{N}} = \underset{\approx}{A}\,\underset{-}{N}$ and $\overset{\circ}{\underset{-}{N}} = \underset{\approx}{A}\,\underset{-}{N} + B$ for an inhomogeneous medium, and this option is also available in ORIGEN.

Generally, solution of this equation takes the familiar form $\underset{-}{N} = exp(\underset{\approx}{A}t)\,\underset{-}{N}(0)$, where N is the nuclide concentration vector and A is the transmutation matrix.

The ORIGEN code is included in the CONKEMO system and is linked to the ABBN-93 system of constants using the COR code, which is a leading program invoking ORIGEN, COUPLE, INTERCON and GIVTAB as subroutines, and which also draws on the EXCHANGE format files, the ORIGEN code neutron and decay data, and the ABBN-93 library of neutron reaction cross-sections. Fig. 2 is a flow diagram showing how the modules and files interact.

Further work on the calculation makes use of one of the ORIGEN binary libraries corresponding to the reactor type under investigation. By default this library should have the number 34 and the file name FT34F001. It contains all the burnup data required for the calculation:

- the main nuclide transmutation chains needed for correct calculation of the burnup;
- the one-group neutron reaction cross-sections, determining the mutual transformations of the isotopes;
- the decay data;
- the fission fragment yields.

Selection of this library is not arbitrary. On the whole, it is used as the format, into which the magnitudes of the cross-sections, calculated on the basis of the ABBN data library, are placed. But in order to take into account several insignificant nuclide transmutation channels, data from the source library can be used directly. Thus, the source library selected should be the one that was created for the reactor most closely related to the one under investigation. We should recall that the standard version of ORIGEN enables the establishment of binary libraries for four reactor types: LWR, THGR, LMFBR and MSBR.

The **first phase** of COR operation is calculation of the average neutron reaction cross-sections on the basis of the ABBN-93 constants and recording them in ORIGEN's working library. To do this, three sources of reaction cross-section data are used:

- the one-group unshielded capture and fission cross-sections calculated by the MAYAK code on the basis of shielded micro-cross-sections from a GMF format file, and the spectra obtained at the physics calculation stage;
- the one-group unshielded reaction cross-sections from the appropriate sections (MF=9) of the ABBN-93 constant system;
- the reaction cross-sections recorded in the ORIGEN working library.

The data sources are listed in descending order of priority That is, the shielded cross-sections averaged by the MAYAK code are used first and, if they are not available, the unshielded cross-sections derived from the MF=9 tables are used. If the ABBN tables do not have the reaction cross-sections needed for the burnup calculation, the cross-section from the ORIGEN working library will be used.

The following general rule is observed: the ORIGEN library should contain all (barring a few exceptions which we will discuss below) the reaction cross-sections that are available in the ABBN library. In other words, reactions that are available in the ABBN should be added to the ORIGEN library. The reverse is not, however, true: if the ORIGEN source library has reactions which are not in the ABBN, then the reaction cross-sections from the basic library are kept.

We note that only 5 nuclides (^{233}U, ^{235}U, ^{238}U, ^{239}Pu, ^{241}Pu) are considered fissile, i.e. nuclides on which fission fragments form.

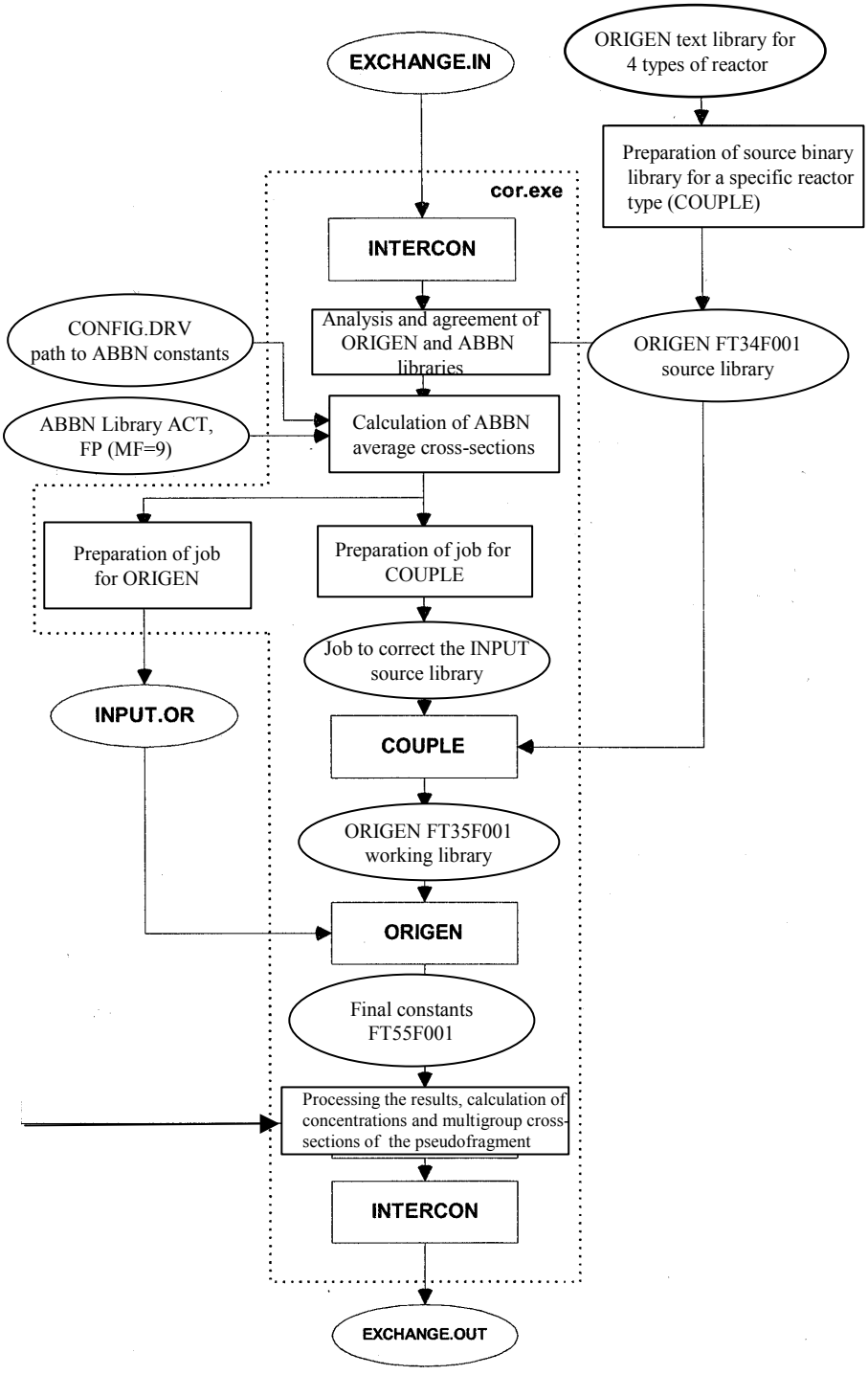

Fig. 2 Flow diagram showing how the modules and files interact

This means that for a large proportion of fissions for any of the more exotic nuclei, the accumulation of fission fragments may be calculated incorrectly. We have encountered this problem when calculating the nuclide composition of new prospective fuel compositions which are designed to burn up actinides with a high content of isotopes such as ^{237}Np and ^{241}Am. To resolve this problem, in the COR code one current nuclide can be replaced with another (for example, replacement of ^{233}U with ^{237}Np or ^{241}Am).

The ORIGEN code uses a three-group configuration to prepare neutron reaction cross-sections. Firstly, it calculates systems with a thermal (neutron) spectrum. For general purposes, it was decided to use the more straightforward method of one-group description. One-group reaction cross-sections divided by the THERM parameter are recorded instead of the thermal cross-sections, and zeros are written instead of the resonance interval and the cross-section in the fast region. Then, when preparing the operation on ORIGEN, the one-group absolute flux for the corresponding region is written instead of the thermal neutron flux. It is easy to see that such a configuration yields the correct rate for the corresponding reaction.

As a result of all the operations described to prepare the cross-sections and their replacement, the COR code generates a job for correction of the ORIGEN source library using the COUPLE code in accordance with its requirements. This job, which basically contains information about the reactions to be replaced, is written to the INPUT text file. The result of the work done by the COUPLE code is that a new library is created with the standard number 35 (file FT35F001), which will also be an ORIGEN working file.

The **second phase** of COR code operation is the generation of a calculation job for the ORIGEN code, which is placed in the INPUT.OR text file. This job essentially contains information about the initial nuclide concentrations, the absolute flux and the duration of the time step.

In the standard version of the code, ORIGEN shows the absolute neutron flux. But ORIGEN has the option of performing a burnup calculation with power conservation in the region being calculated. In physics terms, this means that, during the time step under investigation, the code makes allowance for the change in neutron flux attributable to change in the nuclide composition. As fuel burns up the neutron flux usually increases so that the reactor produces the required thermal power. Of course, this situation can be modelled taking a time step that is sufficiently small for the flux not to undergo any significant change. This, however, requires a large number of reactor and burnup calculations. It is therefore justified to take an approach based on the following approximations:

- there is no significant change in the neutron spectra of the physical regions during the time step;
- also, there is no significant change in the power distribution (neutron flux) in the various physical regions of the reactor.

In this case, calculating the change in neutron flux does not require any neutron physics reactor calculation:

$$\varphi(t) \sim W(t)/V/\Sigma(\rho_i(t)\cdot\sigma_{fi}\cdot Q_{fi}),$$

where $\varphi(t)$ is the neutron flux, $W(t), V$ is the power and volume of the region, $\rho_i(t), \sigma_{fi}, Q_{fi}$ are the concentration, fission cross-section and energy yield during fission on the i-th nuclide. Calculating the change in neutron flux in this way, which is unequivocally linked only to change in the nuclide concentrations, is carried out in the ORIGEN code and is often applied by CONKEMO users.

The command to initiate this algorithm should be stored in the job for the MAYAK code.

The next step (**third phase**) invokes the ORIGEN code directly. The results of calculating the change in isotopic composition is placed in file FT55F001. The text file FT55F001 consists of lines in the following format:

name of the nuclide (for example, 922350), its quantity (in gram-moles).

The number of lines corresponds to the number of isotopes in library FT35F001; first the "light" isotopes are listed, then the actinides and after that the fragments.

In the final, **fourth phase**, COR processes the ORIGEN output data and carries out the following operations:

- a search for the final nuclide concentrations of the "reactor list" for recording in the ZONE section of the EXCHANGE OUT output file:
- calculation of the pseudofragment and pseudo-actinide concentrations;
- calculation of the multigroup neutron capture cross-sections of the pseudofragment and pseudo-actinide, and also of the fission cross-sections of the pseudo-actinide, followed by recording in the MULTIGROUP section of the EXCHANGE OUT file;
- recording of the concentrations of all the ORIGEN nuclides in the SCALEDENSITIES section.

2. Organization of the cyclic calculations with burnup

As has already been said, the CONKEMO system enables cycling of nuclear reactor calculations with burnup in a step-by-step algorithm. On the whole, recycling of the calculations consists of ensuring that the set of information obtained from the previous step is saved and passed on to the following step.

Firstly, the nuclide concentrations obtained as a result of the burnup calculation are saved. We note that it is necessary to save and pass on to the following steps two sets of concentrations: (1) for a limited set of nuclides influencing the neutron balance and taken into consideration in the physics calculation of the reactor system ("reactor list" of nuclides), and (2) for a far broader list of isotopes, needed for correct description of the nuclide transmutation chains ("burnup list"), which the burnup code uses. In the system, information about the "reactor list" concentrations is saved by updating the CONSYST calculation job. When using the ORIGEN code, the concentrations of all the nuclides (approximately 1600) on the "burnup list" are stored in a separate section of the EXCHANGE format file.

Secondly, information about the so-called "pseudonuclides" - the "pseudo fission fragment" and "pseudo actinide" - is prepared and stored. Summing of all the fission fragments, each of which has only an insignificant effect on the neutron balance, to one pseudonuclide - pseudo fission fragment, is the natural and accepted way of keeping the material balance of the physical regions. The pseudofragment concentrations calculated in this way are further multiplied by the microscopic pseudofragment cross-sections in the ABBN system (FP35 or FP39). This enables simulation of the contribution of the fission

fragments to the total macroscopic absorption cross-section of the physical region. Calculation of the "pseudofragment" concentrations is done using both burnup codes (ORIGEN and CARE).

When using ORIGEN, the method is improved as follows. After processing the ORIGEN module, the COR code calculates both the concentrations and the cumulative multigroup average capture cross-sections of the pseudofragment (FPM):

$$\sigma_{FPM}^{g} = \sum \rho_i \sigma_c^i / \sum \rho_i \ ,$$

where summing is performed for the nuclides included in the pseudofragment. This enables more correct calculation of neutron absorption by the fragments. In the ABBN system it is now possible to use the pseudofragment capture cross-section taking into account the characteristics of the nuclide composition of the fragments of a specific reactor and even each physical region in it.

The COR code writes the concentrations and cumulative pseudonuclide cross-sections into the EXCHANGE format file, and the MAYAK code rewrites them in the form of an ABBN table, accessible to the next step of the CONSYST code.

3. Test for calculation of a PWR cell

Given below are the results of a test calculation for a cell with MOX fuel in a PWR type reactor for Pu recycling. This test [15] was proposed by the OECD (Organisation for Economic Co-operation and Development) nuclear research committee. Twelve institutes from nine countries participated. Fourteen versions of the calculations were proposed using various methods and nuclear databases. Our calculations were performed using CONKEMO (TWODANT<S_8>, ORIGEN, 299 groups). Set down below are our results of comparison of k_{eff} and of the change in isotopic composition with respect to burnup with the data from the other test participants. The test shows two calculation versions - A and B, the main difference between them being the isotopic composition of the plutonium (see Table 1).

Table 1

Isotopic composition of Pu

	Option A	**Option B**
^{238}Pu	4%	1.8%
^{239}Pu	36%	59%
^{240}Pu	28%	23%
^{241}Pu	12%	12.2%
^{242}Pu	20%	4.0%

Option A uses plutonium with a very high heavy isotope content and a correspondingly low fraction of plutonium-239, which reflects the composition of recycled MOX fuel and corresponds approximately to a fivefold recycling of plutonium with an average burnup of 50 MW.day/kg of heavy material. From a calculation point of view, Option A is more sensitive to the nuclear data of the high plutonium isotopes and leads to an understanding of the situation in this region.

Option B is based on plutonium with the standard isotopic composition for current commercial PWR reactors using MOX fuel.

In Option A the total plutonium content is 12.5 wt % (6.0 wt % in fissile isotopes), while in Option B the total plutonium content is 4.0 wt % (2.8 wt % in fissile isotopes). The cladding is made of natural zirconium. The temperature of the fuel, cladding and water are 660, 306.3 and 306.3°C, respectively. The boron concentration in the water is taken to be 500 ppm.

The calculated specific power for option A was found to be 183.042 W/cm, and for option B 171.584 W/cm. The time to attain 50 MW day/kg of heavy material burnup was 1400 days.

An infinite height three-zone cylindrical cell model was used. The specific power and fuel burnup are 38.3 W/g and 50 MW day/kg of heavy material, respectively. The CONKEMO calculation was performed with improved group constants for actinides.

Fig. 3 shows the results of the k_∞ calculations for option A. Our results are shown as the solid line, other results simply as symbols. It is clear that we are in the middle range. The qualitative picture is the same for option B.

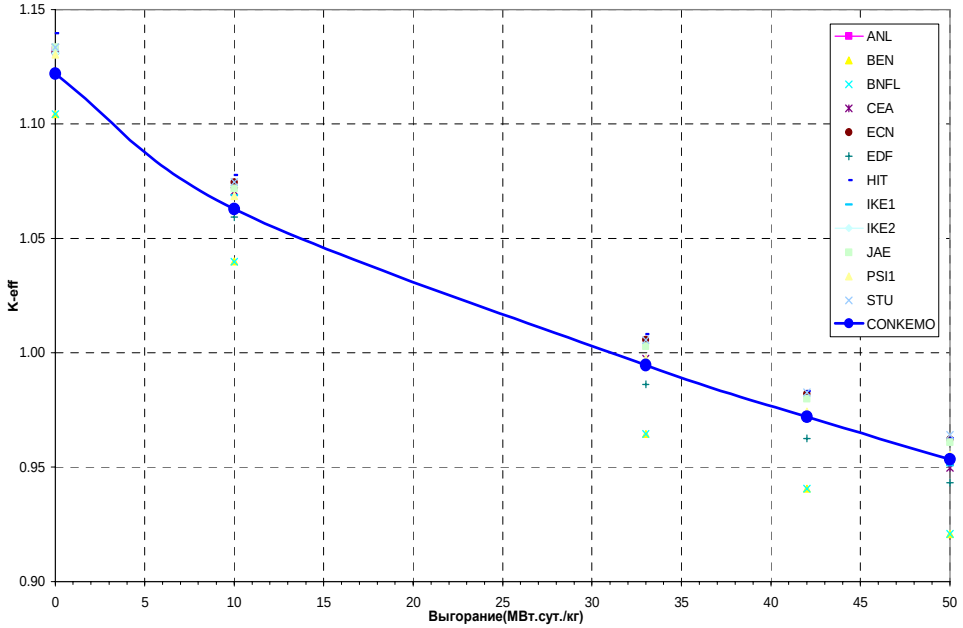

Burnup (MW.day/kg)

Fig. 3 Comparison of K_{eff} for the option A campaign

The next set of results are those for change in the isotopic composition of actinides and fission products with respect to burnup.

Figure 4 shows the minimum and maximum deviation from the mean (calculated for all the participants) concentration of each nucleus at a burnup of 50 MW.day/kg of heavy material. There are two - one dark shaded and one light shaded - rectangles for each nucleus for the A and B options, respectively. The differences between our results and the mean values for all nuclei for both options are shown on the figure as circles.

Basically there are no large calculation deviations from the mean using CONKEMO either for actinides or fission products. The lack of agreement for ^{242m}Am is attributable to the isomeric relationship, which in FOND2.2 is energy dependent whereas the others assume a constant branching fraction, as a rule corresponding to the thermal neutron capture. The reason for the high ^{245}Cm concentration in our calculations is not yet known.

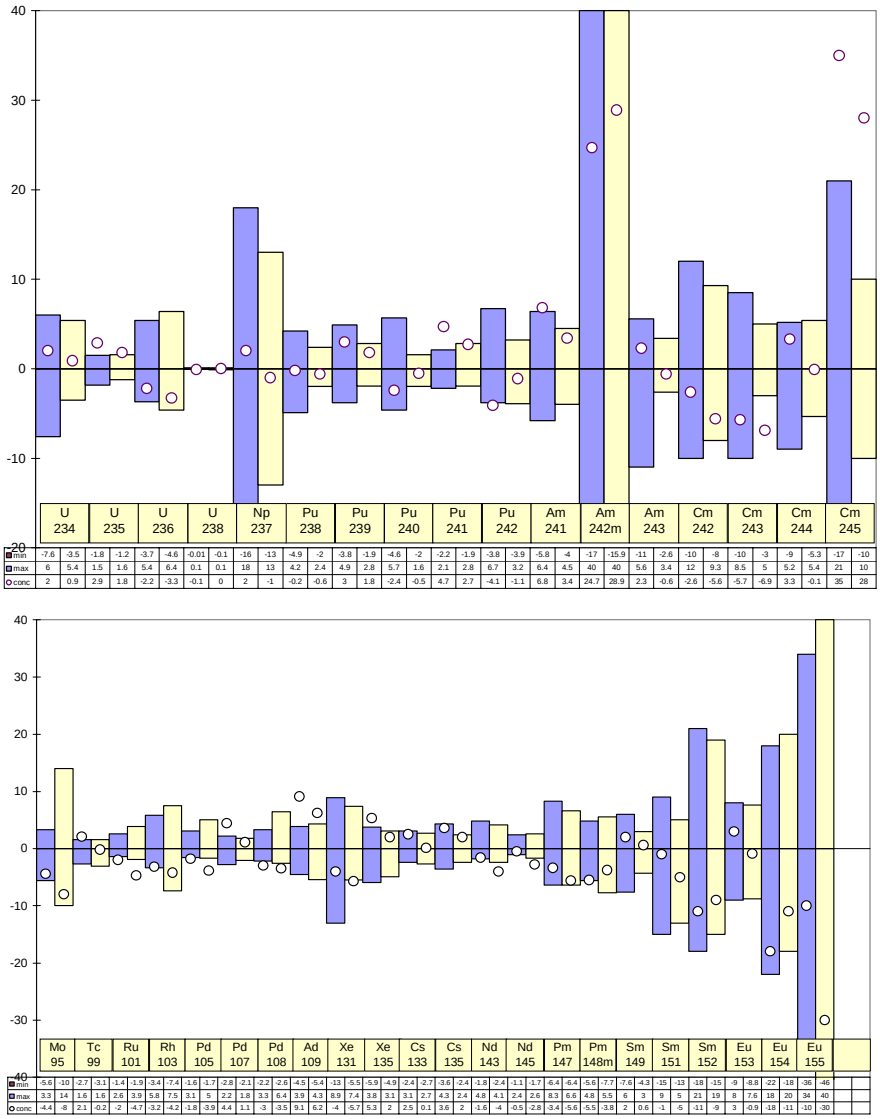

Fig. 4. Deviations from the mean nuclear concentrations for a burnup of 50 MW.day/kg of heavy material for the averaged results of all test participants. The deviation range is shown as rectangles (dark shading - option A, light shading - option B). The circles show the deviations of our data.

References

1. A. Lazarenko, M. Kalugin, S. Bychkov, A. Kalashnikov, Al. Tsiboulia, W. Zwermann, S. Langenbuch, W. Stach, G. Schlosser, M. Delpech, F. Dolci, P. Girieud, M.L. Vergain. Benchmark Calculations for VVER-1000 Fuel Assemblies Using Uranium or MOX fuel // Proceedings of PHYSOR2000 Conference, Pittsburgh, USA, May 7-11, 2000.
2. G.N. Manturov, M.N. Nikolaev, A.M. Tsibulya, ABBN-93 group constants system. Verification report. Inter-departmental committee for validation of reference data in various topics of nuclear science and technology, Moscow 1999, All-Russia Scientific and Technical Information Centre, State Service for Standard Reference Data, certification No. 444, 1 July 1995.
3. L.M. Petrie and N.F. Landers. KENO 5A - An Improved Monte Carlo Criticality Program with Supergrouping // Vol.2, Section F11 from "SCALE: A Modular Code System for Performing Standardized Computer Analyses for Licensing Evaluation", NUREG/CR-0200 Rev.2 (ORNL/NUREG/CSD-2/R2), December 1984.
4. D.F. Hollenbach, L.M. Petrie, N.F. Landers, KENO-VI: A General Quadratic Version of the KENO Program // NUREG/CR-0200 Rev.5, 1995
5. A.A. Blyskavka, G.N. Manturov, M.N. Nikolaev, A.M. Tsibulya, CONSYST/MMKKENO code system for nuclear reactor calculations using the Monte Carlo method in multigroup approximation with indicatrices of P_n-approximation dispersion. Preprint IPPE-2887, Obninsk, 2001.
6. J.F. Briesmeister et al. MCNP-A General Monte Carlo N-Particle Transport Code, Version 4A // Los Alamos National Laboratory Report, LA-12625-M, November 1993.
7. E. Alcouffe, F.W. Brinkley, Jr., D.R. Marr, and D. O'Dell. User's Guide for TWODANT: A Code Package for Two-Dimensional, Diffusion-Accelerated, Neutral-Particle Transport // LA-10049-M, February 1990.
8. O.W. Hermann, R.M. Westfall. ORIGEN-S: SCALE System Module to Calculate Fuel Depletion, Actinide Transmutation, Fission Product Buildup and Decay, and Association Source Terms // SCALE 4.3, Vol.2, Section F7, 1995.
9. A.L. Kochetkov, CARE code - calculation of the isotope kinetics, and the radiation and ecological characteristics of nuclear fuel during irradiation and hold-up, Preprint IPPE-2431, Obninsk 1995.
10. Tatiana Ivanova, Mark Nikolaev, Yevgeny Rozhikhin, Mikhail Semenov, Alexandre Tsiboulia, Validation of the KENO/ABBN-93 Package Based on Data From the International Handbook of Evaluated Criticality Safety Benchmark Experiments // Proceedings of Sixth International Conference on Nuclear Criticality Safety, Versailles, France, September 20-24, 1999.
11. Nikolaev M., Tsiboulia A., Rozhikhin Ye., Ivanova T. On the Internal Inconsistency of Plutonium-Solution Critical-Experiment Data and the Uncertainties // ICNC'99 – The Sixth International Conference on Nuclear Criticality Safety, Versailles, France, September 20-24, 1999.
12. M. Nikolaev, S. Zabrodskaya, T. Ivanova, V. Kosheev, G. Manturov, Y. Rozhikhin, Y. Khomiakov, Al. Tsiboulia, An. Tsiboulia. Nuclear Data Set ABBN-93.2 and its Usage for Nuclear Criticality and Radiation Safety Estimations // International Conference on Nuclear Data in the Science and Technology, Tsukuba, Japan, October 2001.

13. O.W. Hermann, R.M. Westfall. ORIGEN-S: SCALE System Module to Calculate Fuel Depletion, Actinide Transmutation, Fission Product Buildup and Decay, and Association Source Terms // SCALE 4.3, Vol.2, Section F7, 1995.
14. SCALE4.3: System for Computational Analysis and Licensing Evaluations. RSIC Computer Code Collection // ID COC-545, ORNL.
15. Physics of Plutonium Recycling, Volume II, Plutonium Recycling in Pressurized-Water Reactors // OECD, 1995.

Nuclear Data Section
International Atomic Energy Agency
P.O. Box 100
A-1400 Vienna
Austria

e-mail: services@iaeand.iaea.org
fax: (43-1) 26007
cable: INATOM VIENNA
telex: 1-12645
telephone: (43-1) 2600-21710

Online: TELNET or FTP: iaeand.iaea.org
username: IAEANDS for interactive Nuclear Data Information System
usernames: ANONYMOUS for FTP file transfer;
FENDL2 for FTP file transfer of FENDL-2.0;
RIPL for FTP file transfer of RIPL;
NDSONL for FTP access to files saved in “NDIS” Telnet session.
Web: http://www-nds.iaea.org